CONTROLLED RELEASE FROM AGRICULTURAL SPRAY DEPOSITS

CONTROLLED RELEASE FROM AGRICULTURAL SPRAY DEPOSITS

By

FENGYAN WANG, B.Eng. M.Sc.

A Thesis Submitted to the School of Graduate Studies

in Partial Fulfilment of the Requirements

for the Degree of Doctor of Philosophy

McMaster University

DOCTOR OF PHILOSOPHY (2020) McMaster University

(Chemical Engineering) Hamilton, Ontario

TITLE: Controlled Release from Agricultural Spray Deposits

AUTHOR: Fengyan Wang

B.Eng. (Beijing Institute of Technology, China)

M.Sc. (Beijing Institute of Technology, China)

SUPERVISOR: Dr. Robert H. Pelton

NUMBER OF PAGES: VII, 95

Lay Abstract

Agricultural formulations have been developed and widely applied to crops in an effort to maximize yields to keep up with the food demands of the world's ever-growing population. However, there are still many challenges associated with the application of these formulations, such as huge losses due to spray drift, wash-off, and degradation during spraying. These issues can reduce the formulation's overall efficacy and pose serious risks to the environment and human health.

The primary objective of this thesis is to explore the agricultural application of a new environmentally-friendly active ingredient, copper chlorophyllin (CuChl). To this end, this work begins by determining CuChl's colloidal and adsorption behaviors, with a particular focus on its binding tendencies for relevant plant surfaces. Next, a polymer combination was designed as a spray adjuvant to enhance CuChl's rainfastness performance and CuChl's release from dried deposits was characterized. Finally, the distribution of dispersed particles in dried suspoemulsion deposits was determined.

Abstract

Copper chlorophyllin (CuChl) is an antioxidant from renewable sources, which has shown as a potential active ingredient in agricultural crop sprays. The major objectives of this thesis are to understand the colloidal and interfacial behaviors of CuChl, and to develop strategies for improving its effectiveness in field applications. In this project, the following three areas are examined and analyzed.

In practice, CuChl-based formulations are sprayed directly onto a plant's foliage. As such, there is a need to understand how CuChl interacts with relevant plant surfaces. To this end, quartz crystal microbalance with dissipation (QCM-D) was used to quantify the adsorption of CuChl aqueous solutions onto four model surfaces: polystyrene, cellulose, pullulan, and silica. The results showed that cellulose adsorbed the highest amount of CuChl, followed by polystyrene and pullulan. In addition, the results also showed that the surfactants, SDS or DTAB, could alter the binding of CuChl to cellulose when used in concentrations above the critical micelle concentration.

CuChl is composed of water-soluble and dispersed components, therefore it is not intrinsically rainfast, which limits its field application. To immobilize CuChl on leaves, a polymer combination of CMC (carboxymethyl cellulose) and PAE (polyamidoamine-epichlorohydrin) was designed for use as a spray adjuvant. The release behaviors of CuChl from dried spray deposits were investigated using varied polymer compositions and concentrations and compared with those of a water-soluble dye, brilliant sulfaflavine (BSF). The results indicated that a small amount of CuChl was immediately released upon exposure to water whereas BSF's release behavior was dependent on the square root of time. The unusual behavior of CuChl was attributed to the presence of particles in the solution. These nanoparticles were coated with CMC:PAE complex, with the result of being immobilized on parafilm.

Suspoemulsion is the most complex agricultural formulation that is composed of both dispersed particles and emulsion droplets. The objective of this work is to understand the relationship between the solution properties of suspoemulsions and the resulting dried deposits on hydrophobic surfaces. The results showed that the distribution of polychlorinated Cu (II) phthalocyanine (PG7) particles in dried deposits was related to the extent to which PG7 particles were adsorbed on or entrained in oil droplets. The PG7 particles that mainly ended up in the center (dome) area after drying were bound to the oil/water interface in the suspoemulsion, whereas individually dispersed particles ended up in the annulus.

Acknowledgments

Firstly, I would like to thank my supervisor, Dr. Robert Pelton, for his instructions and support throughout my Ph.D. studies. His passion and earnestness show me the world's top researcher's characters and inspire me to think about how to be a better researcher. In addition to scientific thinking and analysis, he also gave me great instructions in oral presentations, mathematical modeling, and paper writing. I am truly grateful to have had the opportunity to work in his research group.

I would like to thank my supervisory committee members, Dr. Michael Brook and Dr. Charles de Lannoy for their helpful advice and discussions on the project. Their insightful questions and recommendations enable me to have a better and deeper understanding of this project.

Also, I would like to thank the staff from Suncor, including Dr. Wenzi Ckurshumova, Dr. Yuichi Terazono, Dr. Ken Ng, Dr. Michael Fefer and Dr. Jun Liu for research and financial support.

Furthermore, I would like to thank our laboratory manager Doug Keller, instrumentation technologist Michael Clarke, research technician Tim Stephens, administrative secretary Sally Watson and graduate assistant Michelle Whalen for their great help in past years. I also want to thank staff and technicians at Biointerfaces Institute and Canadian Centre for Electron Microscopy (CCEM) for their training and help.

I want to thank my lab colleagues, including Dr. Zhen Hu, Dr. Carla Abarca, Dr. Dong Yang, Dr. Yuanhua Li, Dr. Xiaofei Dong, Dr. Qiang Fu, Hongfeng Zhang, Gaoyin He, and Xiao Wu. I really enjoyed the experience of working with you. Many thanks to my friends Lu Zhu, Qianqian Zhang, Dongyang Li, Qun Zhou, Hyejin Lee, Lisha Zhao, Cecilia Chen, Jinlei Li, Xiaodan Ni, Lingli Liu, Yushan Zhang, Naveen Vasudevan, Nan Zhang, Xiaoyun Li, and Yichen Wu.

Last but not least, I would like to express my deepest appreciation to my parents. Their endless love and support encouraged me to go through all the highs and lows.

Table of Contents

List of Abbreviations

AFM	Atomic force microscopy
BSF	Brilliant sulfaflavine
CMC	Sodium carboxymethyl cellulose
$CuCe_6$	Copper chlorin e_6 trisodium salt
CuChl	Copper chlorophyllin
DLS	Dynamic light scattering
DMSO	Dimethyl sulfoxide
DTAB	Dodecyltrimethylammonium bromide
EM	Electrophoretic Mobility
ESI-MS	Electrospray ionization mass spectrometry
MWCO	Molecular weight cut-off
PAE	Polyamidoamine-epichlorohydrin
PBS	Phosphate buffered saline
PDADMAC	Polydiallyldimethylammonium chloride
PG7	Pigment Green 7 (polychlorinated Cu (II) phthalocyanine pigment)
PVSK	Poly(vinyl sulfate) potassium salt
QCM-D	Quartz crystal microbalance with dissipation
SDS	Sodium dodecyl sulfate
SEM	Scanning electron microscope
US	Ultra-sonication
VM	Votex mixing

Chapter 1

Introduction and Objectives

Since their first recorded use by the Sumerians in 2500 B.C., agrochemicals have been employed around the world to ensure sufficient food supplies, either by killing pests and weeds or by enhancing crop yields.[1] Remarkable efforts have been made by industry and academia to improve the effectiveness of agrochemicals, including the development of new active ingredients and adjuvants, as well as more effective delivery methods.[2-5] The application of these innovations is evidenced by data from the Food and Agriculture Organization of the United Nations Statistics Divison (FAO), which shows that over 4 megatons of pesticides were used in 2017.[6]

Typically, agrochemical concentrates are diluted in water before being sprayed onto the foliage. Despite losses during spraying, a small number of droplets will adhere to, spread on, and in some cases penetrate into or translocate inside leaves.[7] Recent researchers have investigated the factors that affect these processes in an attempt to reveal their underlying mechanisms, which would be of tremendous assistance to chemists or formulators in developing new products.[8-11]

This chapter introduces agricultural formulations and leaf surface features and provides an overview of the related research. Finally, the chapter concludes by describing the objectives of this project and providing an outline of this thesis.

1.1 Agricultural formulations

The use of agricultural formulations in modern agriculture has yielded significant economic and social benefits. Commercial agricultural formulations are usually comprised of a variety of ingredients, with bioactivity being regulated by the formulation's active ingredient (AI), which is commonly a chemical or biological agent. Most AIs fall into the general category of pesticides, which are defined by the Food and Agriculture Organization (FAO) as substances or mixtures of substances that are used to control pests, diseases, or unwanted species or to regulate growth during production, storage or transportation.[12] Pesticides can be divided into multiple sub-categories, including herbicides, insecticides, antimicrobials, fungicides, rodenticides, etc. Of these sub-categories, herbicides are among the most commonly used, accounting for more than 40% of all annual pesticide-usage between 2008 and 2012.[13] A brief description of each type of pesticide is provided in Table 1-1.

Table 1-1 Common pesticide categories and related action.

Pesticide category	Action
Herbicides	Kill unwanted plants
Insecticides	Kill insects
Antimicrobials	Kill microorganisms, e.g. bacteria and viruses
Fungicides	Kill fungi, molds, mildew, etc.
Rodenticides	Kill rodents, such as mice and rats

However, pure AIs are not suitable for field practice because they may be water-soluble or instable. To remedy this, AIs are combined with other ingredients, collectively known as adjuvants, to produce useable commercial formulations. Adjuvants can aid or modify the physicochemical characteristics of spray solutions or the action of an AI, thereby enhancing the formulation's efficacy.[14] They may be included in formulations by manufacturers as in-can adjuvants, or they can be added to spray solutions separately by users as tank-mix adjuvants. Common adjuvants can serve a variety of purposes; for example, they can be used as surfactants, spreader-stickers, drift-control agents, and penetrants.

Since most agricultural formulations use water as a carrier to deliver AIs, surfactants are also often added in order to lower the spray solution's surface tension. The addition of surfactants enhances AI retention, as it causes sprayed droplets to flatten out and wet hydrophobic leaf surfaces instead of bouncing off. In particular, researchers have developed a new class of organosilicone surfactants that are capable of lowering the surface tensions to 20 mN/m which allows droplets to infiltrate the stomatal chamber. Furthermore, these new surfactants have also been observed to display rain-resistant properties for some herbicides.[15-17] Surfactants can also self-assemble to micelles above the critical micelle concentration which allows them to solubilize or disperse water-insoluble AIs. Spreader/stickers can also be used to increase the area covered by a spray solution, as well as its ability to stick to target surfaces. Nu Film P® is a commercial non-

ionic spreader/sticker composed of polymeric terpenes, mineral oil and alkyl amine ethoxylate that forms a soft film on the foliage in order to enhance AI contact, wetting and adhesion. Consequently, Nu Film P® also protects the AI from the impact of rainfall, volatilization and UV degradation. Furthermore, a broad range of droplets are produced during spraying with the smallest (<150 μm) being highly susceptible to climatic conditions such as wind, which can cause them to drift to off-target sites.[18] Hence, drift-control agents, such as polyacrylamide or polyvinyl polymers, are added to spray solutions in order to reduce the number of small droplets.[19] Additionally, penetrants can also be added to sprays to promote the translocation or diffusion of AIs into the interior parts of plants as they help soften or dissolve the plant's waxy cuticle barrier. Penetrants are usually oil-based adjuvants, such as crop oil concentrates (emulsifiable petroleum oils) or modified vegetable oils (methylated seed oils).[20] For more details on adjuvants, please see the book, *Adjuvants for Agrichemicals*.[21]

Given the overwhelming variety and availability of adjuvants, it is possible that multiple formulations are on the market for a single AI. For example, glyphosate is a broad-spectrum systemic herbicide that can inhibit the enzyme 5-enolpyruvylshikimate-3-phosphate (EPSP) synthase. Indeed, more than 750 glyphosate-based products have hit the market since Monsanto's introduction of the first one - known by its tradename, Roundup - in 1974.[22]

While it is critical to consider the type of AI when selecting adjuvants, it is also important to consider the formulation type, as this can ensure consistent performance. CropLife International, an international trade association of agrochemical companies, provides a catalog and coding system, which serves as the industry standard for classifying a wide range of agricultural formulations.[23] Table 1-2 provides a list of typical formulation types.

Table 1-2 Typical types of agricultural formulations.

Type	Code	Description
Emulsifiable concentrate	EC	An oil solution comprised of an agrochemical and emulsifiers that emulsifies after dilution in water
Emulsion	EW	Concentrated oil-in-water emulsion
Granule	GR	A non-caking and free-flowing granular formulation consisting of an agrochemical and an adsorbent carrier
Suspension concentrate	SC	A stable suspension of solid particles in oil or water (more common) phase
Suspoemulsion	SE	A mixture of emulsion and suspension
Wettable powder	WP	A powder formulation comprised of an agrochemical, wetting/dispersing agents, and an inert carrier

In this research, copper chlorophyllin (CuChl) was studied as a potential agricultural active ingredient. CuChl is a semi-synthetic derivative of chlorophyll that is prepared *via* saponification to remove the phytyl group and the isocyclic cyclopentanone ring and *via* metal replacement with copper.[24] The resulting CuChl is usually a water-soluble mixture of various chlorins and other materials.[25-26] Much work has been done to analyze and determine the composition of commercial-grade CuChl mostly from Sigma.[26-28] Tumolo's review provides a list of the chemical structures of chlorins that may be detected in commercial products.[29]

Although CuChl is commonly claimed to be water-soluble, Salin *et al.* showed that CuChl solutions could not pass through a dialysis tubing with a cut-off molecular weight of 6-8 kDa.[30] In another work, the presence of particles in CuChl solutions at pH=3 or 5 was also confirmed by dynamic light scattering (DLS).[31]

In addition to its application as a food additive, CuChl has demonstrated the ability to protect against oxidative damages induced by reactive oxygen species (ROS) as well as the ability to inhibit the activities of mutagenic/carcinogenic compounds.[32-33]

1.2 Leaf surface structure

Agricultural formulations are often sprayed directly onto the foliage, which is known as a foliar application. As such, spray droplet retention and deposit structures after dry-down are greatly affected by leaf surface characteristics.

To reduce water loss, the outermost epidermis of most terrestrial plant leaves is covered with a thin protective extracellular membrane, known as a cuticle. Holloway established a theoretical bilayer cuticle model based on ultrastructural features (shown in Figure 1-1).[34] As can be seen, the outer layer, the cuticle proper (CP), consists of alternating layers forming a lamellate region with a thickness of less than 200 nm whereas the inner cuticle layer (CL) displays a reticulate structure with a variable thickness.[35]

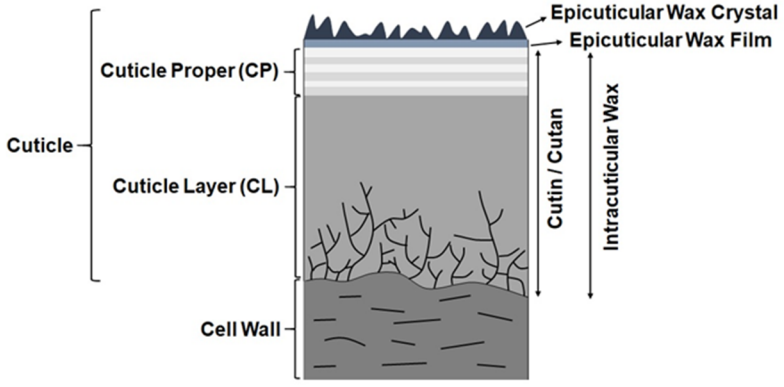

Figure 1-1 Holloway's theoretical plant cuticle structure. Modified from reference[34].

Although the cuticle structure varies between plant species, organs or ontogenic stages, its chemical composition usually consists of two classes of hydrophobic substances: cutin and wax. The cuticle's basic framework is formed by cutin, which is a polyester of C_{16} and C_{18} fatty acids, though in some species it can also be formed by cutan, which is an ether-linked aliphatic biopolymer.[36-37] Wax, either embedded in the network as intracuticular wax or superimposed on the surface as epicuticular wax, is a mixture of long-chain hydrocarbons and sometimes aromatic chemicals.[38-40] Since the cuticle is linked to the epidermal cell wall, it will likely also contain polysaccharides, pectin and phenolics.[41-42]

Epicuticular wax often forms different three-dimensional microstructures along with an underlying two-dimensional wax film; however, these three-dimensional structures may not be present on all species. Much work has been done to characterize the microstructure morphologies of leaf surfaces, particularly through the use of a scanning electron microscope (SEM). For instance, Barthlott's analysis of SEM micrographs of more than 13000 species resulted in the identification of 23 distinct morphologies, with platelets and tubules being the most common.[43] Some examples of these morphologies are shown in Figure 1-2. In addition, several researchers have attempted to correlate morphology with chemistry, with the results of these studies showing that this relationship is strong for certain morphologies. For example, tubules are comprised of four main constituent chemicals: nonacosan-10-ol, β-diketone, alkanediol and δ-lactone.[44-45]

The chemistry and structure of the cuticle enable many functions, including serving as a transport barrier for uptake and loss, as well as water repellency.[46] In particular, lotus leaves derive their superhydrophobic properties from the hierarchical structures of micron-scale epidermal cells (papillae) and nano-scale superimposed hydrophobic wax crystals. To mimic the magic of nature, intensive research has been conducted to prepare anti-adhesive and self-cleaning surfaces based on hierarchical structures.[47-49]

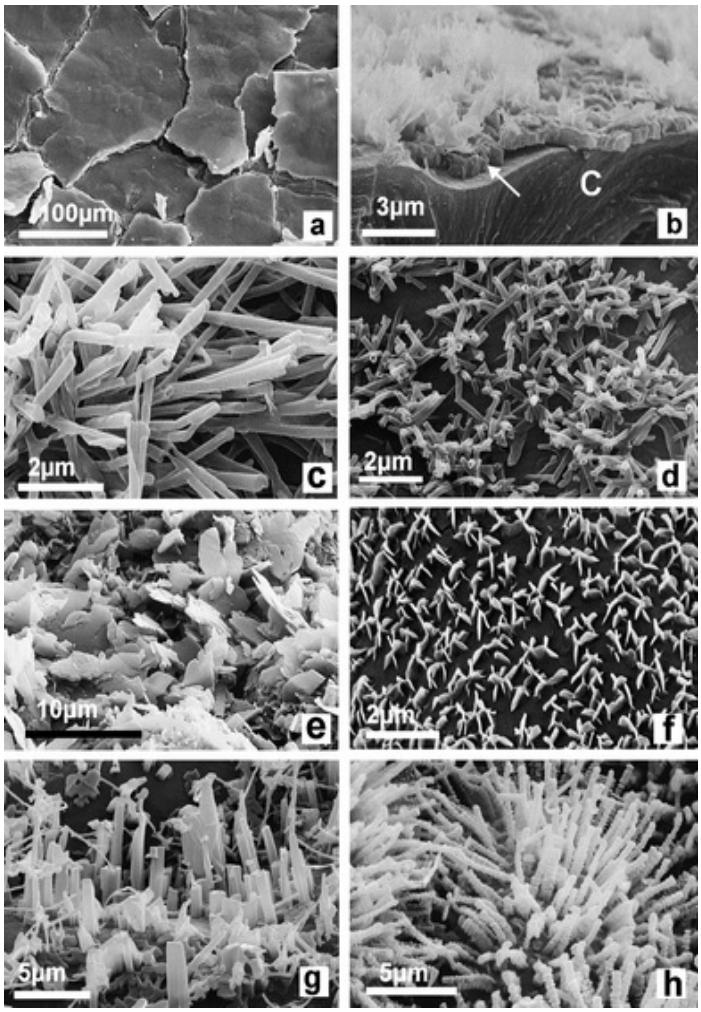

Figure 1-2 SEM micrographs of epicuticular wax microstructures on different leaf surfaces: (a) fissured wax crust on *Crassula ovata*; (b) wax platelets and a wax layer (indicated by an arrow) on *Aloe striata*; (c) β-diketone wax tubules on *Eucalyptus gunnii*; (d) nonacosan-ol tubules on top of *Thalictrum flavum glaucum*; (e) wax plates on *Aloe porphyrostachys*; (f) rosettes of platelets on *Robinia pseudoacaia*; (g) wax rodlets on cabbage (*Brasiica oleracea*); (h) transversely ridged rodlets on *Sassafras albidum*. Figure from reference.[41]

1.3 Recent studies in the literature

As noted above, agricultural formulations are sprayed onto plants to control pests or weeds. A small number of sprayed droplets will adhere to, spread out on and in some cases penetrate through leaf surfaces. The formed dried deposits on leaf surfaces are likely exposed to an irrigation or rain event to be washed off. Numerous researchers have investigated the entire process in an effort to gain a more robust understanding of it. This

section provides an overview of the literature related to deposition, wetting, deposit distribution, rainfastness, and penetration.

1.3.1 Deposition

When spray droplets contact the leaf surface, they may either adhere to it, bounce off of it or shatter into smaller droplets.[50] The spray droplet behavior is usually governed by droplets' size and velocity, the surface tension of the solution, and the leaf's surface features (wettability and surface roughness). Researchers have used high-speed cameras to visualize the impact process and track the trajectories of spray droplets.[51-52]

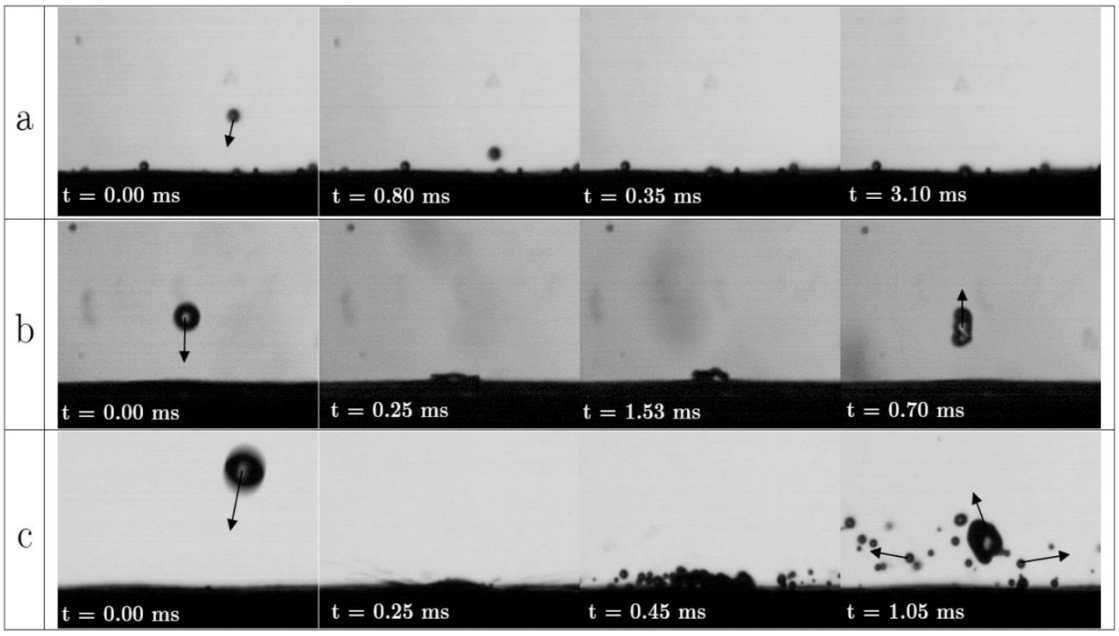

Figure 1-3 Three outcomes of a droplet impacting a surface: a) adhesion; b) bounce; c) shatter. Picture from reference[51].

1.3.1.1 Adhesion or bounce

Sprayed droplets possess kinetic energy that will cause them to spread on leaf surfaces. Due to the surface tension, initial kinetic energy will be partially converted to potential energy stored in the interface.[53] As maximum spreading is reached, the droplet starts to recoil or recede back towards its original shape. The maximum spreading diameter d_{max} is calculated as follows[54]

$$d_{max} = d * \sqrt{\frac{We+12}{3(1-cos\,\theta_A)+{}^{4We}/_{\sqrt{Re}}}} \qquad \text{Equation 1-1}$$

where d is the droplet diameter, and θ_A is the advancing contact angle of the droplet on the leaf surface. The Weber (We) and Reynolds numbers (Re) are determined by,

$$We = \frac{\rho d v^2}{\gamma} \qquad \text{Equation 1-2}$$

$$Re = \frac{\rho v d}{\mu} \qquad \text{Equation 1-3}$$

wherein ρ, γ, and μ are the solution's density, surface tension, and viscosity, respectively, and v is the droplet velocity.

During spreading and recoiling, partial energy loss occurs due to friction. If the energy loss is large enough, the droplet will not be able to detach from the leaf surface and will remain there; conversely, if enough energy is left over after the droplet reforms to a sphere, it will bounce off of the leaf.

1.3.1.2 Shatter

If a droplet impacts the surface with a high amount of energy, it may break up into many smaller droplets. This phenomenon, known as shattering, may enhance retention due to the fact that shattered droplets are slower and therefore more likely to be captured by nearby leaf surfaces. The shattering of droplets will occur if the following criterion is met:[55]

$$We^2 Re > K^4 \qquad \text{Equation 1-4}$$

where K is a constant that is equal to 57.7 for a wide range of substrate roughness, usually including leaves.

1.3.2 Wetting

After being retained, droplets begin to spread out and wet leaves. Although wetting is usually a complicated dynamic process that is influenced by many factors, this section focuses on the static contact angle at equilibrium, as it is considered to be a useful unit for predicting a surface's wettability. Based on static contact angle values, Koch et al. classified four types of surface wettability: superhydrophobic (≥150°), hydrophobic (90°~150°), hydrophilic (10°~90°) and superhydrophilic (0°~10°).[41]

The wetting behavior of a liquid drop on a solid surface is regulated by three interfacial tensions between solid-gas, solid-liquid, and liquid-gas. Complete and zero wetting are two extremes with respective values of 0° and 180°. In most cases, partial wetting is observed with a spherical droplet. For a flat ideal surface that is rigid, smooth and homogeneous, the static (equilibrium) contact angle θ_e can be calculated using Young's equation,[56]

$$\gamma_{sv} = \gamma_{sl} + \gamma_{lv} \cos\theta_e \qquad \text{Equation 1-5}$$

where γ_{sv}, γ_{sl}, γ_{lv} are the interfacial tensions between solid-gas, solid-liquid and liquid-gas respectively.

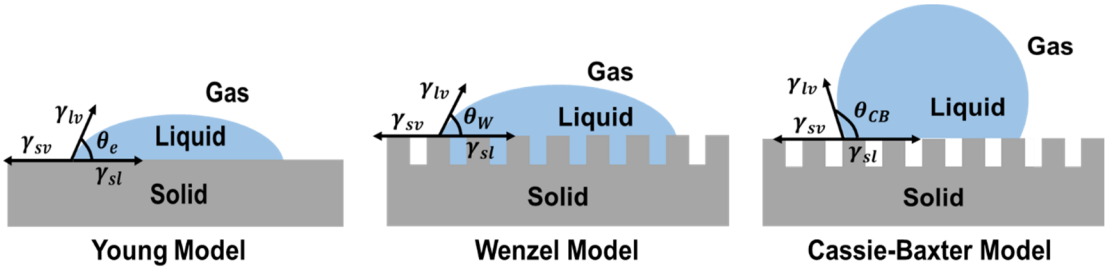

Figure 1-4 Three theoretical models of wetting.

However, real surfaces, such as leaves, are far from ideal. Wenzel integrated the effect of roughness to produce a modified equation for the static contact angle θ_W, assuming the liquid droplet can infiltrate grooves completely,[57]

$$\cos\theta_W = r * \cos\theta_e = r * \frac{\gamma_{sv}-\gamma_{sl}}{\gamma_{lv}} \quad \text{Equation 1-6}$$

wherein the roughness factor, r, is defined as the ratio between actual and projected surface areas. For a smooth surface, r=1, while r>1 for a rough surface.

In other cases, the roughness of the surface greatly reduces the contact area between the droplet and surface underneath. For example, Wagner et al.'s investigation of six species using confocal and atomic force microscopes revealed that hierarchical structures caused a 95% decrease in the contact area of a water droplet compared to the projected area.[58] Cassie and Baxter regarded surface roughness as chemically heterogeneous and calculated the contact angle, θ_{CB}, with individual component wettability.[59] The equation is displayed as follows:

$$\cos\theta_{CB} = f_1 * \cos\theta_1 + f_2 * \cos\theta_2 \quad \text{Equation 1-7}$$

wherein f_1 and f_2 are the fractions of surface types 1 and 2, and θ_1 and θ_2 are corresponding contact angles.

For superhydrophobic surfaces, the air is trapped between the droplet and surface. We define θ_2=180°, and $f_2 = 1 - f_1$ in order to simplify the equation as follows:

$$\cos\theta_{CB} = f * (\cos\theta + 1) - 1 \quad \text{Equation 1-8}$$

wherein f is the ratio between the solid-liquid contact area and its projected area.

1.3.3 Deposit distribution

Evaporation causes spray droplets to dry up on leaf surfaces, leaving residues of different distribution patterns that can affect AI penetration and efficacy. For example, Faers et al.'s investigation of the deposit residues of suspoemulsion formulations revealed that the close association between the AI and adjuvant oil can enhance uptake.[60] The following sub-sections briefly explore three basic distribution patterns of a simple particle-laden solution on a smooth surface and their underlying mechanisms.

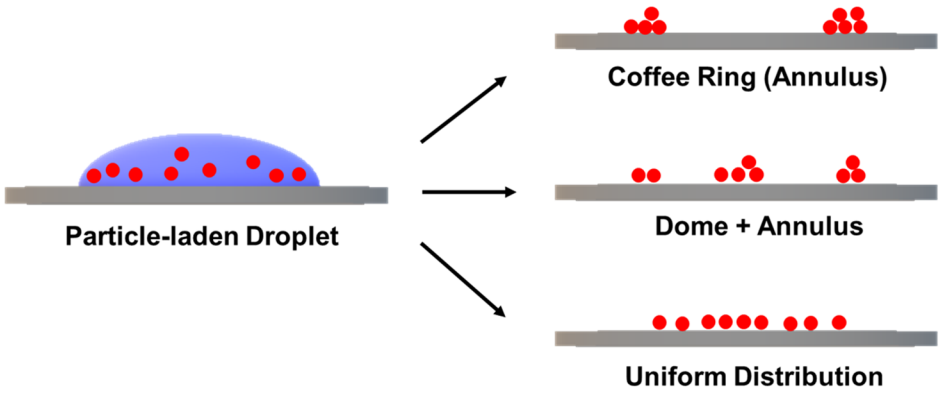

Figure 1-5 Cross-sectional illustration of different deposit distributions formed by drying sessile drops of a particle-laden solution.

1.3.3.1 Coffee-ring distribution

Similar to coffee stains, agricultural droplets containing suspended particles present an annulus or ring-like pattern on leaves after evaporation. In 1997, Deegan et al. proposed a mechanism to explain this phenomenon.[61] Specifically, they suggested evaporation occurs along the surface of an aqueous droplet when it is placed on a solid surface. The evaporation flux $J(r)$ in a sessile drop with a contact angle, θ_c, is given by

$$J(r) \propto (R - r)^{-\lambda} \qquad \text{Equation 1-9}$$

in which

$$\lambda = \frac{\pi - 2\theta_c}{2\pi - 2\theta_c} \qquad \text{Equation 1-10}$$

and R and r are the droplet radius and the radial coordinate, respectively.

Based on Equation 1-9, evaporation flux varies with the position, with the highest evaporation rate being obtained as r approaches R. The pinned contact line of the droplet induces an outward capillary flow to replenish the liquid at the edge, which transports particles outwards as well. For a thin drop with a center height that is far smaller than R, the mass of solute, m_R, in the ring is[62]

$$m_R = m_0\left[1-\left(1-\frac{t}{t_f}\right)^{(1+\lambda)/2}\right]^{2/(1+\lambda)} \quad \text{Equation 1-11}$$

where m_0 is the initial solute mass, and t_f is total drying time.

1.3.3.2 Dome plus annulus distribution

Sometimes, a dome can be observed in the center of annulus residues.[63] Hu et al. have ascribed this formation to a reversed flow, Marangoni flow.[64] Temperatures along the liquid-air surface are non-uniform due to different thermal conduction paths, with the lowest value being found at the top center of the droplet. These variations in temperature result in different surface tensions throughout the droplet. The surface-tension gradient induces an inward flow, termed Marangoni flow, to carry particles back towards the top of the center. [65] As a result, particles can either precipitate to adsorb onto the substrate or be recirculated to the edge. However, Marangoni flow is usually suppressed in water droplets, which is why the coffee ring formation tends to be more common.

Surfactants are also known for their efficiency in altering the surface tension, which allows them to generate different scenarios depending on whether they collaborate or compete with the thermal-induced gradient. For instance, the coffee ring effect can be enhanced or reversed depending on the type or concentration of the surfactant.[66-69] Karapetsas et al. summarized the effect of surfactants as follows:1) they are able to induce the Marangoni flow *via* the surface-tension gradient; 2) they can slow the evaporation rate; 3) they are able to influence the dynamics of the contact line; 4) they can facilitate interactions between particles; and 5) they are able to initiate particle interactions with liquid-solid as well as liquid-gas interfaces.[70-71]

1.3.3.3 Uniform distribution

Uniform distribution may also be observed depending upon the balance between capillary and Marangoni flow or for droplets with a mobile contact line. In addition, uniform distribution has been achieved *via* other methods, such as preparing ellipsoidal particles or heating the substrate, which have been carried out in lab-scale experiments.[72-73]

While uniform distribution is always preferred in printing and coating applications, optimal patterns for agricultural residues vary based on AIs, plants and purposes. For instance, Faers et al. argue that the coffee ring is an acceptable pattern as uptake can be promoted by a strong association between the AI and adjuvant in the ring structure.[60]

1.3.4 Rainfastness

A rain-free period is usually recommended in commercial labels. This recommendation is often related to the product's rainfastness performance, which refers to its ability to resist

loss due to rain or overhead irrigation, thereby maintaining its biological effectiveness.[74] As such, good rainfastness performance can improve retention and reduce application times, which lowers economic costs and risks to the applicators.

In the 1990s, organosilicone surfactants were reported as rainfastness adjuvants for some herbicides.[75-77] The adjuvants that have recently been proposed in the academic literature usually fall into two categories: film-forming materials or encapsulation carriers. Sun et al. from Akzo Nobel Chemicals International B.V. patented methylethylhydroxyethyl cellulose (MEHEC) as a drift-control and rainfastness agent.[78] They mixed the 0.2 wt% MEHEC solution with a water-soluble model dye, tartrazine, at 1:1 ratio and deposited drops of the mixture onto parafilm. The dried deposits were then placed under a simulated rain source, which was produced by quickly pouring 400 g of water into a vessel with small holes at the bottom for 15 seconds. The retained deposits were visually compared before and after simulated rain, with the results suggesting that MEHEC provided better protection than the comparison adjuvant, guar gum. In 2016, Dr. Khutoryanskiy's group developed laboratory-scale and simulated raintower washing methods to evaluate the rainfastness performance of fluorescently labeled poly(vinyl alcohol) (PVA) deposits on *Vicia faba* leaf surfaces. By monitoring coverage with fluorescent microscopy, they found the rainfastness performance of PVA enhanced with molecular weight and crystallinity.[79] In a subsequent study, they found that chitosan displayed better retaining coverage *via* the identical protocol than commercial BOND or PVA.[80] Furthermore, they also created a formulation by combining chitosan with a water-dispersed fungicide, azoxystrobin, and assessed the adjuvancy of chitosan *via* a quantitative spot and wash analysis. After a one-hour rain washing (10 mm/h), nearly 100% of the azoxystrobin was retained under the protection of chitosan.

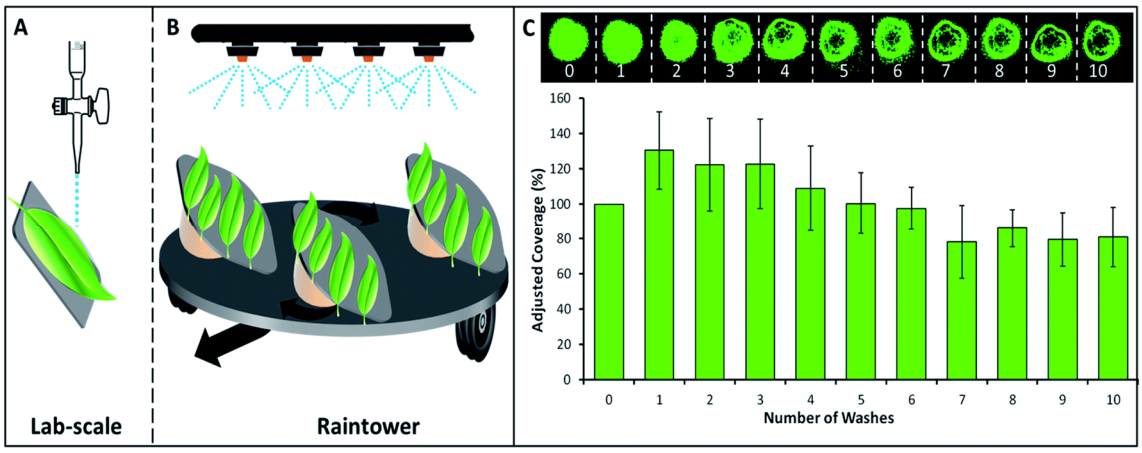

Figure 1-6 (A) and (B) are schematic diagrams of the lab-scale and simulated raintower methods, respectively; (C) is a representative wash-off result. The coverage area of a PVA deposit before and after the wash-off is processed by ImageJ and plotted. Picture from reference.[80]

Although the addition of film-forming adjuvants can be effective, another strategy is to design functional carriers to encapsulate the AI. Yu et al. functionalized poly(lactic acid) nanoparticles with carboxyl, amine and acetyl groups individually in order to encapsulate the biocide, abamectin, and to evaluate their adhesion to cucumber foliage *via* fluorescence imaging and HPLC. The adhesion was found to follow the order of H_2N-PLA-NS > CH_3CO-PLA-NS > HOOC-PLA-NS, owing to hydrogen bonds, electrostatic interaction and covalent bonds. These nanoparticles also displayed additional desirable benefits, such as sustained-release behaviors and higher photostability.[81] In addition, Jia et al. have prepared polydopamine microcapsules *via in-situ* emulsion polymerization at the interface in order to encapsulate avermectin for the purpose of prolonging foliar retention.[82]

1.3.5 Penetration

Foliar penetration is a key factor in the efficiency of systemic agrochemicals that are supposed to translocate in the interior of plants. Foliar penetration is a complex process that is influenced by a number of factors, including the formulation's physicochemical properties, such as molecular weight, lipophilicity and AI concentration, chemistry and microstructure of the leaf surface, including cuticle and stomata, and environmental conditions *viz* temperature and humidity.[83-88] Two possible pathways of foliar penetration, *via* cuticle and *via* stomata, are illustrated in Figure 1-7.[89]

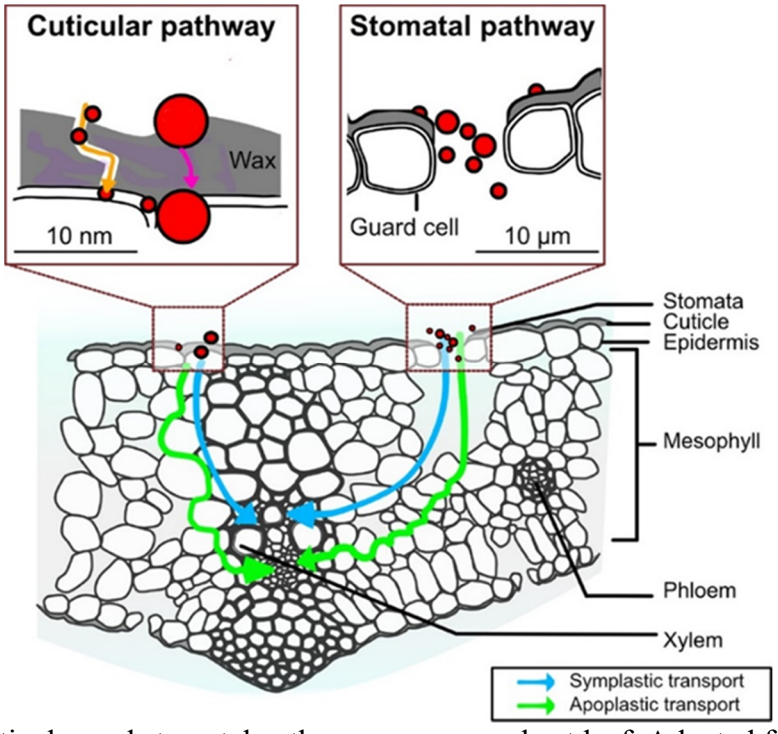

Figure 1-7 Cuticular and stomatal pathways across a wheat leaf. Adapted from reference[89]. (Copyright © 2019 American Chemical Society. Adapted with permission.)

1.3.5.1 Cuticular pathway

Both lipophilic and hydrophilic molecules were observed to penetrate through the cuticle in previous investigations.[90-92] Thus, it was postulated that the cuticle contains two paths of lipophilicity and hydrophilicity. In particular, the hydrophilic path was explained by "polar pores" or "aqueous pores" in the astomatous cuticle which are formed by water adsorption on polar domains consisting of free carboxyl and/or hydroxyl groups in cutin or polysaccharide fibers extending from underlying cell walls.[91, 93-94]

Although cuticular penetration is a continuous diffusion process driven by the concentration gradient, it is usually divided into three separate steps for analysis: sorption into the cuticle, diffusion through the cuticle and desorption from the cuticle. The basic aspects of sorption and transcuticular diffusion will be illustrated in the following sub-sections.

Sorption. Agrochemicals are sorbed into the cuticle as they are applied to the foliage. The sorption equilibrium state is governed by the cuticle/water partition coefficient

$$K_{CW} = \frac{C_C}{C_W} \qquad \text{Equation 1-12}$$

where C_C and C_W represent molecule concentrations in the cuticle and water phase, respectively.

Many efforts have been made to determine K_{CW} experimentally, with the resultant values having been compiled by Riederer.[95] However, it is impractical or tedious to measure all values experimentally due to the variability of agrochemicals and plant species. Thus, Schönherr and Riederer developed a method of predicting K_{CW} that used the physicochemical parameters of agrochemicals. Using this method, they correlated K_{CW} with the 1-octanol/water partition coefficient K_{OW} or water solubility S_W as follows:[92]

$$\log K_{CW} = 0.057 + 0.970 \log K_{OW} \; (r = 0.987) \qquad \text{Equation 1-13}$$

$$\log K_{CW} = 1.118 - 0.569 \log S_W \; (r = 0.978) \qquad \text{Equation 1-14}$$

Transcuticular diffusion. The fundamental equation for steady-state diffusion is given by Fick's first law. When transport occurs across a membrane, within the context of this research, a cuticle, a particular parameter permeance P (m/s) is used. Hence, the flux J (mol/(m^2*s)) is given by

$$J = P(C_i - C_o) \qquad \text{Equation 1-15}$$

wherein C_i and C_o represent molecule concentrations at the cuticle's inner and outer surfaces, respectively.

P is a combined parameter shown in the following equation,[96]

$$P = \frac{DK}{l} \quad \text{Equation 1-16}$$

where D (m^2/s) represents the diffusion coefficient in the cuticle, K is the partition coefficient between the cuticle and the adjacent solution and l (m) is the length of the diffusion path.

As the cuticle is tortuous, Equation 1-16 can be modified by including the tortuosity, τ, of the diffusion path.[84]

$$P = \frac{DK}{l} * \frac{1}{\tau} \quad \text{Equation 1-17}$$

However, the real cuticular penetration process is far more complicated than described by the equations above. For example, the cuticle's heterogeneous structure and non-steady state in actual practice wherein temperature and concentration change with evaporation lead to deviations from the theoretical case.

1.3.5.2 Stomatal pathway

The infiltration of stomata also contributes to the penetration of foliar-applied agrochemicals.[97] Since the critical surface tension of a leaf is usually lower than 30 mN/m, formulations containing organosilicone surfactants, e.g. Silwet L-77, were reported to display stomatal penetration.[15, 98] In addition, hygroscopic chaotropic salts were also demonstrated to reduce the surface tension of solutions and enable the hydraulic activation of stomata (HAS), thereby promoting penetration.[99]

1.4 Challenges in agrochemical development

Although agrochemicals are necessary to ensure that there is an adequate food supply, their overuse has led to great environmental damage, including soil and water contamination, reduced biodiversity, pesticide resistance, and pesticide residues in food commodities.[100-105] These adverse outcomes have provided an impetus for the government and the public to re-evaluate acceptable levels of toxicity in agricultural products and to enact new regulations designed to reduce harm and conserve the environment. One example of such progress was the banning of dichlorodiphenyltrichloroethane (DDT) in a number of countries after Rachel Carson demonstrated its devastating effects on the environment, wildlife and human health in her book "*Silent Spring*".[106-107]

At present, the rational design and use of agrochemicals are widely advocated. Much progress, including the adoption of upgraded application methods and the development of formulations with improved physicochemical properties, has been made. Furthermore, integrated pest management (IPM) was proposed as an ecological and economic approach for keeping pest populations within acceptable levels, while also reducing or minimizing impacts on the environment and human health.[108-109] Indeed, there is a long way to go before the goal of sustainable agriculture is achieved.

1.5 Objectives

Recent work has shown that CuChl, either alone or in combination with synthetic oil, can provide protection for plants facing drought or salt stress.[110-111] With respect to foliar application, it is of importance to understand CuChl's binding tendencies for relevant plant surfaces. Since CuChl is a mixture of water-soluble and dispersed components, it is washed off of leaves during rainfall or irrigation relatively easily. Thus, it is necessary to develop spray adjuvants to immobilize CuChl onto leaves while simultaneously controlling the amount of CuChl that is available to enter leaves.

Another goal of this research is to understand the relationship between the properties of agricultural suspoemulsions and the resulting dried deposits.

Therefore the specific objectives of this research are as follows:

1. To characterize aqueous CuChl solutions and to quantitatively determine the adsorption of CuChl on model surfaces: pullulan, silica, cellulose, and polystyrene;

2. To develop adjuvants to immobilize CuChl on hydrophobic surfaces and to understand the factors affecting the release behaviors of CuChl when dried deposits are exposed to water;

3. To investigate how formulation variables influence the distribution of PG7 particles in the dried deposits of suspoemulsion sessile drops on parafilm.

1.6 Outline

Chapter 1 presents the background information of the project, including an overview of agricultural formulations and leaf surface structures, and a review of studies related to spray droplet deposition, wetting, deposit distribution, rainfastness and penetration. Chapter 1 also introduces the objectives of this project and provides an outline of this thesis.

Chapter 2 presents an evaluation of the colloidal and interfacial properties of aqueous CuChl solutions. The adsorption behaviors of CuChl on model surfaces, such as polystyrene, cellulose, pullulan and silica, are quantified with QCM-D and compared with the behaviors of an authentic standard, $CuCe_6$. In addition, paper chromatography is used to assess the effects of surfactants on CuChl's ability to bind to cellulose. This work has been published on *Colloids and Surfaces A: Physicochemical and Engineering Aspects*.

Chapter 3 details how the polymer pair of CMC and PAE can be used to immobilize CuChl onto hydrophobic parafilm surfaces. To demonstrate this, the release behaviors of dry deposits containing CuChl and the polymers are quantified and compared with dry

deposits containing a water-soluble dye, BSF and polymers. The significant differences in their release behaviors are also analyzed and explained. This chapter is in preparation for publication.

Chapter 4 investigates how formulation variables affect the deposit structures that form when sessile drops of suspoemulsions are dried on waxy parafilm surfaces. This work has been published on *Colloids and Surfaces A: Physicochemical and Engineering Aspects*.

Chapter 5: This chapter summarizes the contributions of this thesis.

Reference

1. Flint, M. L.; van den Bosch, R., A History of Pest Control. In *Introduction to Integrated Pest Management*, Flint, M. L.; van den Bosch, R., Eds. Springer US: Boston, MA, 1981; pp 51-81.
2. Matthews, G., *Pesticide application methods*. John Wiley & Sons: 2008.
3. Foy, C. L.; Pritchard, D. W., *Pesticide formulation and adjuvant technology*. CRC press: 1996.
4. Ware, G. W., *The pesticide book*. Thomson Publications: 2000.
5. Matolcsy, G.; Nádasy, M.; Andriska, V., *Pesticide chemistry*. Elsevier: 1989; Vol. 32.
6. Food and Agriculture Organization of the United Nations (FAO): 2018.
7. Knowles, A., Adjuvants for agrochemicals. *Pesticide Outlook* **2001,** *12* (5), 183-184.
8. Taylor, P., The wetting of leaf surfaces. *Current Opinion in Colloid & Interface Science* **2011,** *16* (4), 326-334.
9. Damak, M.; Mahmoudi, S. R.; Hyder, M. N.; Varanasi, K. K., Enhancing droplet deposition through in-situ precipitation. *Nature communications* **2016,** *7* (1), 12560.
10. Wirth, W.; Storp, S.; Jacobsen, W., Mechanisms controlling leaf retention of agricultural spray solutions. *Pesticide Science* **1991,** *33* (4), 411-420.
11. Hull, H. M., Leaf structure as related to absorption of pesticides and other compounds. In *Residue Reviews: Residues of Pesticides and Other Foreign Chemicals in Foods and Feeds*, Gunther, F. A., Ed. Springer Berlin Heidelberg: Berlin, Heidelberg, 1970; pp 1-150.
12. *International Code of Conduct on the Distribution and Use of Pesticides (Revised Version)*. Food and Agriculture Organization of the United Nations: 2003.
13. *Pesticides Industry Sales and Usage 2008 - 2012 Market Estimates*; United States Environmental Protection Agency: 2017.
14. Standard Terminology Relating to Agricultural Tank Mix Adjuvants. ASTM International.

15. Field, R. J.; Bishop, N. G., Promotion of stomatal infiltration of glyphosate by an organosilicone surfactant reduces the critical rainfall period. *Pesticide Science* **1988,** *24* (1), 55-62.
16. Krishna, N. R.; Singh, M., Organosilicone Adjuvant Effects on Glyphosate Efficacy and Rainfastness. *Weed Technology* **1992,** *6* (2), 361-365.
17. Frank, C. R.; Loston, R.; Donald, P.; Len, P.; Richard, B., Increasing Postemergence Herbicide Efficacy and Rainfastness with Silicone Adjuvants. *Weed Technology* **1990,** *4* (3), 576-580.
18. Wolf, R. *Strategies to Reduce Spray Drift*; University of Illinois at Urbana-Champaign: The cutting edge.
19. CURRAN, W. S. *Adjuvants for Enhancing Herbicide Performance*; Pennsylvania State University: 1999.
20. Ferrell, J. *Spray Adjuvants: A User's Guide*; University of Florida.
21. Foy, C. L., *Adjuvants for Agrichemicals*. CRC Press: 2018.
22. Guyton, K. Z.; Loomis, D.; Grosse, Y.; El Ghissassi, F.; Benbrahim-Tallaa, L.; Guha, N.; Scoccianti, C.; Mattock, H.; Straif, K., Carcinogenicity of tetrachlorvinphos, parathion, malathion, diazinon, and glyphosate. *The Lancet Oncology* **2015,** *16* (5), 490-491.
23. International, C., Technical Monograph 2, 7th Edition. In *Catalogue of pesticide formulation types and international coding system*, 2017.
24. Humphrey, A. M., Chlorophyll. *Food Chemistry* **1980,** *5* (1), 57-67.
25. Mortensen, A.; Geppel, A., HPLC–MS analysis of the green food colorant sodium copper chlorophyllin. *Innovative Food Science & Emerging Technologies* **2007,** *8* (3), 419-425.
26. Inoue, H.; Yamashita, H.; Furuya, K.; Nonomura, Y.; Yoshioka, N.; Lib, S., Determination of copper (II) chlorophyllin by reversed-phase high-performance liquid chromatography. *Journal of Chromatography A* **1994,** *679* (1), 99-104.
27. Ferruzzi, M. G.; Failla, M. L.; Schwartz, S. J., Sodium Copper Chlorophyllin: In Vitro Digestive Stability and Accumulation by Caco-2 Human Intestinal Cells. *Journal of Agricultural and Food Chemistry* **2002,** *50* (7), 2173-2179.
28. Chernomorsky, S.; Rancourt, R.; Virdi, K.; Segelman, A.; Poretz, R. D., Antimutagenicity, cytotoxicity and composition of chlorophyllin copper complex. *Cancer Letters* **1997,** *120* (2), 141-147.
29. Tumolo, T.; Lanfer-Marquez, U. M., Copper chlorophyllin: A food colorant with bioactive properties? *Food Research International* **2012,** *46* (2), 451-459.
30. Salin, M. L.; Alvarez, L. M.; Lynn, B. C.; Habulihaz, B.; Fountain iii, A. W., Photooxidative Bleaching of Chlorophyllin. *Free Radical Research* **1999,** *31* (sup1), 97-105.
31. Selig, M. J.; Gamaleldin, S.; Celli, G. B.; Marchuk, M. A.; Smilgies, D.-M.; Abbaspourrad, A., The stabilization of food grade copper-chlorophyllin in low pH solutions through association with anionic polysaccharides. *Food Hydrocolloids* **2020,** *98*, 105255.

32. Kamat, J. P.; Boloor, K. K.; Devasagayam, T. P., Chlorophyllin as an effective antioxidant against membrane damage in vitro and ex vivo. *Biochimica et Biophysica Acta (BBA)-Molecular and Cell Biology of Lipids* **2000,** *1487* (2), 113-127.
33. Dashwood, R. H.; Breinholt, V.; Bailey, G. S., Chemopreventive properties of chlorophyllin: inhibition of aflatoxin B1 (AFB1)-DNA binding in vivo and anti-mutagenic activity against AFB1 and two heterocyclic amines in the salmonella mutagenicity assay. *Carcinogenesis* **1991,** *12* (5), 939-942.
34. Holloway, P. J., Plant cuticles: physicochemical characteristics and biosynthesis. In *Air pollutants and the leaf cuticle*, Springer: 1994; pp 1-13.
35. Jeffree, C., Structure and ontogeny of plant cuticles. *Plant cuticles: an integrated functional approach* **1996**, 33-82.
36. Holloway, P. In *chemical constitution of plant cutins*, Linnean Society symposium series, 1982.
37. Nip, M.; Tegelaar, E. W.; de Leeuw, J. W.; Schenck, P. A.; Holloway, P. J., A new non-saponifiable highly aliphatic and resistant biopolymer in plant cuticles. *Naturwissenschaften* **1986,** *73* (10), 579-585.
38. Kunst, L.; Samuels, A. L., Biosynthesis and secretion of plant cuticular wax. *Progress in Lipid Research* **2003,** *42* (1), 51-80.
39. Jetter, R.; Kunst, L.; Samuels, A. L., Composition of plant cuticular waxes. *Biology of the plant cuticle* **2008,** *23*, 145-181.
40. Jetter, R.; Schäffer, S., Chemical composition of the Prunus laurocerasus leaf surface. Dynamic changes of the epicuticular wax film during leaf development. *Plant physiology* **2001,** *126* (4), 1725-1737.
41. Koch, K.; Bhushan, B.; Barthlott, W., Diversity of structure, morphology and wetting of plant surfaces. *Soft Matter* **2008,** *4* (10), 1943-1963.
42. Domínguez, E.; Cuartero, J.; Heredia, A., An overview on plant cuticle biomechanics. *Plant Science* **2011,** *181* (2), 77-84.
43. Barthlott, W.; Neinhuis, C.; Cutler, D.; Ditsch, F.; Meusel, I.; Theisen, I.; Wilhelmi, H., Classification and terminology of plant epicuticular waxes. *Botanical Journal of the Linnean Society* **1998,** *126* (3), 237-260.
44. Jeffree, C. E., The fine structure of the plant cuticle. *Biology of the plant cuticle* **2006,** *23*, 11-125.
45. Jetter, R.; Riederer, M., Homologous long-chain δ-lactones in leaf cuticular waxes of Cerinthe minor. *Phytochemistry* **1999,** *50* (8), 1359-1364.
46. Bargel, H.; Koch, K.; Cerman, Z.; Neinhuis, C., Structure-function relationships of the plant cuticle and cuticular waxes - a smart material? *Functional Plant Biology* **2006,** *33* (10), 893-910.
47. Bhushan, B.; Jung, Y. C.; Koch, K., Self-Cleaning Efficiency of Artificial Superhydrophobic Surfaces. *Langmuir* **2009,** *25* (5), 3240-3248.
48. Bhushan, B.; Jung, Y. C.; Niemietz, A.; Koch, K., Lotus-Like Biomimetic Hierarchical Structures Developed by the Self-Assembly of Tubular Plant Waxes. *Langmuir* **2009,** *25* (3), 1659-1666.

49. Koch, K.; Bhushan, B.; Jung, Y. C.; Barthlott, W., Fabrication of artificial Lotus leaves and significance of hierarchical structure for superhydrophobicity and low adhesion. *Soft Matter* **2009,** *5* (7), 1386-1393.
50. Mercer, G.; Sweatman, W., Process driven models for spray retention of plants. **2006**.
51. Massinon, M.; De Cock, N.; Forster, W. A.; Nairn, J. J.; McCue, S. W.; Zabkiewicz, J. A.; Lebeau, F., Spray droplet impaction outcomes for different plant species and spray formulations. *Crop Protection* **2017,** *99*, 65-75.
52. Dong, X.; Zhu, H.; Yang, X., Characterization of droplet impact and deposit formation on leaf surfaces. *Pest Management Science* **2015,** *71* (2), 302-308.
53. Yarin, A. L., Drop impact dynamics: splashing, spreading, receding, bouncing…. *Annu. Rev. Fluid Mech.* **2006,** *38*, 159-192.
54. Pasandideh‐Fard, M.; Qiao, Y.; Chandra, S.; Mostaghimi, J., Capillary effects during droplet impact on a solid surface. *Physics of fluids* **1996,** *8* (3), 650-659.
55. Mundo, C.; Sommerfeld, M.; Tropea, C., On the modeling of liquid sprays impinging on surfaces. *Atomization and sprays* **1998,** *8* (6).
56. Young, T., III. An essay on the cohesion of fluids. *Philosophical transactions of the royal society of London* **1805,** (95), 65-87.
57. Wenzel, R. N., Resistance of solid surfaces to wetting by water *Industrial & Engineering Chemistry* **1936,** *28* (8), 988-994.
58. Wagner, P.; Fürstner, R.; Barthlott, W.; Neinhuis, C., Quantitative assessment to the structural basis of water repellency in natural and technical surfaces. *Journal of Experimental Botany* **2003,** *54* (385), 1295-1303.
59. Cassie, A. B. D.; Baxter, S., Wettability of porous surfaces. *Transactions of the Faraday Society* **1944,** *40* (0), 546-551.
60. Faers, M. A.; Pontzen, R., Factors influencing the association between active ingredient and adjuvant in the leaf deposit of adjuvant-containing suspoemulsion formulations. *Pest Manag Sci* **2008,** *64* (8), 820-33.
61. Deegan, R. D.; Bakajin, O.; Dupont, T. F.; Huber, G.; Nagel, S. R.; Witten, T. A., Capillary flow as the cause of ring stains from dried liquid drops. *Nature* **1997,** *389* (6653), 827-829.
62. Deegan, R. D.; Bakajin, O.; Dupont, T. F.; Huber, G.; Nagel, S. R.; Witten, T. A., Contact line deposits in an evaporating drop. *Physical Review E* **2000,** *62* (1), 756-765.
63. Wang, F.; Hu, Z.; Abarca, C.; Fefer, M.; Liu, J.; Brook, M. A.; Pelton, R., Factors Influencing Agricultural Spray Deposit Structures on Hydrophobic Surfaces. *Colloids and Surfaces A: Physicochemical and Engineering Aspects* **2018,** *553*.
64. Hu, H.; Larson, R. G., Marangoni Effect Reverses Coffee-Ring Depositions. *The Journal of Physical Chemistry B* **2006,** *110* (14), 7090-7094.
65. Hu, H.; Larson, R. G., Analysis of the Effects of Marangoni Stresses on the Microflow in an Evaporating Sessile Droplet. *Langmuir* **2005,** *21* (9), 3972-3980.
66. Truskett, V. N.; Stebe, K. J., Influence of Surfactants on an Evaporating Drop: Fluorescence Images and Particle Deposition Patterns. *Langmuir* **2003,** *19* (20), 8271-8279.

67. Still, T.; Yunker, P. J.; Yodh, A. G., Surfactant-Induced Marangoni Eddies Alter the Coffee-Rings of Evaporating Colloidal Drops. *Langmuir* **2012,** *28* (11), 4984-4988.
68. Crivoi, A.; Duan, F., Effect of Surfactant on the Drying Patterns of Graphite Nanofluid Droplets. *The Journal of Physical Chemistry B* **2013,** *117* (19), 5932-5938.
69. Marin, A.; Liepelt, R.; Rossi, M.; Kähler, C. J., Surfactant-driven flow transitions in evaporating droplets. *Soft Matter* **2016,** *12* (5), 1593-1600.
70. Karapetsas, G.; Sahu, K. C.; Matar, O. K., Evaporation of Sessile Droplets Laden with Particles and Insoluble Surfactants. *Langmuir* **2016,** *32* (27), 6871-6881.
71. Lunkenheimer, K.; Zembala, M., Attempts to study a water evaporation retardation by soluble surfactants. *Journal of colloid and interface science* **1997,** *188* (2), 363-371.
72. Yunker, P. J.; Still, T.; Lohr, M. A.; Yodh, A. G., Suppression of the coffee-ring effect by shape-dependent capillary interactions. *Nature* **2011,** *476* (7360), 308-11.
73. Li, Y.; Yang, Q.; Li, M.; Song, Y., Rate-dependent interface capture beyond the coffee-ring effect. *Scientific Reports* **2016,** *6* (1), 24628.
74. Standard Terminology Relating to Pesticides. *ASTM International*.
75. Roggenbuck, F. C.; Rowe, L.; Penner, D.; Petroff, L.; Burow, R., Increasing postemergence herbicide efficacy and rainfastness with silicone adjuvants. *Weed Technology* **1990,** *4* (3), 576-580.
76. Boydston, R. A.; Al-Khatib, K., DC X2-5309 organosilicone adjuvant improves control of kochia (Kochia scoparia) with bentazon and bromoxynil. *Weed technology* **1994,** *8* (1), 99-104.
77. Reddy, K. N.; Locke, M. A.; Howard, K. D., Bentazon spray retention, activity, and foliar washoff in weed species. *Weed technology* **1995,** *9* (4), 773-778.
78. Sun, J. S.; He, Q.; Zhu, S.; Dempsey, L.; Walters, M.; Westbye, P., Cellulose ether as a drift control agent and rainfastness agent. Google Patents: 2017.
79. Symonds, B. L.; Thomson, N. R.; Lindsay, C. I.; Khutoryanskiy, V. V., Rainfastness of Poly (vinyl alcohol) Deposits on Vicia faba Leaf Surfaces: From Laboratory-Scale Washing to Simulated Rain. *ACS applied materials & interfaces* **2016,** *8* (22), 14220-14230.
80. Symonds, Brett L.; Lindsay, C. I.; Thomson, N. R.; Khutoryanskiy, V. V., Chitosan as a rainfastness adjuvant for agrochemicals. *RSC Advances* **2016,** *6* (104), 102206-102213.
81. Yu, M.; Yao, J.; Liang, J.; Zeng, Z.; Cui, B.; Zhao, X.; Sun, C.; Wang, Y.; Liu, G.; Cui, H., Development of functionalized abamectin poly(lactic acid) nanoparticles with regulatable adhesion to enhance foliar retention. *RSC Advances* **2017,** *7* (19), 11271-11280.
82. Jia, X.; Sheng, W.-b.; Li, W.; Tong, Y.-b.; Liu, Z.-y.; Zhou, F., Adhesive polydopamine coated avermectin microcapsules for prolonging foliar pesticide retention. *ACS applied materials & interfaces* **2014,** *6* (22), 19552-19558.
83. Wang, C. J.; Liu, Z. Q., Foliar uptake of pesticides—Present status and future challenge. *Pesticide Biochemistry and Physiology* **2007,** *87* (1), 1-8.

84. Stagnari, F., A review of the factors influencing the absorption and efficacy of lipophilic and highly water-soluble post-emergence herbicides. *European Journal of Plant Science and Biotechnology* **2007,** *1* (1), 22-35.
85. Bauer, H.; Schönherr, J., Determination of mobilities of organic compounds in plant cuticles and correlation with molar volumes. *Pesticide Science* **1992,** *35* (1), 1-11.
86. Schönherr, J.; Schreiber, L., Size selectivity of aqueous pores in astomatous cuticular membranes isolated from Populus canescens (Aiton) Sm. leaves. *Planta* **2004,** *219* (3), 405-411.
87. Baker, E. A.; Hayes, A. L.; Butler, R. C., Physicochemical properties of agrochemicals: their effects on foliar penetration. *Pesticide Science* **1992,** *34* (2), 167-182.
88. Stevens, P. J.; Baker, E. A.; Anderson, N. H., Factors affecting the foliar absorption and redistribution of pesticides. 2. Physicochemical properties of the active ingredient and the role of surfactant. *Pesticide Science* **1988,** *24* (1), 31-53.
89. Avellan, A.; Yun, J.; Zhang, Y.; Spielman-Sun, E.; Unrine, J. M.; Thieme, J.; Li, J.; Lombi, E.; Bland, G.; Lowry, G. V., Nanoparticle Size and Coating Chemistry Control Foliar Uptake Pathways, Translocation, and Leaf-to-Rhizosphere Transport in Wheat. *ACS Nano* **2019,** *13* (5), 5291-5305.
90. Schönherr, J., A mechanistic analysis of penetration of glyphosate salts across astomatous cuticular membranes. *Pest Management Science* **2002,** *58* (4), 343-351.
91. Schönherr, J., Calcium chloride penetrates plant cuticles via aqueous pores. *Planta* **2000,** *212* (1), 112-118.
92. Schönherr, J.; Riederer, M., Foliar penetration and accumulation of organic chemicals in plant cuticles. In *Reviews of environmental contamination and toxicology*, Springer: 1989; pp 1-70.
93. Schönherr, J., Water permeability of isolated cuticular membranes: the effect of pH and cations on diffusion, hydrodynamic permeability and size of polar pores in the cutin matrix. *Planta* **1976,** *128* (2), 113-126.
94. SCHREIBER, L., Polar Paths of Diffusion across Plant Cuticles: New Evidence for an Old Hypothesis. *Ann. Bot.* **2005,** *95* (7), 1069-1073.
95. Riederer, M., Partitioning and transport of organic chemicals between the atmospheric environment and leaves. *Plant contamination. Lewis/CRC Press, Boca Raton, FL, USA* **1995**, 153-190.
96. Crank, J., *The mathematics of diffusion*. Oxford university press: 1979.
97. Schönherr, J.; Bukovac, M. J., Penetration of Stomata by Liquids. *Plant Physiology* **1972,** *49* (5), 813.
98. Stevens, P. J. G.; Gaskin, R. E.; Hong, S.-O.; Zabkiewicz, J. A., Contributions of stomatal infiltration and cuticular penetration to enhancements of foliar uptake by surfactants. *Pesticide Science* **1991,** *33* (3), 371-382.
99. Basi, S.; Burkhardt, J.; Noga, G.; Hunsche, M., Hygroscopic salts support the stomatal penetration of glyphosate and influence its biological efficacy. *Weed biology and management* **2014,** *14* (3), 186-197.
100. Ritter, W., Pesticide contamination of ground water in the United States - A review. *Journal of Environmental Science & Health Part B* **1990,** *25* (1), 1-29.

101. Beketov, M. A.; Kefford, B. J.; Schäfer, R. B.; Liess, M., Pesticides reduce regional biodiversity of stream invertebrates. *Proceedings of the National Academy of Sciences* **2013,** *110* (27), 11039-11043.
102. Wauchope, R. D., The Pesticide Content of Surface Water Draining from Agricultural Fields—A Review1. *Journal of Environmental Quality* **1978,** *7* (4), 459-472.
103. Flury, M., Experimental Evidence of Transport of Pesticides through Field Soils—A Review. *Journal of Environmental Quality* **1996,** *25* (1), 25-45.
104. Picó, Y.; Blasco, C.; Font, G., Environmental and food applications of LC–tandem mass spectrometry in pesticide-residue analysis: An overview. *Mass Spectrometry Reviews* **2004,** *23* (1), 45-85.
105. Boudh, S.; Singh, J. S., Pesticide Contamination: Environmental Problems and Remediation Strategies. In *Emerging and Eco-Friendly Approaches for Waste Management*, Bharagava, R. N.; Chowdhary, P., Eds. Springer Singapore: Singapore, 2019; pp 245-269.
106. Carson, R., *Silent spring*. Houghton Mifflin Harcourt: 2002.
107. Agency, U. S. E. P. DDT - A Brief History and Status. https://www.epa.gov/ingredients-used-pesticide-products/ddt-brief-history-and-status.
108. Ehler, L. E., Integrated pest management (IPM): definition, historical development and implementation, and the other IPM. *Pest management science* **2006,** *62* (9), 787-789.
109. Elliott, N.; Farrell, J.; Gutierrez, A.; van Lenteren, J. C.; Walton, M.; Wratten, S., *Integrated pest management*. Springer Science & Business Media: 1995.
110. Fefer, M.; Liu, J.; NG, k.; Terazono, Y.; Teshler, I.; Ckurshumova, W.; Nash, B. Macrocyclic tetrapyrrole compounds, compositions and methods for increasing abiotic stress resistance in plants. 2019.
111. Zhang, X.; Goatley, M.; Conner, J.; Wilkins, M.; Teshler, I.; Liu, J.; Fefer, M.; Ckurshumova, W., Copper Chlorophyllin Impacts on Growth and Drought Stress Tolerance of Tomato Plants. *HortScience horts* **2019,** *54* (12), 2195-2201.

Chapter 2

Adsorption of Copper Chlorophyllin on Model Surfaces

To employ CuChl as a potential agricultural active ingredient, chapter 2 first details the colloidal properties of aqueous CuChl solutions. CuChl's binding tendencies for model surfaces are measured *via* QCM-D in order to understand how CuChl interacts with relevant plant surfaces. Furthermore, the effect of surfactants, which are commonly used in commercial products, on CuChl's ability to bind to cellulose is assessed *via* paper chromatography.

All experiments, except AFM, were carried out by myself. Xiao, Dr. Niinivaara, and Daniel helped with AFM measurements. Dr. Terazono assisted me in analyzing MS results. Dr. Liu and Dr. Fefer reviewed the paper and provided useful comments. I summarized the data and wrote the draft. Dr. Pelton helped me rewrite the draft to the final version.

Adsorption of Aqueous Copper Chlorophyllin Mixtures on Model Surfaces

Fengyan Wang, Yuichi Terazono, Jun Liu, Michael Fefer, Robert Pelton

Colloids and Surfaces A: Physicochemical and Engineering Aspects 2020, 592, 124578.

https://doi.org/10.1016/j.colsurfa.2020.124578

Colloids and Surfaces A 592 (2020) 124578

Contents lists available at ScienceDirect

Colloids and Surfaces A

journal homepage: www.elsevier.com/locate/colsurfa

Adsorption of aqueous copper chlorophyllin mixtures on model surfaces

Fengyan Wang[a], Yuichi Terazono[b], Jun Liu[b], Michael Fefer[b], Robert H. Pelton[a,*]

[a] Department of Chemical Engineering, McMaster University, 1280 Main Street West, Hamilton, ON L8S 4L7, Canada
[b] Suncor AgroScience, 2489 North Sheridan Way, Mississauga, L5K 1A8, Canada

GRAPHICAL ABSTRACT

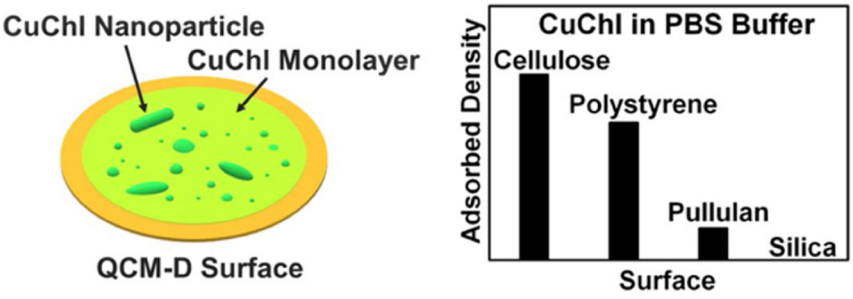

ARTICLE INFO

Keywords:
Copper chlorophyllin
Colloidal properties
Adsorption on surfaces
Particle size
Quartz crystal microbalance

ABSTRACT

Measured were the colloidal and adsorption properties of copper chlorophyllin (CuChl), a complex mixture derived from chlorophyll that is used as a food additive and in other applications. CuChl has an "apparent solubility" (it is a mixture) of 0.1 g/L in PBS buffer. Dynamic light scattering of dilute solutions showed the presence of particles with diameters in the range 10 − 800 nm. Nanoparticle tracking analysis (NanoSight LM10) showed the majority of nanoparticles had hydrodynamic diameters 100 − 200 nm. Dialysis experiments revealed that 58 % of a 0.1 g/L CuChl was present as dispersed particles. QCM-D measurements showed that aqueous CuChl adsorbs on surfaces giving a maximum adsorbed coverage, $\Gamma_{max,}$ that is sensitive to the type of surface; cellulose > polystyrene > > pullulan > silica = 0. No adsorption was observed on silica. Centrifuged $CuCe_6$, a pure chlorin, showed essentially the same adsorption behaviors as centrifuged CuChl mixtures on polystyrene, suggesting that chlorins are the dominant adsorbed species from CuChl mixtures on hydrophobic surfaces. Centrifuged CuChl and $CuCe_6$ usually gave lower Γ_{max} values compared to non-centrifuged samples. In all cases, rinsing with buffer after CuChl or $CuCe_6$ adsorption resulted in the immediate removal of some of the adsorbed chlorins. With cellulose there was no further dissolution, whereas with polystyrene, the adsorbed layer eventually was entirely removed. AFM measurements showed the adsorbed materials included nanoparticles. The surfactants SDS or DTAB could displace CuChl adsorbed on cellulosic filter paper only if the surfactant concentrations were above the critical micelle concentration.

1. Introduction

Copper chlorophyllin (CuChl) is a green dye found in some foods, [1,2] it is sold as a health food, and CuChl has been the subject of many investigations of potential applications including biomedical [3], photocatalytic [4] and photovoltaic devices [5]. This interest reflects the attractive properties of CuChl, including it is inexpensive, it has approvals for use in some foods, and CuChl is green, figuratively and

* Corresponding author.
E-mail address: peltonrh@mcmaster.ca (R.H. Pelton).

https://doi.org/10.1016/j.colsurfa.2020.124578
Received 12 December 2019; Received in revised form 7 February 2020; Accepted 10 February 2020
Available online 13 February 2020

literally. We are interested in the potential application of CuChl and related chlorins for the protection of agricultural crops. [6]

CuChl is extracted from the hydrolytic degradation of chlorophyll. The manufacturing process includes the replacement of the magnesium ligand with copper 2^+, yielding a more stable product compared to the parent chlorophyll. Ryan and Senge in their 2015 review [5] estimated CuChl production was only "several thousand tonnes worldwide".

Although there is much literature describing potential applications of CuChl, there is little information regarding some of the most basic physical-chemical properties. This contribution describes some properties of aqueous CuChl including water-solubility, particle size and the adsorption/desorption behaviors with model surfaces. These are non-trivial measurements because, as discussed below, aqueous CuChl is a mixture of chemicals, some of which are present as nanoparticles. We believe this information may contribute to understanding CuChl mechanisms in a variety of applications. The following paragraphs summarize the results from some relevant prior work.

1.1. CuChl composition

CuChl is a chemical mixture, and much like commercial lignin or starch, the composition of the mixture depends upon the source, the extraction and the purification processes. The chemical composition of food grade CuChl has been summarized in recent reviews [1–3]. Fig. 1 shows the structures of the most relevant chlorins and the nomenclature used herein; a more extensive set of chlorin structures is given in Tumolo's review [1].

In early work, Inoue et al. reported the composition of four (unnamed) commercial CuChl mixtures; $CuCe_4$ was the major component (35–60 wt %), with minor amounts of $CuCe_6$, rodin g_7 and pheophorbide a [7]. The contents of non-chlorin materials ranged from 8 to 43 wt%. Presumably these were other chlorophyll breakdown products and inorganic salts. Chernomorsky et al. used measurements of copper and nitrogen elemental compositions to estimate the purity of four lots of CuChl. The purities ranged from 23 to 60 % [8].

Many published studies used CuChl from Sigma-Aldrich without purification. Sigma Canada sells two grades of CuChl, "Commercial Grade" and "Pharmaceutical Secondary Standard; Certified Reference Material"; in both cases Sigma gives the structure as $CuCe_6$. Based on copper analysis, Ferruzzi et al. estimated the purity of Sigma CuChl to be 48 % assuming the only chlorophyllin was $CuCe_4$ [9]. In a more detailed analysis of CuChl from Sigma, Mortensen and Geppel reported Cu chlorin e_6, Cu chlorin p_6, and Cu isochlorin e_4 were the main constituents [10]. To summarize, whereas biomedical applications ideally require pure copper chlorins [11], food coloring, textile dying and many other potential applications could be served by CuChl mixtures. Herein we report properties of CuChl mixtures, making some comparisons with pure $CuCe_6$.

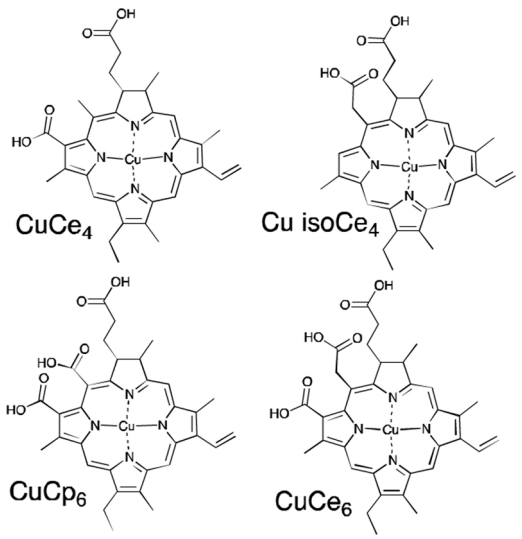

Fig. 1. Structure of major components of CuChl.

1.2. CuChl water solubility

We have found no reported water solubility values for CuChl in the literature. In spite of the fact that some authors claim CuChl mixtures are water-soluble [12], CuChl solutions contain dispersed particles. Salin et al. reported in 1999 that aqueous Sigma CuChl could not pass through 6 − 8 kDa cut off dialysis tubing, suggesting the presence of particles [13]. Aydin et al. prepared spin coated films of $CuCe_6$ and observed 40 nm particles on the film surface [14]. Dynamic light scattering (DLS) showed similar sized particles. A very recent publication also presented DLS evidence that CuChl was aggregated [15]. They further showed that the particle size was reduced by the presence of sodium alginate or xanthan gums; presumably the polysaccharides are acting as colloidal stabilizers.

The octanol-water partition coefficient, Kp, is a measure of solute hydrophilicity. Kp has been reported for metal ligand-free Ce_6 in PBS buffer [16]. Kp ranged from 10 at pH 6.7 down to about 3 at pH 7.6. By contrast the Kp of chlorophyll is about 275 in water [17]. Kp values have little meaning for mixtures of solutes and thus we have found no values for CuChl. The above values for Ce_6 should be a good approximation for $CuCe_6$.

The water-soluble components of CuChl could be surface active. However, we have found no reports of CuChl surface activity. A recent paper describing the use of flotation to purify CuChl suggests that some chlorins must be surface active [18]. In summary, the literature suggests CuChl is a water-borne material that is present as a mixture of particles, large and small, plus truly water-soluble components.

1.3. CuChl interactions with surfaces

Whether it is dying fabrics [19] or fabricating devices [18], many CuChl applications involve immobilizing the green dye on surfaces. Hou et al. reported a kinetic study of CuChl adsorption onto silk [20]. The CuChl was 50 % actives, of which 85 % was $CuCe_4$ and 15 % $CuCe_6$. The binding results were obtained as a function of CuChl concentration, pH (6–8), temperature (70 − 90 °C) and NaCl concentration. Most experiments were conducted at pH 8 because CuChl precipitated at pH 6. The binding kinetics and isotherm results suggested high affinity binding. The adsorption capacity of the silk in 9 g/L NaCl solution was ~ 4 times greater than in salt-free water. Increasing the temperature from 70 to 90 °C caused a decrease in adsorption capacity. In a similar study it was shown that the CuChl adsorbs onto cotton [21]. The amount of bound CuChl was increased by pre-treating the cotton with cationic chitosan. Other surfaces capable of binding CuChl include hydrotalcite, a synthetic cationic clay [22,23], and TiO_2 [24]. Few of these studies address desorption, and none seems to address the presence of CuChl particles.

Herein we report on our efforts to characterize aqueous CuChl solutions in terms of the presence of dispersed particles. In addition, we present quartz crystal microbalance (QCM-D) measurements of CuChl binding results to model surfaces (silica, cellulose, polystyrene, and grafted pullulan). The adsorption measurements were made to give initial insights into CuChl binding to various surfaces in leaves when CuChl is applied as a crop spray. Finally, we illustrate the conditions under which some surfactant solutions can remove CuChl adsorbed on cellulose.

2. Experimental section

2.1. Materials

Commercial-grade sodium copper chlorophyllin (CuChl) fine powder (Batch NO. S005.S00201.G0034.170207) was obtained from Organic Herb Inc., Hunan, China. The total copper content is 5.3 % as specified by the manufacturer, which is at the high end of the Sigma commercial grade specification. Authentic standard of Cu chlorin e_6 trisodium salt ($CuCe_6$), above 95 % purity, was obtained from Frontier Scientific (Logan, UT). Cysteamine hydrochloride, sodium cyanoborohydride ($NaBH_3CN$), 37 % hydrochloric acid (HCl), deuterium oxide (D_2O) and dodecyltrimethylammonium bromide (DTAB) were purchased from Sigma–Aldrich. Dimethyl sulfoxide (DMSO) and acetone were obtained from Caledon Laboratories (ON, Canada). Sodium hydroxide (NaOH) was acquired from LabChem Inc. (Zelienople, PA). 95 % ethanol was supplied by Greenfield Global Inc. (Canada). Phosphate buffered saline (PBS, 10 X liquid concentrate) and sodium dodecyl sulfate (SDS) were obtained from Bioshop Canada Inc. Food-grade pullulan was purchased from Hayashibara Co., LTD. (Japan). All chemicals were used without further purification. All water used in the experiments was deionized and further purified by an EMD Millipore Milli-Q® Advantage A10 System (Thermo Scientific).

Standard regenerated cellulose membranes (pre-wetted Spectra/Por® 6, MWCO 1 kDa, product number 132640 and Spectra/Por® 4, MWCO 12 − 14 kDa, product number 132706) were purchased from Spectrum Laboratories, US. Schleicher & Schuell® filter paper (grade 602H, diam. 125 mm) was obtained from Sigma-Aldrich. Gold, cellulose, silica and polystyrene sensors were supplied by Q-sense (Sweden). Falcon® 96-Well tissue culture treated black microplates with clear bottom were purchased from VWR.

2.2. CuChl and $CuCe_6$ stock buffer dispersions

Most experiments were performed in three buffers that were prepared from phosphate buffered saline (PBS) concentrate that was diluted to give PBS, 0.1 PBS and 0.01 PBS. CuChl buffer solutions were prepared by adding 5.0 mg of dry CuChl to 50 mL buffer in a 90 mL Leakbuster™ specimen container. The mixture was dispersed (vortexed) with a vibromixer (Mini Vortex Mixer, VWR) at 3000 rpm for 1 min. $CuCe_6$ stock buffer solutions were sonicated (Branson 3510 ultrasonic cleaner) for 3 h in an ice bath. Fresh stock solutions were prepared daily.

In an effort to remove dispersed particles, some dispersions were centrifuged with a Beckman L-80 XP) at 50,000 rpm (260,000*g*) for 30 min at 23 °C. The supernatant concentrations were typically 0.095 g/L for CuChl and 0.082 g/L for $CuCe_6$. Stock solutions that were employed directly in experiments after preparation are termed "untreated", whereas "centrifuged" solutions consisted of the supernatant after ultracentrifugation.

2.3. Composition analysis

Mass spectrometry (electrospray ionisation-ESI, Bruker maXis 4 G Q/ToF) was employed in both positive and negative ion modes to analyze the composition of CuChl. The solvent used was methanol. $CuCe_6$ was also characterized as a reference.

2.4. CuChl dialysis

20 mL of 0.1 g/L CuChl 0.1 PBS solution was placed in 29 mm diameter dialysis tubing with a MWCO of 12 − 14 kDa. The tubing was placed in a beaker containing 2 L of 0.1 PBS solution which was gently stirred with a magnetic stir bar in the dark. The external solution was replaced every 12 h and the experiment was terminated after 7 days. In parallel, a solution of CuChl in 0.1 PBS was stored in the dark for the same period. Based on the absorbance at 404 nm the CuChl concentration decreased by 15 % after 7 days, a result consistent with the literature [25].

After 7 days of dialysis, the volume of retentate, v_r, was measured with a 25 mL graduated cylinder. The CuChl concentration in the retentate, c_r, was determined by the absorbance at 404 nm after 10-fold dilution with 0.1 PBS. The biggest assumption in this analysis is that absorbance changes reflect the change in concentration of all the materials in the CuChl mixture.

2.5. Dynamic light scattering (DLS) particle size distributions

The hydrodynamic diameters of CuChl and $CuCe_6$ particles in buffer solutions were measured with a Malvern Zetasizer Nano ZS which is equipped with a He-Ne 4.0 mW laser operating at 633 nm and a detector angle of 173°. 1 mL of 0.1 g/L sample solution was put in a cuvette (four-sided clear polystyrene, 10 mm, 4.5 mL) and then equilibrated in the light scattering cell for 1 min at 23 °C. Measurements were performed in triplicate with the measurement position fixed at 4 mm, with an attenuation index of 11. The data were analyzed using Zetasizer software, version 7.01 where the CONTIN algorithm was fitted to obtain the size distribution.

2.6. NanoSight particle size distributions

Untreated or centrifuged CuChl and $CuCe_6$ stock solutions in 0.1 PBS solutions were diluted with 0.1 PBS buffer to have a final concentration of 6 mg/L. NanoSight measurements were performed with a Malvern NanoSight LM10 instrument equipped with a LM14C laser with a wavelength of 532 nm and a syringe pump (Harvard Apparatus, Catalog NO. 98-5362). Samples were injected into the chamber at a flow rate of 0.1 mL/min, captured by a CMOS camera and analyzed by NanoSight NTA 3.4 software.

2.7. UV–vis absorbance

The Infinite® M1000 (Tecan) was used to record the UV–vis absorbance of CuChl and $CuCe_6$ buffer solutions. In a typical experiment, 200 μL of 0.1 g/L sample solution was deposited into one well of the Falcon® 96-well flat-bottom tissue culture treated microplate (polystyrene, black with clear bottom) and measured with a wavelength range between 300 and 800 nm. For each sample, four replicas were measured.

2.8. Synthesis of thiolated-pullulan

Our procedures for the hydrolysis and thiolation of pullulan were based upon the literature with minor changes [26]. 5 g of pullulan was dissolved in 250 mL of water and heated to 80 °C in an oil bath. The pH was adjusted to 2 by adding 37 % HCl dropwise. The hydrolysis proceeded under reflux and magnetic stirring at 400 rpm for 72 h. Then the solution was cooled to room temperature and neutralized with 1 M NaOH to pH 7. The solution was purified by dialysis with 29 mm diameter tubing with a MWCO of 1 kDa against water for 7 days and freeze dried.

0.8 g of hydrolyzed pullulan, 202.1 mg of cysteamine hydrochloride and 195.6 mg of $NaBH_3CN$ were dissolved in 50 mL of DMSO sequentially. The solution was held at 60 °C and stirred magnetically at 400 rpm for 72 h. After the solution was cooled to room temperature, 100 mL of acetone was then added to precipitate the polymer. The product was dissolved in water and dialyzed against a mixture of ethanol and water (v/v, 50/50) for 3 days and against water for 7 days, followed by freeze-drying.

2.9. Quartz crystal microbalance Adsorption/desorption (QCM-D)

Gold sensors were cleaned by UV/ozone Procleaner™(BioForce

Table 1
Some properties of CuChl and $CuCe_6$ solutions in diluted PBS buffer. ε is the molar extinction coefficient. The solubility error estimates are the standard deviation of two replicates.

Buffer Conc.	pH		ε at 404 nm (m^2/mol)		Apparent Solubility (g/L)	
	CuChl 0.1 g/L	$CuCe_6$ 0.1 g/L	CuChl	$CuCe_6$	CuChl	$CuCe_6$
0.01 PBS	7.6	6.3	3.68×10^3	3.12×10^3	0.097 ± 0.001	0.048 ± 0.001
0.1 PBS	7.3	7.0	3.44×10^3	4.56×10^3	0.095 ± 0.006	0.082 ± 0.007
PBS	7.4	7.4	3.24×10^3	3.71×10^3	0.095 ± 0.003	0.085 ± 0.002

Nanosciences) for 10 min and placed in a mixture solution of water, ammonia (25 %) and hydrogen peroxide (30 %) (v:v:v, 5:1;1) for 5 min at 75 °C. After rinsing with water, the sensors were dried with nitrogen gas and treated with UV/ozone for another 10 min. The cleaning protocol for silica sensors was similar except that they were immersed in a 2% SDS solution for 30 min at room temperature after the initial UV/ozone treatment. The polystyrene sensors were immersed in the solution of 1% Deconex 11 for 30 min at 30 °C and rinsed with water. They were kept in water for 2 h followed by the rinsing with 99 % ethanol and drying with nitrogen gas. The cellulose sensors were rinsed with water and dried with nitrogen gas. Moreover, cellulose sensors were soaked in water overnight to ensure equilibrium swelling before adsorption experiments.

Adsorption experiments were carried out with an E4 QCM-D instrument from Q-sense AB (Sweden) where the frequency and dissipation data from the third overtone were used to analyze the adsorption behaviors. All the experiments were performed with PBS buffers of different dilution factors at 23 °C. The flow rate of the solution was constant at 0.1 mL/min.

For cellulose, silica and polystyrene sensors, injections sequence was as follows: (1) a buffer feed until a stable baseline was obtained; (2) 0.1 g/L sample in buffer solution until the frequency shift was less than 1.0 Hz in 10 min; and, (3) a buffer rinse to characterize desorption. To obtain the pullulan-coated surface, 1 g/L thiolated-pullulan buffer solution was pumped through a gold QCM-D sensor followed by the three steps above.

2.10. Surfactant displacement of CuChl and $CuCe_6$ from cellulose

5 µL of 0.1 g/L CuChl or $CuCe_6$ buffer solution (0.1 PBS) was deposited on a filter paper (grade 602H, Schleicher & Schuell®) strip (5.5 × 1 cm^2) about 10 mm from the bottom and left to dry at room temperature for 2 h. The paper strip was supported vertically above a 90 mL Leakbuster™ specimen container containing surfactant in buffer solution. Upon contacting the solution, the liquid was allowed to climb to near the top of the paper, taking between 5 and 25 min. The paper strip was then removed, and allowed to dry for two hours. The location of colored CuChl after surfactant elution was obtained from images taken with a ChemiDoc™ MP imaging system (Biorad, nr. 170–8280) running Image Lab™ 4.1 software. The strips were illuminated by UV Trans for 0.1 s. The SDS concentrations were 1.6 mM, 8.2 mM, and 41 mM, whereas the DTAB concentrations were 2.8 mM, 14 mM, and 70 mM.

2.11. Atomic force microscopy (AFM)

Images of QCM-D sensor surfaces, after adsorption experiments, were recorded with an Asylum MFP-3D instrument (Asylum Research, US) in tapping mode and processed in Igor Pro 6.37 running Asylum research 13.03.17 software. The images were taken under ambient conditions using a NANOSENSORS™ Super SharpSilicon™-Non-contact/Tapping mode-High resonance Frequency (SSS-NCHR) tip with a spring constant of 49 N/m and a resonance frequency of 333 kHz in tapping mode. The length, mean width and thickness of the tip were 125, 30 and 4.3 µm respectively.

3. Results

3.1. CuChl composition

The chemical structures of relevant chlorins are shown in Fig. 1. According to the CuChl supplier (Organic Herb Inc.), the copper content was 5.3 wt%. Assuming all the copper is present as a chlorin ligand and that the predominant chlorin structure was $CuCe_4$, the copper chlorin content of our CuChl was 54 wt%. Based on mass spectra, $CuCe_6$, iso-$CuCe_4$ and Cu chlorin p_6 are the main components of our CuChl (see spectra Figs. S1, S2 and assignments Table S1 in the supporting information).

3.2. Solution properties

Measurements of CuChl and $CuCe_6$ were performed in three buffer solutions: PBS (137 mM NaCl, 2.7 mM KCl, 8 mM Na_2HPO_4, and 2 mM KH_2PO_4); PBS buffer diluted by a factor of 10 (0.1 PBS); or, in PBS diluted by a factor of 100 (0.01 PBS). Some properties of CuChl and $CuCe_6$ buffer solutions are summarized in Table 1. For many of the experiments herein, the CuChl and $CuCe_6$ concentrations were 0.1 g/L, which corresponds to 0.14 mM for pure $CuCe_6$. For undiluted PBS buffer solutions, the pH of both chlorins was 7.4. $CuCe_6$, which has 3 carboxylic groups per molecule (see Fig. 1) gave lower pH values in the diluted buffers. By contrast the CuChl mixtures showed only small pH variations with dilution.

UV-Vis spectra were obtained for CuChl and $CuCe_6$ (see Fig. S3 in the SI file) for concentrations between 0.005 and 0.02 g/L. Absorbance at 404 nm versus concentration plots were linear (Fig. S4) and the corresponding molar extinction coefficients, ε, are summarized in Table 1. The CuChl values increased somewhat with PBS dilution, the $CuCe_6$ results showed a greater variation, with the greatest value at the intermediate PBS concentration. Scuiti et al. reported $\varepsilon = 1.11 \times 10^3$ m^2 /mol for Sigma CuChl in water, only 1/3 of the values we observed in PBS [27].

We attempted to measure CuChl solubility in three buffers by adding excess CuChl, mixing, and centrifuging at 260,000*g* for 30 min. The CuChl concentration in the supernatant was determined from the UV absorbance of diluted supernatant solutions at 404 nm. The results, summarized in Table 1, show "apparent solubilities" because, as shown in the following paragraphs, dispersed nanoparticles are present in the solution phase even after aggressive centrifugation. The CuChl solubilities were independent of the extent of buffer dilution, whereas $CuCe_6$ lowered the pH of the most dilute buffer to 6.3, giving a lower solubility.

3.3. CuChl colloidal properties

The electrophoretic mobility of untreated CuChl (13 mg/L) in 0.1 PBS was -1.62 ± 0.03 × 10^{-8} m^2/V·s. This result is consistent with the presence of carboxyl groups on the structures in Fig. 1. Dynamic light scattering (DLS) and NanoSight experiments were performed to characterize dispersed particles in the CuChl buffer mixtures. Measurements were made with a Malvern Zetasizer Nano ZS whose laser has a wavelength of 633 nm, corresponding to Q band peaks in the chlorin

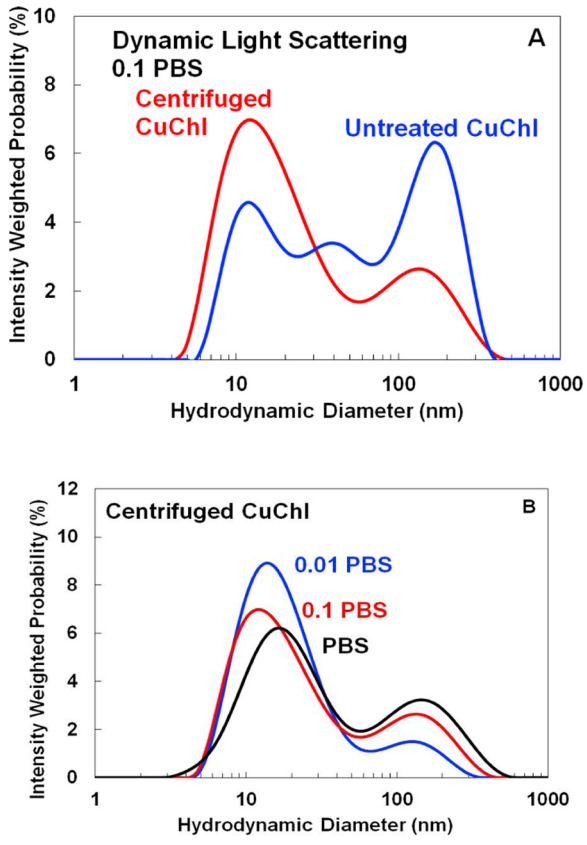

Fig. 2. Dynamic light scattering particle size distributions of 0.1 g/L CuChl solutions: A before (i.e. untreated) and after ultracentrifugation (260,000*g* for 30 min); and, B as a function of buffer dilution.

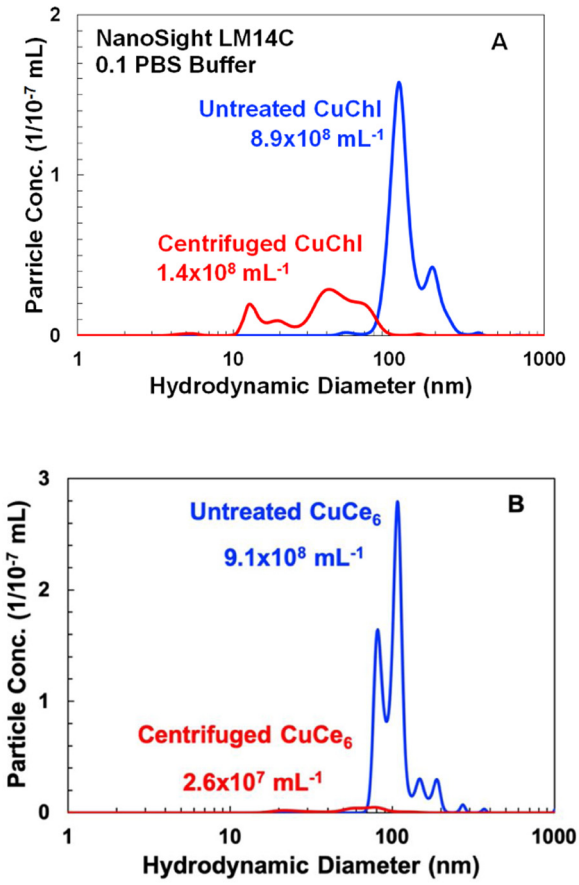

Fig. 3. NanoSight particle size distributions of 6 mg/L CuChl and CuCe6 dispersions in 0.1 PBS before and after ultracentrifugation. The numbers beside the labels are the total particle concentrations.

solution spectra (see Fig. S3). We measured freshly prepared CuChl solutions dispersions before and after centrifugation (260,000*g* for 30 min.) and the results are summarized in Fig. 2. Note, the intensity weighted particle size distribution emphasizes the larger particles, and one should be suspicious of distributions with multiple peaks [28]. We interpret the untreated result as a broad distribution between 10 and 800 nm. After centrifugation, the CONTIN fits showed two populations (see Fig. 2A), one with a peak around 20 nm and the other around 160 nm. The presence of large particles was surprising in view of the aggressive ultracentrifugation. Either the density of particles was very close to the supporting buffer or new aggregates formed quickly after centrifugation. Fig. 2B shows the fraction of larger particles increased with increasing ionic strength (i.e. less buffer dilution).

The Zetasizer software could not generate CONTIN fits for any of the $CuCe_6$ samples to give particle size distributions, possibly because of the absorption of the laser light by the green chlorins. However, identical instrument settings were used for all DLS experiments, facilitating comparisons of the mean count rates of back-scattered light. DLS count rates are normally a sensitive measure of turbidity. However, in these experiments the scattered intensity will be attenuated by light absorbance by both soluble and dispersed species. Table 2 summarizes the results. Both CuChl and $CuCe_6$ showed substantial decreases in count rates as a result of centrifugation, further likely due to the removal of dispersed particles. Comparing the particle-free buffer results with the centrifuged $CuCe_6$, there was no indication of particles in centrifuged PBS or in 0.1 PBS. Whereas in 0.01 PBS, the count rate was high, suggesting particles were forming at pH 6.3 with the diluted buffer.

Table 2
Dynamic light scattering mean count rates (kilo-counts per second).

Buffer Concentration	Buffer	CuChl (0.1 g/L) Untreated	CuChl (0.1 g/L) Centrifuged	$CuCe_6$ (0.1 g/L) Untreated	$CuCe_6$ (0.1 g/L) Centrifuged
0.01 PBS	32	95	51	838	130
0.1 PBS	32	96	64	128	45
PBS	28	201	90	119	33

CuChl and $CuCe_6$ dispersions in PBS were also characterized by NanoSight measurements. This instrument tracks individual particles and estimates the diameter from the observed diffusion coefficients. Centrifugation removed the larger particles from CuChl, whereas the concentration of smaller particles increased. By contrast centrifugation removed virtually all of the $CuCe_6$ particles.

Given that the total particle concentration in untreated CuChl is 8.9×10^8 mL^{-1} (see Fig. 3) and the mean particle diameter is 148 nm, the corresponding mass concentration can be calculated assuming the density of CuChl in the particles. If we assume a density of 1 g/mL, the particles represent 25 % of the total CuChl concentration – this should be an overestimate as it does not account for the water content of the particles.

3.4. Dialysis of CuChl dispersions

Further evidence for particles in the CuChl solutions came from dialysis experiments. Following the lead of Salin et al., [13] 0.1 g/L CuChl solution was exhaustively dialyzed through a 12–14 kDa membrane and only 42 wt% of the CuChl passed through the membrane. Following the same procedures, 86 % of the $CuCe_6$ passed through the membrane. Taken as a whole, the above results suggest that CuChl in PBS buffer is present as both soluble and dispersed particles. Furthermore, the colloidal fraction of CuChl does not dissolve in buffer with

dilution or dialysis. $CuCe_6$ is essentially particle-free at higher pH values after centrifugation.

3.5. CuChl adsorption on polystyrene

Our ultimate interests involve understanding the transport of CuChl and related chlorins into plants. Because transport is slowed by tendency of CuChl to adsorb on surfaces, the goal of the following studies was to determine the binding tendencies of the CuChl mixtures on 4 surfaces - grafted pullulan, silica, crystalline cellulose, and polystyrene. The measurements were made with a quartz crystal microbalance (QCM-D) instrument. All the QCM-D sensor surfaces, except the pullulan coated ones, were purchased from Q-Sense. The pullulan surface was prepared by treating a gold coated sensor with thiolated pullulan.

We first focus on CuChl adsorption onto the polystyrene, the most hydrophobic of the 4 surfaces. The QCM-D experiments involved the continuous flow of aqueous solution over the polystyrene coated quartz sensor in three sequential stages: 1) initial equilibration with buffer; 2) exposure to CuChl solution; and, 3) rinsing with buffer. Each experiment generates two curves, one is the change in frequency (Δf_3) versus elution time and the other corresponds to the dissipation (ΔD). The Δf_3 values are the frequencies minus the initial frequency. The subscript 3 denotes the data were based on the third overtone. Many examples of the dissipation curves are given in supporting information.

Fig. 4A shows QCM-D Δf_3 curves for untreated and centrifuged of CuChl on polystyrene. For both samples, the addition of CuChl resulted in an initial rapid increase in the absolute value of Δf_3, leveling to a steady-state value. The negative sign corresponds to an increase in mass on the sensor surface. When the rate of change of Δf_3 was < 1 Hz in 10 min, the instrument switched from flowing CuChl solution to the buffer rinse. Initially rinsing gave a rapid decrease in adsorption, (i.e.

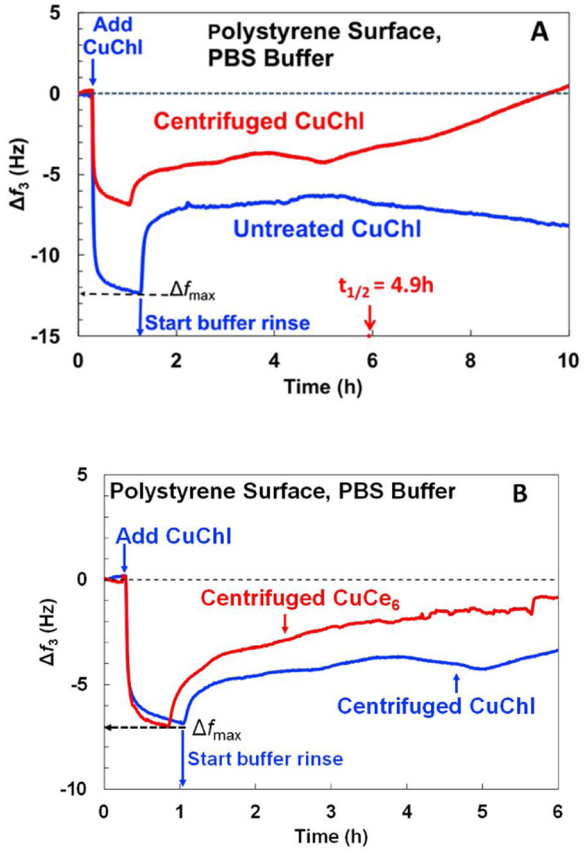

Fig. 4. The adsorption of CuChl 0.1 g/L and $CuCe_6$ 0.1 g/L in PBS (pH 7.4) onto polystyrene QCM-D sensor surfaces.

Δf_3 became less negative). However, after the initial phase of rinsing the centrifuged sample show a slow, continual desorption.

Two values were extracted from the Δf_3 curves: Δf_{max} the maximum negative value of Δf_3 before rinsing; and, $t_{½}$ the rinsing time required for Δf_3 to decrease to 0.5 Δf_{max}. $t_{½}$ is a measure of the desorption/dissolution rate, the lower $t_{½}$ the faster was the CuChl removal from the surface. Δf_{max} is a measure of the surface adsorption capacity. The adsorption of CuChl on polystyrene was repeated three times over a year, serving as a measure of reproducibility. The resulting Δf_{max} values were -9.2, -11.4, and -12.1 Hz – the latter value corresponds to the curve in Fig. 4. Δf_3 versus elution time curves of the three replicates are compared in Fig. S5.

Fig. 4A shows that centrifugation of the CuChl dispersion impacts the QCM-D binding curves. The untreated (i.e. not centrifuged) CuChl dispersion gave a large Δf_{max} and a $t_{½} = 19.3$ h (beyond the plotted range in Fig. 4, see the extended data in Fig. S6). However much of the bound material was quickly removed when the CuChl feed was replaced by rinsing buffer. By contrast, the centrifuged CuChl dispersion gave a smaller Δf_{max}, and with a $t_{½} = 4.9$ h, indicating the desorption was much faster compared to the untreated CuChl. Therefore whether centrifuged or not, CuChl adsorption on polystyrene was reversible.

Fig. 4B compares the adsorption characteristics of centrifuged pure $CuCe_6$ with the centrifuged commercial CuChl mixture. The adsorption capacities, Δf_{max}, values of the two curves were equal within experimental uncertainty. This is indirect support for the suggestion that although CuChl is a complex mixture in which ~50 % of the material is unidentified, the main adsorbing species from CuChl are the chlorins, not the other components.

To further elucidate the nature of the CuChl adsorbed layer on polystyrene, we used atomic force microscopy (AFM) to examine the dry QCM-D sensor surfaces after the adsorption/desorption experiments. The top row of images in Fig. 5 shows the dry polystyrene sensor surface removed before the buffer rinsing would normally commence – the conditions corresponding to Δf_{max}. The surface is covered with particles with a broad particle size distribution. In the middle row, the very large particles, seen in the top row image, are gone leaving mainly nm scale particles more akin to the particle size distributions shown in Fig. 2. The AFM image of a cleaned, unused polystyrene sensor showed no particles and is shown in Fig. S7.

The bottom images in Fig. 5 show a polystyrene surface after adsorption of $CuCe_6$. In spite of the high purity of the chlorin, and having been centrifuged, there are many particles in the $CuCe_6$ adsorbed layer. Recall that the NanoSight measurements in Fig. 3B gave a total nanoparticle concentration of 2.6×10^7 mL^{-1}.

3.6. Comparing CuChl and $CuCe_6$ adsorption on cellulose and polystyrene

CuChl adsorbs onto cellulose surfaces, hence the interest in CuChl as a textile dye. Fig. 6 shows QCM-D curves for centrifuged CuChl and $CuCe_6$ adsorption on cellulose from PBS buffer. In both cases buffer rinsing removed weakly bound material, however, the remaining adsorbed material did not desorb. More CuChl adsorbed on cellulose compared to $CuCe_6$. This is in contrast to the corresponding behavior on polystyrene (see Fig. 4B) where both chlorins gave the same amount of adsorption.

Table 3 compares QCM-D adsorption results for CuChl with $CuCe_6$, on the two surfaces with two buffer concentrations. Because for all of our results, $\Delta D/\Delta f_3 < 1\,0^{-7}$ s [29] we applied the Sauerbrey equation to convert Δf_{max} values to mass coverage Γ_{max} (mg/m^2). The main observations from Table 3 are: 1) CuChl and $CuCe_6$ give very similar adsorption (Γ_{max}) values in spite of CuChl being a crude mixture including particles; 2) only a small fraction of adsorbed material was removed with buffer rinsing from cellulose; and 3) PBS solutions always gave more adsorption than 0.1 PBS solutions.

The Γ_{max} values in Table 3 span the range 1.09–3.48 mg/m^2; are these values reasonable? Assuming $CuCe_6$ as representative of CuChl,

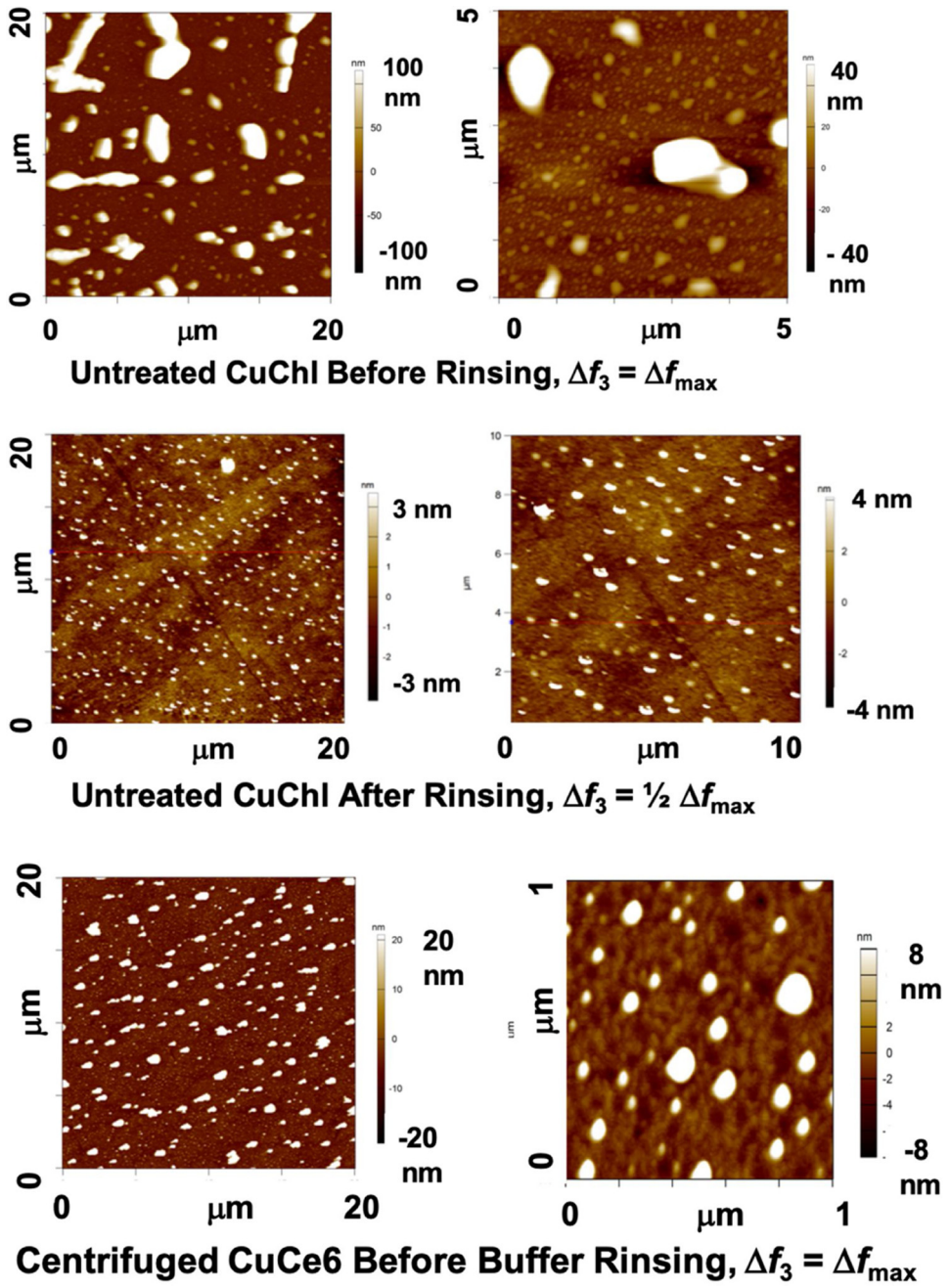

Fig. 5. Atomic force microscopy images polystyrene of dried QCM-D surfaces after exposure to untreated 0.1 g/L chlorin dispersion in PBS.

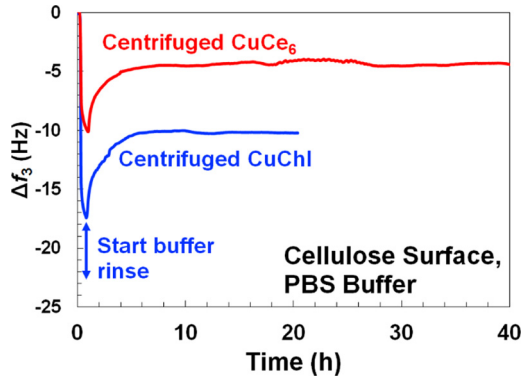

Fig. 6. The adsorption of centrifuged CuChl and $CuCe_6$ on cellulose in PBS buffer, pH 7.4.

Table 3
Summary of QCM-D results for untreated CuChl and untreated $CuCe_6$ adsorption on polystyrene and crystalline cellulose. Γ_{max} is the maximum coverage adsorbed chlorin before the buffer rinse and $t_{1/2}$ is the buffer rinsing time required to remove ½ of adsorbed material, $\Gamma_{max}/2$.

		Buffer	$\Delta D_3/\ \Delta f_{max}$ (10^{-7} s)	Γ_{max} (mg/m^2)	$t_{1/2}$ (h)
Cellulose	CuChl	0.1 PBS	0.7	1.60	> 18.4
		PBS	0.5	2.92	> 0.5
	$CuCe_6$	0.1 PBS	1.0	1.57	12.0
		PBS	0.6	2.67	> 19.9
Polystyrene	CuChl	0.1 PBS	0.4	1.09	0.2
		PBS	0.3	2.16	18.0
	$CuCe_6$	0.1 PBS	0.3	2.05	0.08
		PBS	0.2	3.48	3.5

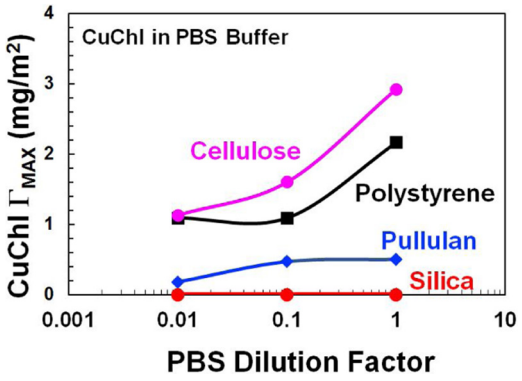

Fig. 7. The maximum density of adsorbed untreated CuChl (Γ_{max}) on four surfaces as functions of the PBS dilution factor. The pH values resulting from buffer dilution were: 7.4 for DF = 1, 7.3 for DF = 0.1; and, 7.6 for DF = 0.01.

the projected area of a single molecule lying flat on a surface was estimated to be 1.8 nm^2 using the software Avogadro. If the surface is fully covered with a monolayer of $CuCe_6$ lying flat, the corresponding mass coverage is Γ_{max} = 0.66 mg/m^2. Since no surface is completely covered, a more reasonable estimate for an adsorbed layer of individual chlorin molecules is Γ_{max} = 0.5 mg/m^2. The experimental values in Table 3 are up to 5 times greater than this estimate. Clearly the particles observed in the AFM images in Fig. 5 contribute to the adsorbed mass.

3.7. Comparing CuChl adsorption on four model surfaces

Fig. 7 summarizes the CuChl maximum adsorption values (Δf_{max}) o n the four model surfaces. Cellulose and polystyrene adsorbed the most CuChl, whereas there was no adsorption on silica, and very little on pullulan. Adsorption increased with PBS concentration on cellulose and polystyrene. The corresponding QCM-D plots are in Fig. S6 - polystyrene, Fig. S8 – cellulose, Fig. S9 – pullulan, and Fig. S10 – silica. The lack of adsorption on silica could be explained by electrostatic repulsion. The electrophoretic mobility of CuChl particles was $-1.62 \pm 0.03 \times 10^{-8}$ $m^2/V{\cdot}s$, giving repulsive interactions with negatively charged silica at neutral pH.

3.8. Removal of adsorbed CuChl with surfactants

The application of CuChl in formulated products is likely to include surfactants which could influence both the adsorption and removal of CuChl from surfaces. We deposited drops of CuChl dispersions on strips of filter paper and, after drying, we dipped the end of the filter paper into solutions of sodium dodecyl sulfate (SDS) or dodecyl trimethyl ammonium bromide (DTAB) in PBS buffer. In what is essentially a paper chromatography experiment, the surfactant solution moves up the paper strip by the capillary driven flow. The adsorbed CuChl did not move with surfactant-free buffer or with surfactant solutions below the critical micelle concentration (CMC) of either surfactant. At concentrations above their CMCs, both SDS and DTAB transported the CuChl up the paper. Fig. 8 shows a typical set of photographs. The white line zones at the top correspond to the final positions of the elution fronts. Only the high DTAB concentration removed the CuChl deposit from the bottom of the strip. Presumably the CuChl is solubilized in the surfactant micelles. Others have shown that Cu chlorophyll (i.e. no CuChl) binds to nonionic surfactant micelles. [17]

4. Conclusions

Based on the copper content, our commercial grade CuChl is mixture of about 54 wt% copper chlorins plus 46 % other materials, presumably from the degradative processing of chlorophyll. Dialysis results suggested that 58 % of CuChl is present as dispersed particles compared

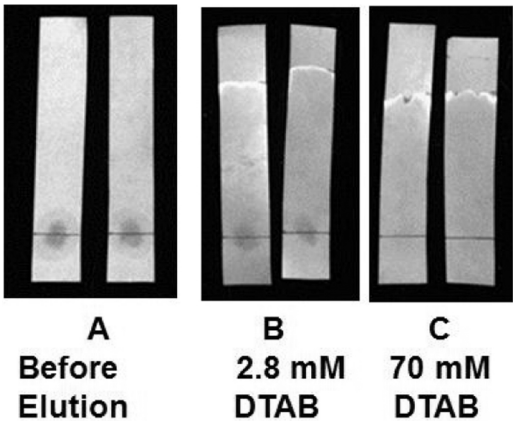

Fig. 8. Dried, 1 cm wide filter paper strips: A) CuChl spotted and dried on filter paper; B) after elution with DTAB 0.2 times CMC in water; and, C) after elution with DTAB 5 times the CMC in water. Photographs made by a ChemiDoc™ MP imaging system with the UV transilluminator illumination. The horizontal pencil lines indicate the location of the CuChl spotting.

to 14 % for $CuCe_6$. The dispersed particles are colloidally stable and do not dissolve when diluted in PBS buffer. DLS and NanoSight results suggest a broad distribution of sizes between 10 and 800 nm. Many of the larger particles could be removed by ultracentrifugation leaving approximately 20 nm aggregates as the dominant particle size. Publications describing commercial CuChl from other sources gave similar descriptions [13–15]. The adsorption studies of CuChl and $CuCe_6$ on various surfaces can be summarized as follows:

1 Aqueous CuChl adsorbs on surfaces giving a maximum adsorbed coverage, Γmax, that is sensitive to the type of surface, cellulose > polystyrene > > pullulan. No adsorption was observed on silica.
2 Centrifuged pure $CuCe_6$ showed essentially the same adsorption behaviors as centrifuged CuChl mixtures on polystyrene, suggesting that chlorins are dominant adsorbed species from CuChl mixtures on hydrophobic surfaces.
3 Centrifuged CuChl and $CuCe_6$ usually gave lower Γmax values compared to non-centrifuged samples reflecting the contribution of nanoparticles.
4 In all cases, rinsing with buffer after CuChl or $CuCe_6$ adsorption resulted in the immediate removal of some of the adsorbed material. With cellulose, there was no further dissolution, whereas with polystyrene, the adsorbed layer eventually was entirely removed.
5 The surfactants SDS or DTAB could displace CuChl adsorbed on cellulosic filter paper only if the surfactant concentrations were above the critical micelle concentration.

CRediT authorship contribution statement

Fengyan Wang: Writing - original draft, Methodology, Investigation. **Yuichi Terazono:** Writing - review & editing. **Jun Liu:** Writing - review & editing. **Michael Fefer:** Writing - review & editing, Funding acquisition. **Robert H. Pelton:** Conceptualization, Supervision, Writing - review & editing, Project administration.

Declaration of Competing Interest

The authors report no conflicts of interest.

Acknowledgments

We thank the National Sciences and Engineering Research Council of Canada (NSERC) and Suncor Energy for funding this project. Most of

the experiments were conducted at the McMaster Biointerfaces Institute, funded by the Canadian Foundation for Innovation. R. H. Pelton holds the Canada Research Chair in Interfacial Technologies. Carla Abarca, Dong Yang and Wenzi Ckurshumova are thanked for useful discussion and Xiao Wu, Elina Niinivaara, and Daniel Osorio for help with the AFM measurements.

Appendix A. Supplementary data

Supplementary material related to this article can be found, in the online version, at doi:https://doi.org/10.1016/j.colsurfa.2020.124578.

References

[1] T. Tumolo, U.M. Lanfer-Marquez, Copper chlorophyllin: a food colorant with bioactive properties? Food Res. Int. 46 (2012) 451–459.
[2] I. Viera, A. Pérez-Gálvez, M. Roca, Green natural colorants, Molecules 24 (2019) 154.
[3] S. Nagini, F. Palitti, A.T. Natarajan, Chemopreventive potential of chlorophyllin: a review of the mechanisms of action and molecular targets, Nutr. Cancer 67 (2015) 203–211.
[4] D. Cannella, K.B. Möllers, N.U. Frigaard, P.E. Jensen, M.J. Bjerrum, K.S. Johansen, C. Felby, Light-driven oxidation of polysaccharides by photosynthetic pigments and a metalloenzyme, Nat. Commun. 7 (2016) 11134.
[5] A.A. Ryan, M.O. Senge, How green is green chemistry? Chlorophylls as a bioresource from biorefineries and their commercial potential in medicine and photovoltaics, Photochem. Photobiol. Sci. 14 (2015) 638–660.
[6] M. Glueck, C. Hamminger, M. Fefer, J. Liu, K. Plaetzer, Save the crop: photodynamic inactivation of plant pathogens I: bacteria, Photochem. Photobiol. Sci. 18 (2019) 1700–1708.
[7] H. Inoue, H. Yamashita, K. Furuya, Y. Nonomura, N. Yoshioka, S. Lib, Determination of copper (II) chlorophyllin by reversed-phase high-performance liquid chromatography, J. Chromatogr. A 679 (1994) 99–104.
[8] S. Chernomorsky, R. Rancourt, K. Virdi, A. Segelman, R.D. Poretz, Antimutagenicity, cytotoxicity and composition of chlorophyllin copper complex, Cancer Lett. 120 (1997) 141–147.
[9] M.G. Ferruzzi, M.L. Failla, S.J. Schwartz, Sodium copper chlorophyllin: in vitro digestive stability and accumulation by Caco-2 human intestinal cells, J. Agric. Food Chem. 50 (2002) 2173–2179.
[10] A. Mortensen, A. Geppel, Hplc–Ms analysis of the green food colorant sodium copper chlorophyllin, innovative food sci, Emerging Technol. 8 (2007) 419–425.
[11] R.H. Dashwood, The Importance of Using Pure Chemicals In (Anti) Mutagenicity Studies: Chlorophyllin as a Case In Point, Mutation Research, Fundamental and Molecular Mechanisms of Mutagenesis vol. 381, (1997), pp. 283–286.
[12] M.J. Scotter, L. Castle, D. Roberts, Method development and hplc analysis of retail foods and beverages for copper chlorophyll (E141[I]) and chlorophyllin (E141[Ii]) food colouring materials, Food Addit. Contam. 22 (2005) 1163–1175.
[13] M.L. Salin, L.M. Alvarez, B.C. Lynn, B. Habulihaz, A.W. Fountain iii, Photooxidative bleaching of chlorophyllin, Free Radic. Res. Commun. 31 (1999) 97–105.
[14] M.E. Aydin, A.A.M. Farag, M. Abdel-Rafea, A.H. Ammar, F. Yakuphanoglu, Device characterization of organic nanostructure based on sodium copper chlorophyllin (Scc), Synth. Met. 161 (2012) 2700–2707.
[15] M.J. Selig, S. Gamaleldin, G.B. Celli, M.A. Marchuk, D.-M. Smilgies, A. Abbaspourrad, The stabilization of food grade copper-chlorophyllin in low pH solutions through association with anionic polysaccharides, Food Hydrocoll. (2019) 105255.
[16] B. Čunderlíková, L. Gangeskar, J. Moan, Acid–base properties of chlorin E6: relation to cellular uptake, J. Photochem. Photobiol. B 53 (1999) 81–90.
[17] A.P. Gerola, T.M. Tsubone, A. Santana, H.P.M. de Oliveira, N. Hioka, W. Caetano, Properties of chlorophyll and derivatives in homogeneous and microheterogeneous systems, J. Phys. Chem. B 115 (2011) 7364–7373.
[18] J. Xia, L. Ni, J. Han, Y. Wang, Y. Li, Y. Li, Y. Tian, Simultaneous aqueous two-phase flotation of sodium chlorophyllin and removal of sugars from saponified solution of bamboo leaves, Chem. Eng. Process. Process. Intensif. 101 (2016) 41–49.
[19] Shahid-ul-Islam, G. Sun, Thermodynamics, Kinetics, and Multifunctional Finishing of Textile Materials with Colorants Extracted from Natural Renewable Sources, ACS Sustainable Chem. Eng. 5 (2017) 7451–7466.
[20] X. Hou, R. Yang, H. Xu, Y. Yang, Adsorption kinetic and thermodynamic studies of silk dyed with sodium copper chlorophyllin, Ind. Eng. Chem. Res. 51 (2012) 8341–8347.
[21] S.J. Park, Y.M. Park, Eco-dyeing and antimicrobial properties of chlorophyllin copper complex extracted from Sasa veitchii, Fibers Polym. 11 (2010) 357–362.
[22] A. Sommer, A. Romero, G. Fetter, E. Palomares, P. Bosch, Exploring and tuning the Anchorage of chlorophyllin molecules on anionic clays, Catal. Today 212 (2013) 186–193.
[23] G. Rocha Oliveira, L.J. Dias Do Amaral, M. Giovanela, J. Da Silva Crespo, G. Fetter, J.A. Rivera, A. Sampieri, P. Bosch, Bactericidal performance of chlorophyllin-copper hydrotalcite compounds, Water Air Soil Pollut. 226 (2015) 226–316.
[24] K. Siwińska-Ciesielczyk, O. Bartlewicz, P. Bartczak, A. Piasecki, T. Jesionowski, Functional titania–Silica/Chlorophyllin hybrids: design, fabrication, comprehensive physicochemical characteristic and photocatalytic test, Adsorption (2019) 1–15.
[25] M.G. Ferruzzi, S.J. Schwartz, Thermal degradation of commercial grade sodium copper chlorophyllin, J. Agric. Food Chem. 53 (2005) 7098–7102.
[26] J. Hoypierres, V. Dulong, C. Rihouey, S. Alexandre, L. Picton, P. Thébault, Two methods for one-point anchoring of a linear polysaccharide on a gold surface, Langmuir 31 (2015) 254–261.
[27] L.F. Sciuti, L.H.Z. Cocca, A.R.L. Caires, P.J. Gonçalves, L. de Boni, Picosecond dynamic of aqueous sodium-copper chlorophyllin solution: an excited state absorption study, Chem. Phys. Lett. 706 (2018) 652–657.
[28] Malvern, Dynamic light scattering: an introduction in 30 minutes, Technical Note Malvern, (2012), pp. 1–8 MRK656-01.
[29] I. Reviakine, D. Johannsmann, R.P. Richter, Hearing what you cannot see and visualizing what you hear: interpreting quartz crystal microbalance data from solvated interfaces, Anal. Chem. 83 (2011) 8838–8848.

Supporting Information

Adsorption of Aqueous Copper Chlorophyllin Mixtures on Model Surfaces

Fengyan Wang, [a] Yuichi Terazono,[b] Jun Liu, [b] Michael Fefer,[b] and Robert H. Pelton*[a]

[a] Department of Chemical Engineering, McMaster University, 1280 Main Street West, Hamilton, ON L8S 4L7, Canada

[b] Suncor AgroScience, 2489 North Sheridan Way, Mississauga, ON L5K 1A8, Canada

*Corresponding author: peltonrh@mcmaster.ca

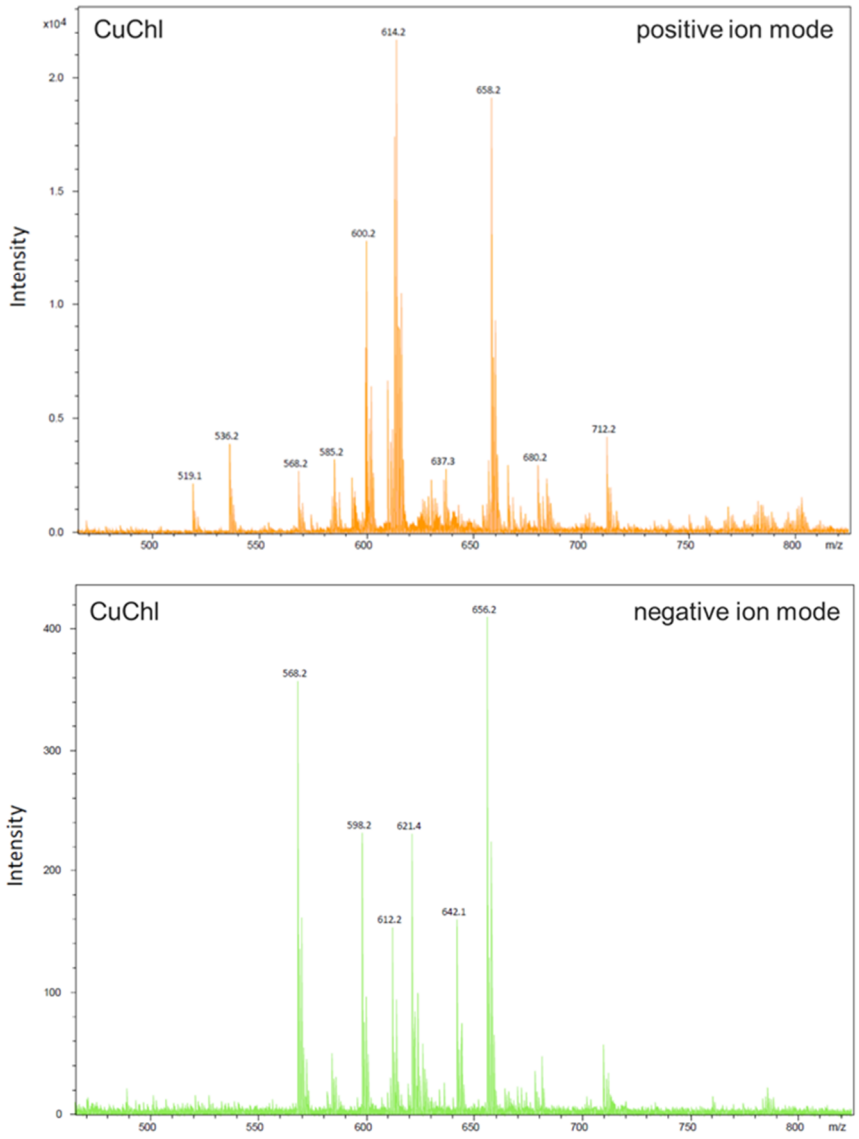

Figure S1 CuChl mass spectra.

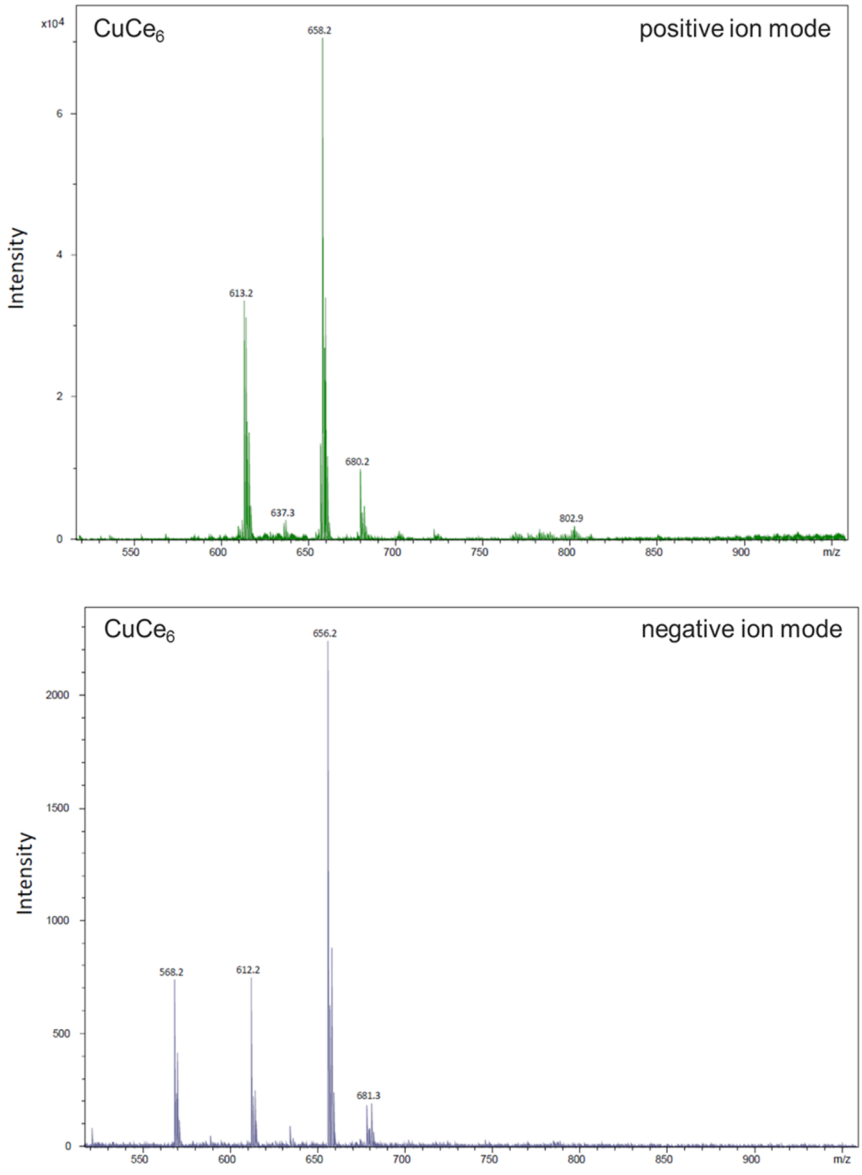

Figure S2 $CuCe_6$ mass spectra.

Table S1 Mass spectrometric data and assignments of the major components in CuChl.

ESI-MS	m/z	Assignment
Positive ion mode	658.2, 614.2	$CuCe_6$
	614.2	iso-$CuCe_4$
	600.2	Cu chlorin p_6
Negative ion mode	656.2, 612.2, 568.2	$CuCe_6$
	642.1, 598.2	Cu chlorin p_6
	612.2, 568.2	iso-$CuCe_4$

Figure S3 compares the UV-Vis spectra of CuChl and $CuCe_6$ in three buffer solutions. The CuChl spectra were rather insensitive to buffer dilution, whereas the $CuCe_6$ showed greater changes with buffer dilution. Porphyrins and chlorins are known to form aggregates in aqueous solutions and aggregation and precipitation are promoted by lowering pH and increasing ionic strength. Furthermore, the aggregates have a lower extinction coefficient compared to dissolved chlorins. When diluting buffers, the pH drops with $CuCe_6$, promoting aggregation, whereas the ionic strength decreases, promoting solubility.

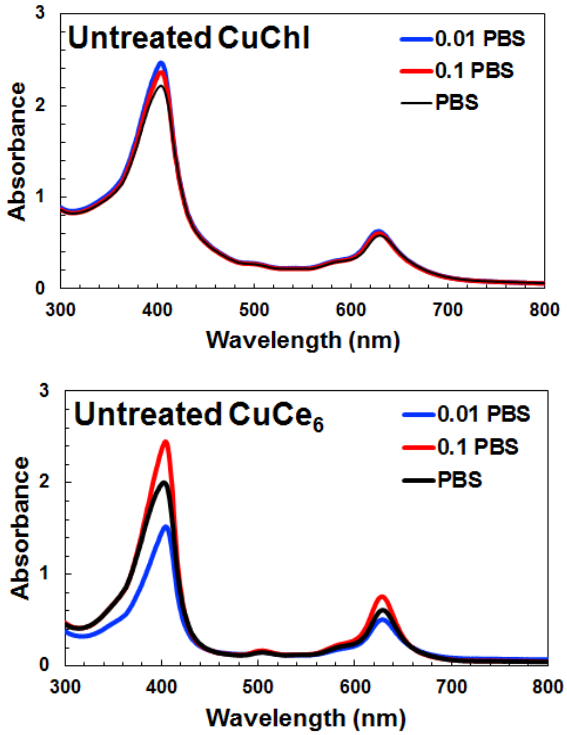

Figure S3 UV-Vis spectra for 0.1 g/L CuChl and $CuCe_6$

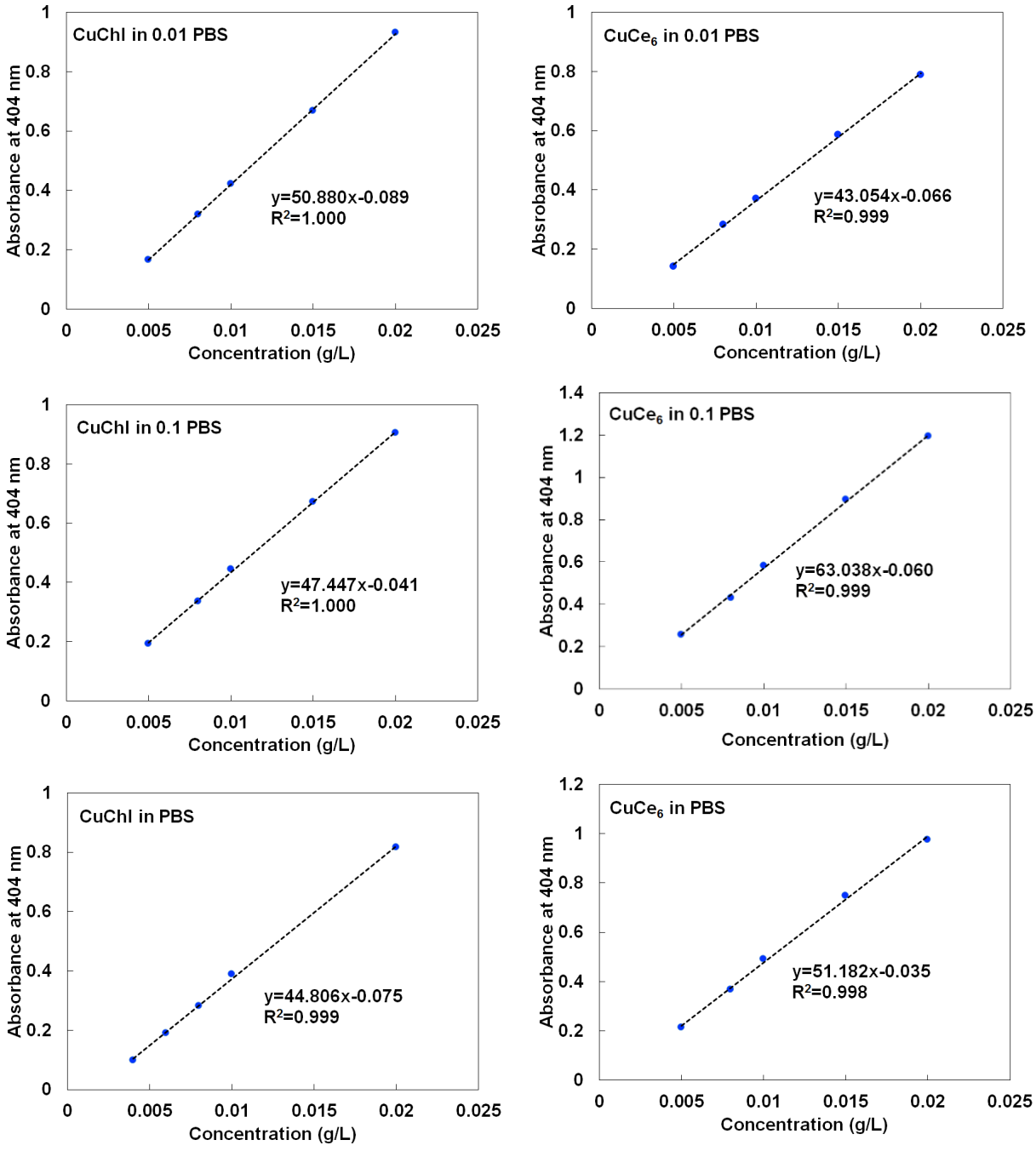

Figure S4 Calibration curves of CuChl and $CuCe_6$ in PBS solutions.

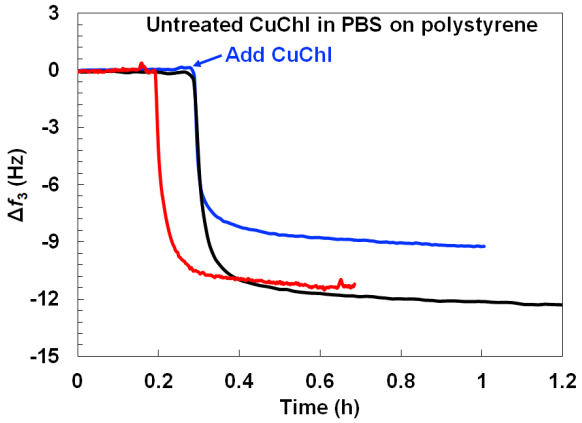

Figure S5 Δf_3 (ΔD_3) versus time for QCM-D studies of polystyrene exposed to 0.1 g/L CuChl PBS buffer solutions (reproducibility).

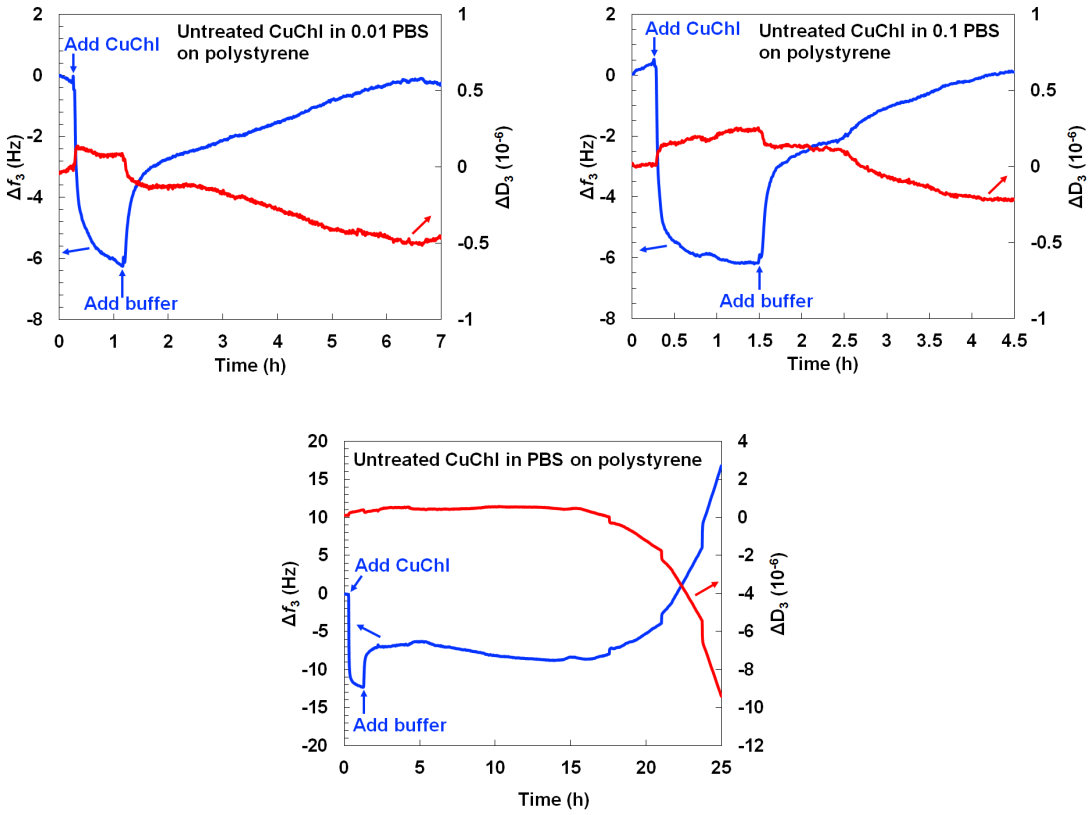

Figure S6 Δf_3 (ΔD_3) versus time for QCM-D studies of polystyrene exposed to 0.1 g/L CuChl PBS buffer solutions.

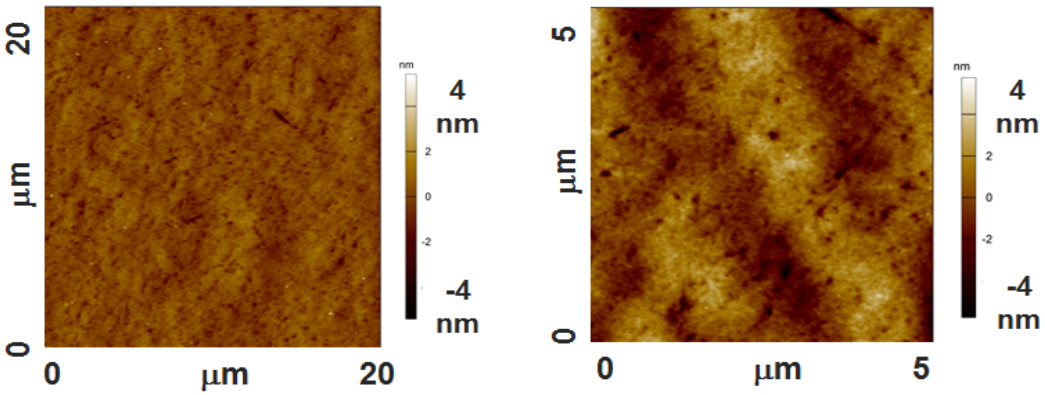

Figure S7 Atomic force microscopy images of a cleaned polystyrene QCM-D sensor.

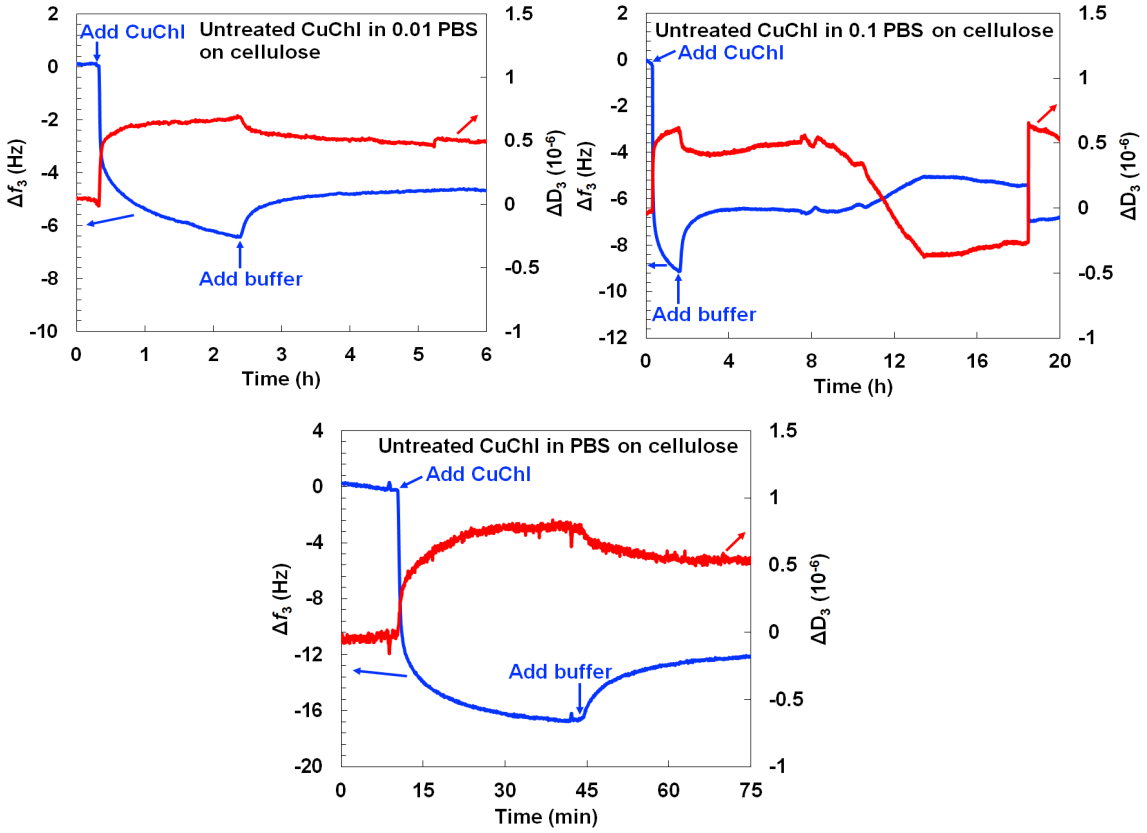

Figure S8 Δf_3 (ΔD_3) versus time for QCM-D studies of cellulose exposed to 0.1 g/L CuChl PBS buffer solutions.

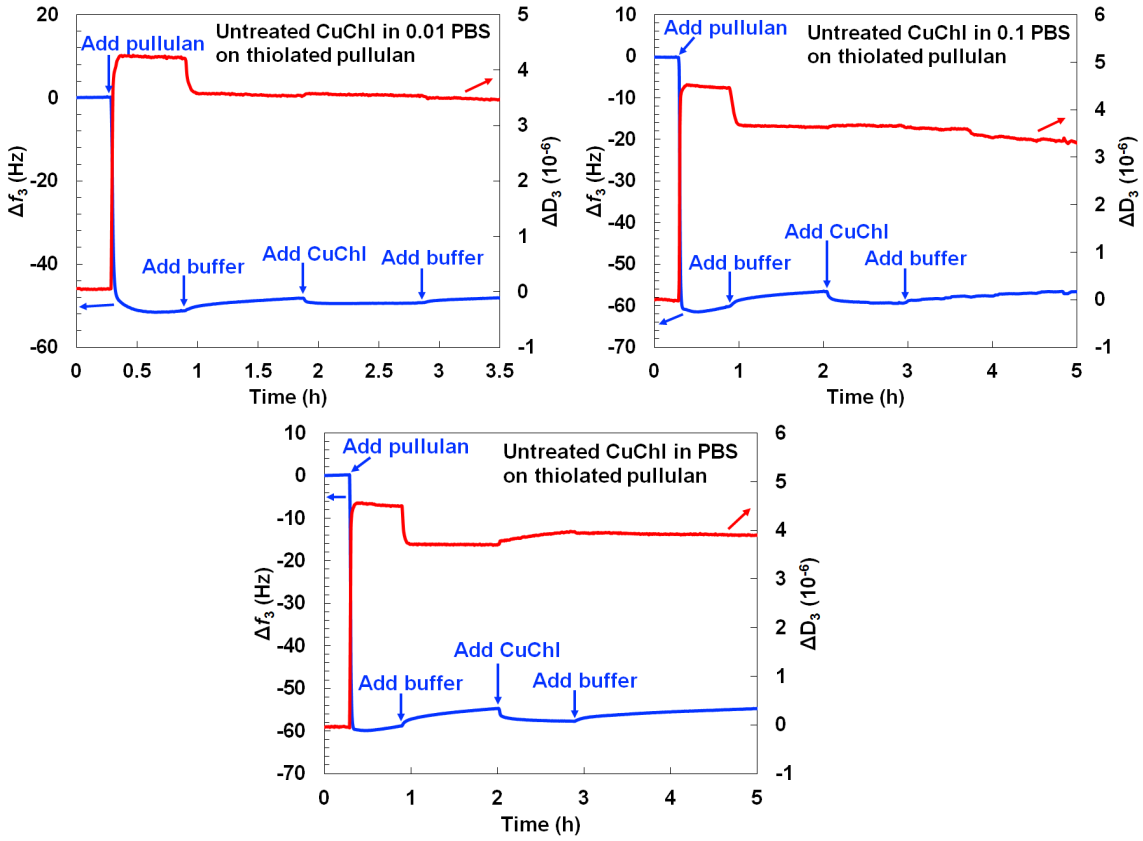

Figure S9 Δf_3 (ΔD_3) versus time for QCM-D studies of thiolated-pullulan exposed to 0.1 g/L CuChl PBS buffer solutions.

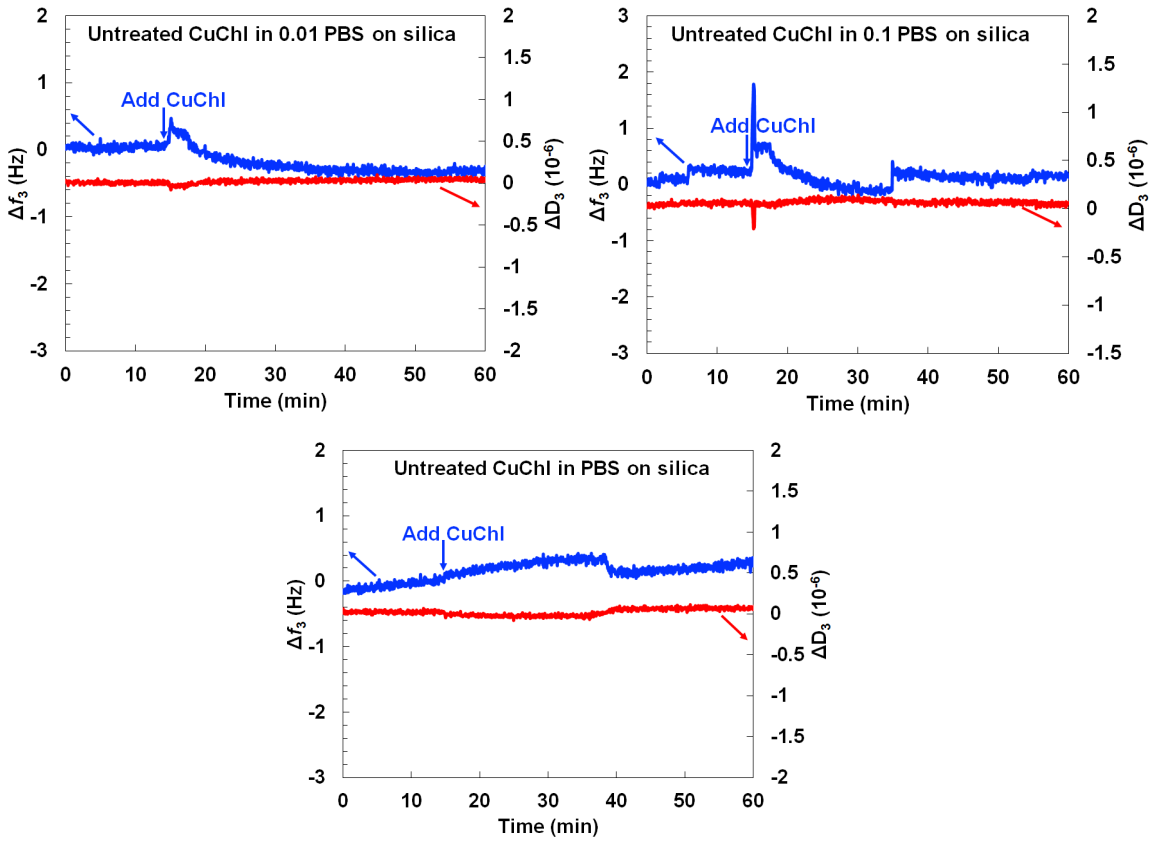

Figure S10 Δf_3 (ΔD_3) versus time for QCM-D studies of silica exposed to 0.1 g/L CuChl PBS buffer solutions.

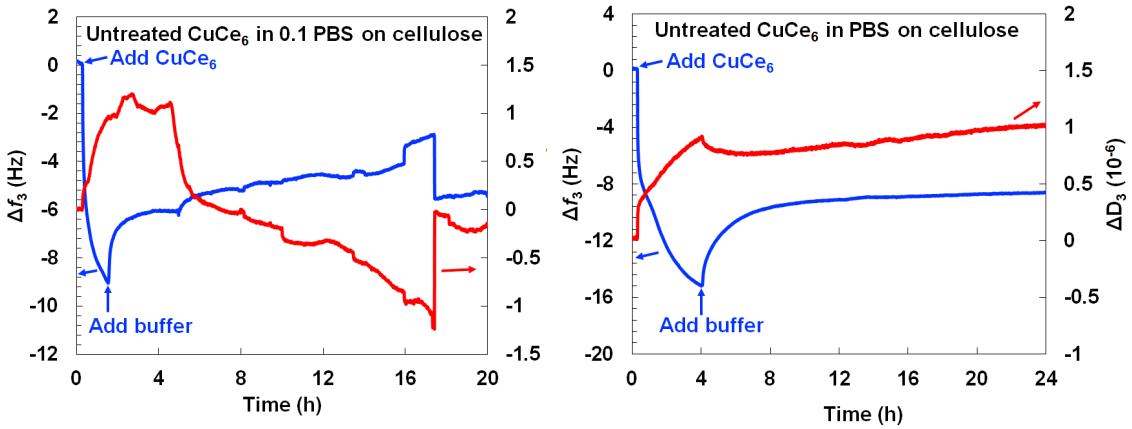

Figure S11 Δf_3 (ΔD_3) versus time for QCM-D studies of polystyrene exposed to 0.1 g/L $CuCe_6$ PBS buffer solutions.

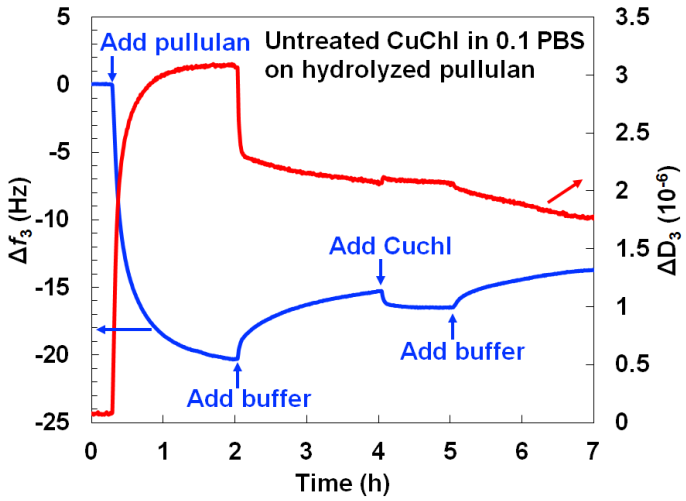

Figure S12 Δf_3 (ΔD_3) versus time for QCM-D studies of hydrolyzed-pullulan exposed to 0.1 g/L CuChl 0.1 PBS buffer solution.

Chapter 3

Release of Copper Chlorophyllin From Deposits on Hydrophobic Surfaces

To enhance CuChl's poor intrinsic rainfastness performance, a polymer combination of CMC and PAE is proposed as a spray adjuvant to immobilize CuChl onto hydrophobic surfaces in this chapter. To demonstrate this, the release behaviors of CuChl from dried deposits are quantified and compared with those of a water-soluble dye, BSF. In addition, explanations are presented for the markedly different release behaviors between CuChl and BSF.

The experiment design and data collection were done by myself. Dr. Ckurshumova, Dr. Liu and Dr. Fefer reviewed the paper and provided useful comments. I wrote the draft and Dr. Pelton helped revise it to the final version.

This chapter is in preparation for publication.

Controlling the Release of Copper Chlorophyllin From Crop Spray Deposits on Hydrophobic Surfaces

Fengyan Wang, [a] Wenzi Ckurshumova, [b] Jun Liu, [b] Michael Fefer, [b] Robert H. Pelton*[a]

[a] Department of Chemical Engineering, McMaster University, 1280 Main Street West, Hamilton, ON, L8S 4L7, Canada

[b] Suncor AgroScience, 2489 North Sheridan Way, Mississauga, ON L5K 1A8, Canada

*Corresponding author: peltonrh@mcmaster.ca

Key Words: copper chlorophyllin, rainfastness, crop spray

Abstract

The chlorophyll derivative copper chlorophyllin (CuChl) and related chlorins have promise as environmentally friendly agricultural chemicals, however, spray application is hindered by the propensity to be washed off of leaf surfaces during rain or irrigation. This work evaluates polyelectrolyte complexes formed between anionic carboxymethyl cellulose (CMC) and cationic polyamidoamine-epichlorohydrin (PAE) as adjuvants for controlling the release of CuChl from dried sessile drops on parafilm, a physical model for crop spray drop deposits on hydrophobic leaf surfaces. When a dried CMC:PAE deposit containing CuChl is immersed in the buffer, there is an immediate (burst) release of some CuChl whereas the remainder is immobilized on the parafilm. By contrast, the near-complete release of Brilliant Sulfaflavine (BSF), an anionic water-soluble dye, follows the typical square root of time dependence. The unusual behavior of CuChl is attributed to the presence of nanoparticles when CuChl is dispersed in water. The nanoparticles are encased in CMC:PAE complex that adheres to parafilm. The fraction of the added CuChl lost in the burst release can be controlled by varying the CMC:PAE composition and concentration.

Introduction

Copper chlorophyllin (CuChl) is a green material derived from chlorophyll and is sold as a health food [1] and as a food colorant [2-3]. Being relatively inexpensive and from renewable sources, CuChl has been studied for applications ranging from cancer treatment [4] to textile dying. [5] Our interests involve the potential use of CuChl as an active component of agricultural crop sprays targeting plant leaves (foliar application). [6] In most cases, crop sprays are aqueous solutions or dispersions of an active chemical plus one or more additives (adjuvants). [7] An important role for adjuvants is to promote the transport of the active ingredients to specific locations in the plant. The desired locus of actives varies. In one extreme, formulations promote the immediate transport of the active solutions into the leaf tissue, stimulating a desired response in the plant. In the other extreme, adjuvants fix the actives on the leaf surfaces as solid deposits formed when the spray drop deposits dry. Spray deposits immobilized on leaf surfaces can kill pathogens through direct contact, [8] by stimulating the plant's defenses against pathogens, [9] or by acting as a physical barrier inhibiting spore adhesion.[10] The focus of this work is to understand how some water-borne polymeric adjuvants can control the release of CuChl when dried spray deposits on leaf surfaces are exposed to rain, foliar irrigation or dew.

Crop spray formulation is a mature technology mainly developed by crop protection chemical companies over many decades and described in many patents. Whereas most crop protection actives are low molecular synthetic chemicals with specific structures, commercial-grade CuChl is a complex mixture. Many publications describe experiments with Sigma-Aldrich commercial-grade CuChl; Sigma gives the structure as that of copper chlorin e_6 ($CuCe_6$ - see structure Figure 1). The conclusions regarding commercial-grade CuChl from the literature are: 1) CuChl is a mixture of at least four chlorophyllin structures representing about ½ of the material. The remainder of the material is poorly defined and is likely to include inorganic salts from processing and other chlorophyll breakdown products; [1-3] 2) CuChl is not completely water-soluble, with a significant content of dispersed colloidal particles that cannot pass through 6-8 kDa dialysis membranes. [11-13] We show herein that the complexity of CuChl leads to unusual release characteristics when dried spray deposits are exposed to water.

One of the challenges with any hydrophilic crop protection chemical is rainfastness. CuChl, like other water-soluble actives, has no intrinsic rainfastness – an adjuvant-free CuChl deposit easily is washed off of surfaces. Both the patent and scientific literature describe many approaches to increased rainfastness [14] including embedding in film-forming polymers [15-17] and encapsulation. [18] Herein we evaluate polyelectrolyte complexes from mixtures of carboxymethyl cellulose (CMC) and polyamidoamine-epichlorohydrin (PAE) as adjuvants for CuChl spray application. The polymer structures are shown in Figure 1. Although the CMC and PAE are not new materials, we believe this is the first time this combination has been evaluated as spray adjuvants. Reported below are measurements of CuChl release from dried deposits that are immersed in water. Comparison of release results from commercial grade CuChl, the material of interest, to

pure $CuCe_6$ and to brilliant sulfaflavine (BSF) a water-soluble anionic dye, led to unexpected results.

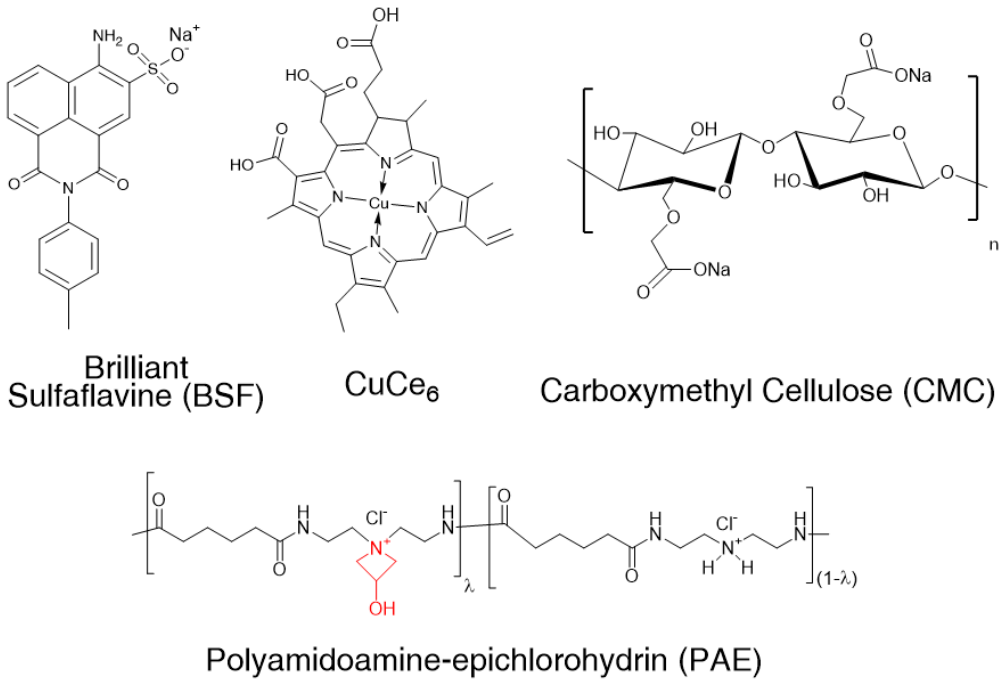

Figure 1 Chemical structures of dyes (BSF, $CuCe_6$) and polymers (PAE, CMC). The AZ (azetidinium) moiety on PAE is shown in red.

Experimental section

Materials. Commercial-grade sodium copper chlorophyllin (CuChl) fine powder (Batch NO. S005.S00201.G0034.170207, Organic Herb Inc., Hunan, China) was supplied by Suncor Energy (Mississauga, ON, Canada). Brilliant sulfaflavine (BSF) was purchased from MP Biomedicals. Polyamidoamine-epichlorohydrin (PAE) (Kymene™ 5221, Solenis) was dialyzed against water for 8 hours using 29 mm diameter tubing with an MWCO of 3.5 kDa (Spectra/Por® 3, Spectrum Laboratories, US) to have a final solid concentration of 2.13 wt%. Sodium carboxymethyl cellulose (CMC, average Mw 90,000, carboxymethyl groups per anhydroglucose unit 0.7), potassium phosphate monobasic and parafilm (PARAFILM® M) were obtained from Sigma–Aldrich. Sodium phosphate (dibasic, anhydrous) was purchased from EMD Millipore. Sodium dihydrogen phosphate monohydrate was obtained from Anachemia (a VWR company). Potassium phosphate dibasic was purchased from Caledon laboratories Ltd. 0.001 N PVSK and 0.001 N PDADMAC were obtained from BTG Americas Inc. (US). All chemicals were used without further purification. All water used was deionized and further purified by an EMD Millipore Milli-Q® Advantage A10 System (Thermo Scientific).

Falcon® 96-well tissue culture treated black microplates with clear bottom and Falcon® polystyrene petri dishes (35 * 10 mm) were purchased from VWR. Millex® - SV 5.00 μm filter units (low protein binding Durapore® (PVDF) membrane) were purchased from EMD Millipore.

Spray Formulations. Most solutions were prepared with 5 mM phosphate (pH=7.0) buffer (2.9 mM Na_2HPO_4 and 2.1mM NaH_2PO_4). 10 mg of dye (CuChl or BSF) was added to 9.99 g of phosphate buffer in a 20 mL vial and mixed with a vibromixer (Mini Vortex Mixer, VWR) at 3000 rpm for 1 min. 1 wt% CMC stock solution was prepared by dissolving 0.5 g of CMC powder to 49.5 g of phosphate buffer and stirred for overnight. Prior to use, the CMC solution was passed through a 5.00 μm filter.

A typical spray solution was prepared by adding 1.4559 g of buffer to a VWR® glass vial (4 Dr), followed by 1.5 g of 0.1 wt% CuChl solution, and then 0.03g of 1.0 wt% CMC solution. The mixture was stirred for 3 min at 1000 RPM. 14.1 μL of PAE stock solution (2.13 wt% in water) was added dropwise with stirring for 3 more minutes. The final spray solution composition for this example was 0.05 wt% CuChl, 0.01 wt% CMC and 0.01 wt% PAE. All spray solution compositions are expressed as mass fractions, that includes the buffer.

Deposit Formation. To make respective UV absorbance in release experiments within an optimal range, 15 μL of CuChl or 30 μL of BSF 5 mM spray solutions were deposited with a 20 or 100 μL pipette on PARAFILM® M surfaces supported on a petri dish and dried overnight in a humidity chamber (ESPEC) at 25 ℃ and 45% relative humidity.

Dynamic Light Scattering (DLS). The hydrodynamic diameters of samples were measured with a Malvern Zetasizer Nano ZS fitted with a He-Ne 4.0 mW laser operating at 633 nm. The detector angle was fixed at 173°. 10 μL of spray solution, diluted with 990 μL of 5 mM phosphate buffer, was placed in a polystyrene cuvette (10 mm, 4.5 mL) and then equilibrated in the light scattering cell for 1 min at 23 ℃. In a typical experiment, the measurement position was fixed at 4.65 mm with an attenuation index of 9. For every sample, three replicates were measured. The data were analyzed with Zetasizer software, version 7.01 using the CONTIN algorithm to generate the intensity size distribution. The cumulants analysis was performed to obtain the polydispersity index (PDI).

Electrophoretic Mobility (EM). The EM values were measured with a ZetaPlus (Brookhaven Instruments, US). Samples were diluted with 5 mM phosphate buffer solution, placed in a four-sided clear polystyrene cuvette (10 mm, 4.5 mL) and measured in triplicate with each measurement consisting of 10 runs.

Mütek Polyelectrolyte Titration. The net charge densities of soluble polymers were determined by polyelectrolyte titration with 0.001 N PVSK for cationic samples or 0.001 N PDADMAC titrants for anionic polymers. The titration endpoints were measured with

the Mütek PCD 03 (BTG, Switzerland) streaming current detector. [19] The polymers were diluted with the buffer to give PAE 0.005% wt/wt, CuChl 0.01%, and CMC 0.005%. The PCD LabX software gave the titrant volumes corresponding to zero streaming potential. The results were expressed as milliequivalents per gram of dry polymer.

Deposit Diameters. Deposits on parafilm were placed in a ChemiDoc™ MP imaging system (Biorad, nr. 170-8280) beside a ruler for distance calibration. Images were made with a UV transillumination excitation source, standard filter and an exposure time of 2 milliseconds. Images were obtained and exported for analysis by Image Lab™ 4.1. The images were analyzed with ImageJ software that determined the deposit boundaries and reported the Feret diameter, the longest distance between any two points along the boundary. The 10-mm scale was set globally and then the threshold of the image was usually adjusted to default. For CuChl deposits, the wand tool was used to determine the boundaries whereas the oval tool was employed for BSF deposits.

Dye Release. For release time up to 30 minutes, each parafilm-supported dry deposits was trimmed to 1.5 x 1 cm^2 and placed in a polystyrene weighing dish. 300 μL of 5 mM phosphate buffer was delivered by a pipette to give a sessile drop of release buffer covering the entire deposit. After a specific release time, the release buffer was aspirated with a 1 mL pipette and stored in a 1.7 mL graduated microtube (flat top, SPE155-N).

For longer release time experiments, each parafilm-supported deposit was placed in a 1.7 mL graduated microtube followed by the addition of 300 μL of 5 mM phosphate buffer. The microtubes were sealed to minimize evaporation, however, the tubes were not agitated.

The dye concentrations in the release buffer were measured by UV absorbance. 0.2 mL of dye-containing solutions were placed in 96-well plate and the absorbance was measured at 404 nm for CuChl and $CuCe_6$ or at 452 nm for BSF. Dye concentrations were calculated from linear calibration curves. Every release experiment was repeated in triplicate and the error was reported as a standard deviation.

Optical Microscopy Bright-field and fluorescent optical micrographs were obtained with an Olympus IX51 microscope (model IX51) equipped with a Retiga-2000R digital camera, and a FITC filter with an excitation range of 475-485 and an emission range of 485-536.

Results

In experiments designed to model some aspects of the spray application of aqueous agricultural chemicals on leaves, individual drops of a "spray solution" were deposited onto smooth, hydrophobic parafilm sheets. With drying, spray solutions were transformed to dry deposits consisting of an active, two polymer adjuvants and dried buffer salts. Our goal was to determine the factors influencing the release of CuChl when dry deposits were exposed to water (rainfall, irrigation or dew). Figure 2 shows photographs of a typical release experiment in which a sessile drop of spray solution was placed on parafilm. The drop was allowed to dry, forming a deposit. Finally, the deposit was covered with a larger drop of buffer to initiate the release of CuChl. Before presenting the release results, properties of the components and the deposits are now presented.

Figure 2 Photographs of the three steps in a release experiment. The spray solution composition was 0.05% CuChl + 0.01% CMC + 0.01% PAE in 5 mM phosphate buffer at pH 7.

Dyes and Polymers. Three actives were compared, BSF, commercial-grade CuChl, and $CuCe_6$ – see structures in Figure 1. Since all three materials are colored but not necessarily active in the agricultural context, herein we refer to these materials as "dyes". From an application perspective, we are primarily interested in the CuChl, which is approximately 54 wt% chlorin mixture. [13] Although claimed to be water soluble, aqueous mixtures at neutral pH include particles ranging in diameters from 10 to 800 nm. As much as 58 wt% of CuChl does not pass through 12-14 kDa MW cut-off dialysis tubing. [13]

$CuCe_6$ was chosen as a representative of the chlorin content of CuChl. The purity of $CuCe_6$, according to the supplier was above 95%, a value much higher than CuChl. BSF was chosen as an ideal dye that tends not to adsorb on anionic surfaces and does not spontaneously form aggregates in water. Hence BSF has been used to characterize water percolation through the soil. [20]

Most of the results herein involve a mixture of CMC (carboxymethyl cellulose), an anionic water-soluble polyelectrolyte and PAE a cationic polymer – see structures in Figure 1. In solution, mixtures of CMC plus PAE form polyelectrolyte complexes and upon water removal and heating, the AZ (azetidinium) groups form crosslinks with both carboxyls on CMC and amine groups on the PAE backbone. [21-22] The crosslinked structures are shown in Figure S 1. PAE crosslinking is widely used in the paper industry to strengthen wet paper such as coffee filters. [23] However, the drying temperatures in papermaking are above 100 ºC, so crosslinking is unlikely to be significant over the range of temperatures relevant to agricultural crops. The use of CMC and PAE as crop spray adjuvants is of interest because they are effective and are commercially available. Some properties of the above spray drop components are summarized in Table 1.

Table 1 Charge and molecular weights of spray solution components.

Spray Solution Component	Designation	Charge at pH7 (meq/g)	MW
Copper chlorophyllin	CuChl	-1.8 [a]	-
Copper $CuCe_6$ sodium salt	$CuCe_6$	-2.8 [b, c]	724 Da
Brilliant Sulfaflavine	BSF	-2.5 [b]	404.4 Da
Polyamine epichlorohydrin	PAE	+3.0 [a]	-
Carboxymethyl cellulose	CMC	-4.5 [a]	90 kDa

[a] Mütek polyelectrolyte titration (For CuChl, only dispersed particles were measured). [b] from the structure. [c] assuming 2 carboxyls are ionized.

Spray Solution Properties. Most solutions in this work were made with 5 mM phosphate buffer at pH 7. The exception was 5 mM phosphate (pH=8) was used to increase the solubility of $CuCe_6$. Most spray solutions were prepared by the sequential addition of dye, CMC, and PAE to a stirred 5 mM phosphate buffer solution at pH 7. With or without dye, colloidal polyelectrolyte complexes form immediately – CMC:PAE complexes have been reported in the papermaking technology literature. [21-22] Table S 1 summarizes the average particle size from dynamic light scattering, the electrophoretic mobility, and hydrogel net charge content calculated assuming all added dye and polymers end up as colloidal hydrogels. In all cases the colloids had a net negative charge, reflecting the contribution of both CMC and the dyes. Upon exposure to CMC, the mobility of CuChl particles was reduced, suggesting CMC adsorbed onto the CuChl particle surfaces before the PAE was added. In all cases the mobility distributions were monomodal.

Higher polymer concentrations gave larger hydrogels, although the average diameters only ranged from 176 to 379 nm. Without CMC, mixtures of PAE and dyes form large precipitates, not suitable for agricultural sprays. Thus it appears that the colloidal complexes contain a mixture of CMC, PAE and dye. We believe that the CMC enhances the colloidal stability of the colloidal complexes, presumably by electrostatic mechanisms. Figure S 3 shows the average diameter of the polyelectrolyte complex hydrogel particles did not change over 5 days, the length of the experiment. Furthermore,

there was no evidence of sedimentation or deposition on anionic surfaces. Colloidal stability is an important property for commercial spray applications.

Deposit Properties. Deposits were formed by placing sessile drops of spray solution onto parafilm and allowing them to dry. Figure 3 shows optical and fluorescent micrographs of BSF deposits formed from 30 μL of 0.05% BSF + 0.1% PAE + 0.1% CMC in phosphate buffer. The corresponding mass fractions in the dried deposits are 0.3 buffer solids, 0.14 BSF, 0.28 CMC and 0.28 PAE. The dried deposit (left-hand images) showed complex shapes with dense areas of material. The right-hand images show the deposit after three minutes' exposure to release solution (5 mM buffer), which was then aspirated leaving a damp deposit. While under the release solution, the periphery of the deposit lifted up and folded upon itself with the aspiration of the release solution. Comparing the fluorescent images, before and after exposure to release buffer, suggests that most of the BSF was released in the first three minutes. Quantitative BSF release measurements are presented in the next section.

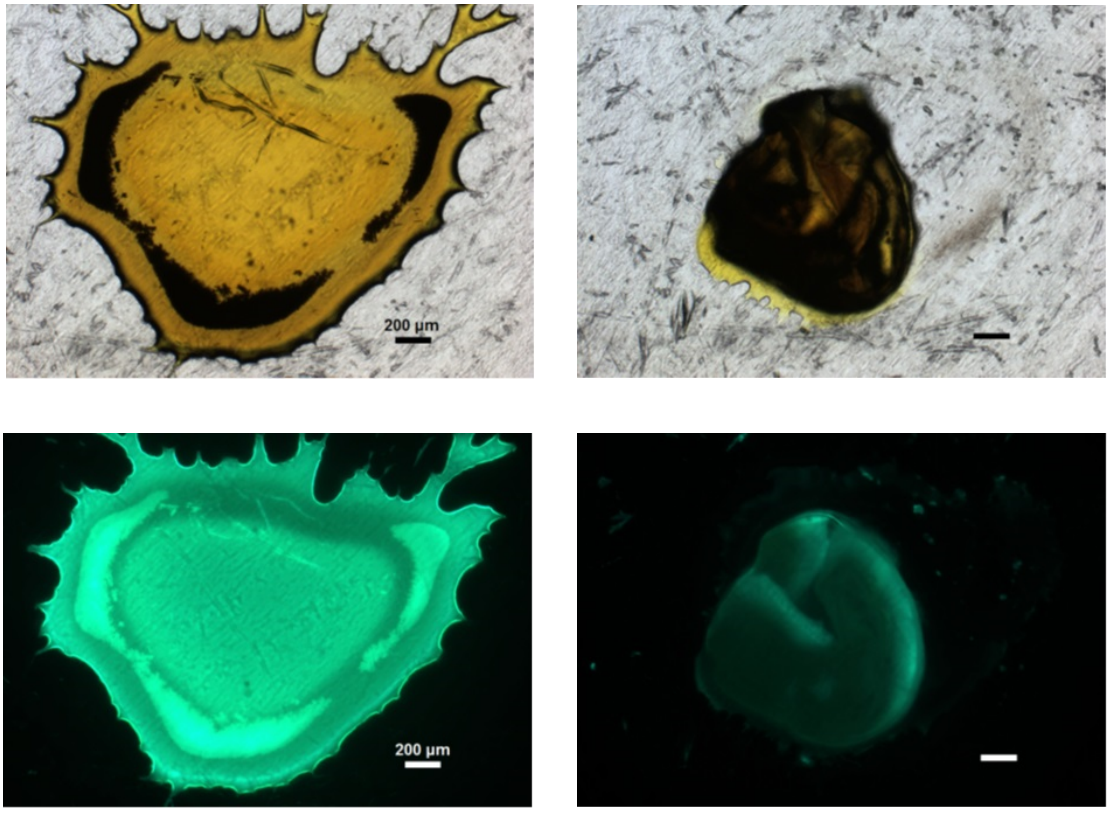

Figure 3 Bright-field (top) and fluorescent (bottom) micrographs of a BSF deposit dried at 25 ºC on parafilm. The left images are of the original air-dried deposit, the right images are the deposit after three minutes' release followed by the aspiration of the release solution leaving a damp deposit. The deposit was formed from 30 μL of spray

solution with a composition of 0.05% BSF + 0.1% PAE + 0.1% CMC. Images were taken under identical settings with a FITC filter. The scale bars represent 200 μm.

The deposit image in Figure 2 shows that CuChl formed circular deposits with a significant annulus (coffee ring). Figure S 4 shows a deposit of slightly higher magnification made from a spray solution where the polymer concentration was ten times high than the deposit in Figure 2.

Figure 4 shows the diameters of dried deposits as functions of CMC:PAE contents for CuChl and BSF spray solutions. For the circular CuChl deposits the diameters were unequivocal. In the case of the ragged BSF deposits, the ImageJ software determined the largest diameter spanning the deposit. The CuChl deposit diameters were high and independent of the CMC:PAE content. BSF deposits had smaller footprints than CuChl deposits even though the BSF had twice the mass of the CuChl deposit.

The square points in Figure 4 show two examples of the diameters of the fresh sessile drops. The CuChl diameter increased with drying, an indication of the slow spreading of the drying drop. By contrast, the BSF footprint decreased with drying. Assuming the sessile drops were spherical caps, the corresponding contact angles of the newly formed drops on parafilm were 97° for CuChl and 85° for BSF.

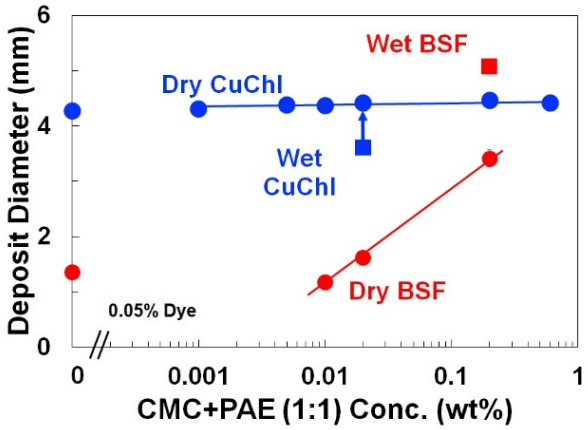

Figure 4 Diameters of dried deposits, on parafilm, as functions of the CMC+PAE concentrations in the spray solutions. The spray solution drop volume for CuChl was 15 μL whereas for BSF the volume was 30 μL. The squares denote the diameters of initially formed sessile drops.

BSF Release from Dried Spray Drop Deposits. BSF is an example of low molecular weight, anionic dye that does not form aggregates in water. Two formats of release studies were performed – for experiments of up to thirty minutes a sessile drop of release buffer was placed over the deposit and after a fixed time (see example in Figure 2), the

drop was aspirated and the BSF concentration in the release buffer was measured by UV absorbance. For longer time experiments the deposit was exposed to the release buffer in a closed tube to limit complications from evaporation.

An obvious, but important result - there was no retention of CuChl or BSF on parafilm after exposure to release buffer if the sessile spray solution drop was not allowed to dry and thus form a deposit (see Figure S 5 for BSF and Figure S 8 for CuChl). Figure 5A shows BSF release as a function of time for two deposit compositions. The deposit compositions on the graphs are presented as the composition of the spray solutions whereas the corresponding dry deposit compositions are given in Table S 2. Herein release results are presented as the mass of released dye divided by the original mass of dye in the deposit. In both cases in Figure 5A, the release was linear with the square root of time over the first thirty minutes. At longer times there was a slow release up to a plateau value of 0.8. Surprisingly, the two polymer concentrations gave similar results in spite of one being ten times greater than the other. Nevertheless, the polymer combinations are necessary. The results in Figure 5B show that with no polymer or with only CMC, all of the BSF is quickly released. Both release results are slightly above 1 due to the different sensitivity of employed analytical methods. Note, using PAE only generated large precipitates in the spray solution. Comparing the three CMC:PAE curves in Figure 5B, shows that release is not very sensitive to the CMC:PAE ratio. To summarize, without CMC:PAE polymers, BSF dissolves immediately. With the polymers, most of the BSF is released in 30 min with the remainder firmly fixed in the deposit. Taken as a whole, BSF release seems to follow the classic behavior of Fickian-diffusion release from a polymer matrix. [24]

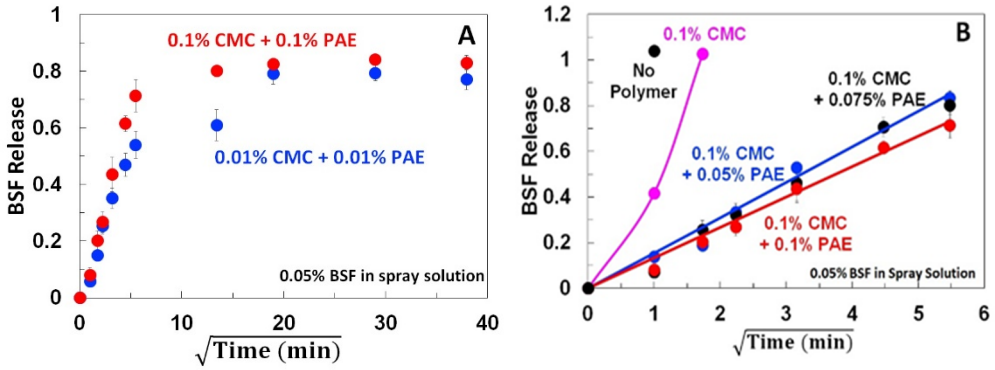

Figure 5 The fraction of BSF released from CMC+PAE deposits as a function of the exposure time to phosphate buffer (5 mM, pH 7) release solution. The deposit compositions are expressed as the polymer wt% in the spray solution used to form the deposits.

Finally, when CMC:PAE polyelectrolyte complexes are dried and heated, the AZ groups in PAE form covalent crosslinks with carboxyl groups in CMC and with secondary amine

groups in PAE – see chemistry in Figure S 1. Heating BSF:CMC:PAE to 70 ºC slows BSF release because of crosslink formation – see Figure S 6. However, for crop spray applications, high-temperature treatments are not relevant.

CuChl and $CuCe_6$ Release Figure 6 shows CuChl release from deposits containing CMC and PAE. In this case, the total mass of CMC+PAE was about ½ the mass of the CuChl. The inset shows the same results plotted against the square root of time. The release behaviors of CuChl is in stark contrast to BSF in the previous figure. There was a burst of CuChl release observed after one-minute exposure to the release buffer and accounting for most of the release in 24 h. There is a secondary slow release over the first three hours after which there was no further release.

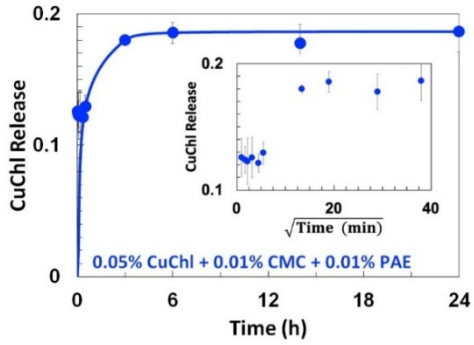

Figure 6 CuChl releases over time. The inset figure shows the same results plotted against the square root of time.

The role of CMC:PAE 1:1 concentration is illustrated in Figure 7 which shows release at 10 minutes as a function of total polymer concentrations. The inset shows three examples of release versus time experiments used to obtain the release result in Figure 7, which shows the main release is equilibrated at 10 minutes.

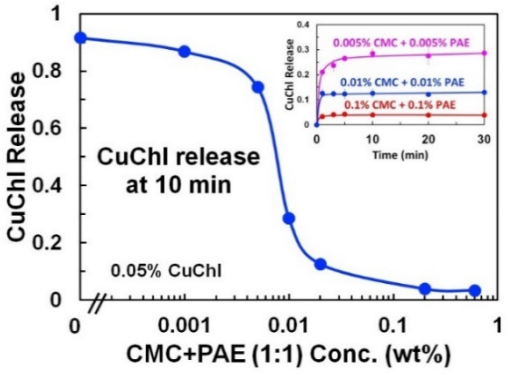

Figure 7 CuChl release at 10 minutes as a function of total CMC:PAE 1:1 concentration in the spray solution. The inset figure shows release/time behaviors for three CMC:PAE concentrations.

A remarkable feature of the CuChl release results is that it takes very little CMC:PAE (1:1) to fix CuChl in the deposit. For example, at equal weight CMC+PAE = 0.05% = CuChl, the release interpolated from in Figure 7 was less than 0.1. From an application perspective, the extent of burst release can be controlled by the quantity of CMC:PAE.

CMC is important because, without it, PAE produces macroscopic precipitates when mixed with CuChl. However, the release is not very sensitive to the amount of CMC in the spray solution. Figure 8 shows CuChl release as a function of the CMC concentration in the spray solution. Whereas the release associated with the initial burst is a strong function of the total concentration of CMC + PAE (Figure 7), the burst release is insensitive to the CMC:PAE mass ratios from 0.1 to 10.

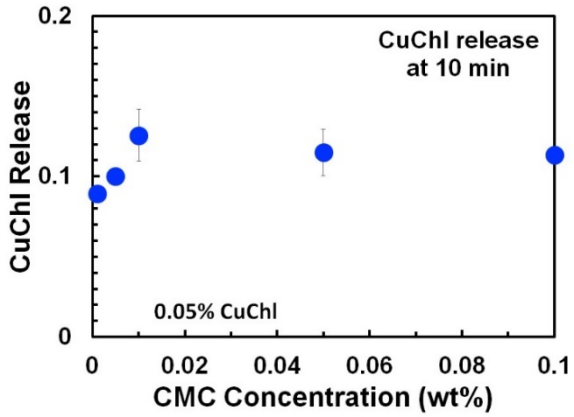

Figure 8 The influence of CMC:PAE on the release of 0.05% CuChl. The PAE spray solution content was 0.01%.

Comparing CuChl and $CuCe_6$ Release. Because CuChl is a mixture, one cannot assign an absolute solubility. In previous work, we employed UV to measure the supernatant concentrations of CuChl and $CuCe_6$ dispersions after aggressive ultracentrifugation. For commercial-grade CuChl, the apparent solubility was about 0.01% and the corresponding value for $CuCe_6$ was a little less. [13] Therefore in virtually all of the experiments herein involving CuChl we expect the presence of nanoparticles in the spray solution. The particle size of the dispersed components was broadly dispersed with a mean around 200 nm for both chlorins. [13] In this work, we compared the release behaviors of CuChl and $CuCe_6$ with and without ultracentrifugation of the chlorin stock solutions used to prepare spray solutions. The release results are shown in Figure 9. For both chlorins, centrifugation has little influence. Note, the pH of $CuCe_6$ spray solution was 8 instead of the 7 used for all CuChl experiments. $CuCe_6$ should be more soluble than at higher pH, possibly contributing to the higher burst release.

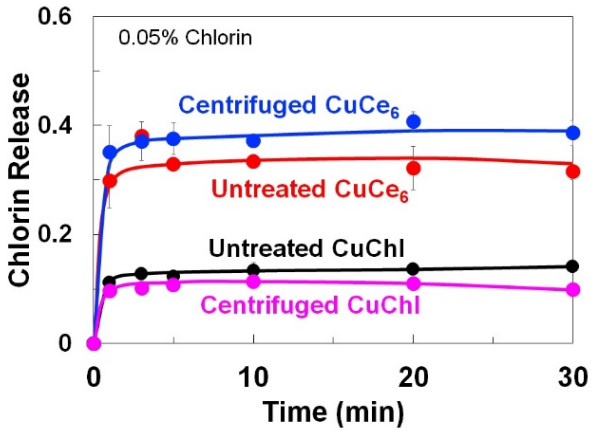

Figure 9 The influence of ultracentrifugation of chlorin stock solutions on release. The spray solution compositions were 0.05 % dye + 0.01% CMC + 0.01% PAE and the pH of CuChl solution was 7 whereas the pH of the $CuCe_6$ solution was 8.

Discussion

Why are polyelectrolyte complexes formed by CMC plus PAE so effective at fixing CuChl on parafilm surfaces? Additionally, why does the small fraction that does release do so in a burst fashion? These behaviors contrast those of BSF, an anionic dye that displays nearly complete release, following a square root of time dependence. BSF shows classical release behaviors driven by Fickian diffusion whereas CuChl does not. Because commercial-grade CuChl is a complex mixture, it is difficult to have a definitive explanation of why the release behaviors of CuChl and BSF are so different. Any explanations must also account for the following observations: 1) the CMC:PAE deposits must first dry in order to fix CuChl to parafilm; 2) there was little impact of the removal of colloidal particles from stock solutions of CuChl and from $CuCe_6$ (Figure 9); 3) the minimum mass of CMC:PAE required to fix most of CuChl was about same as the mass of CuChl (Figure 7); and, 4) although some CMC was required to prevent large aggregate formation upon addition of PAE to CuChl, the release was not very sensitive to the amount of CMC added (Figure 8). In the following paragraphs, we first highlight the key differences in the deposit structures formed with CuChl and BSF, followed by our explanation of the release behaviors upon immersing the deposits into water.

Deposit formation by drying sessile spray drops on parafilm is a complex process. During evaporation, convection of material within the drop leads to the much-discussed annulus or coffee ring formation. [25] [26] In addition, as water is removed the ionic strength increases to the point where buffer components come out of solution. Simultaneously, polymer concentrations increase leading to large viscosity increases. Ionic interactions will be attenuated by increasing buffer concentration whereas depletion interactions will increase

with the increasing polymer concentrations. In spite of these complexities, we now provide the following tentative explanations for our results.

BSF deposit structure. Figure 10 summarizes our vision of the spray solution properties and the resulting deposits structures. The BSF spray solution is a mixture of dispersed CMC:PAE polyelectrolyte hydrogel particles about 250 nm in diameter plus dissolved BSF. With evaporation, the sessile drop retracts (Figure 4) suggesting that neither the CMC:PAE complexes or the dissolved BSF promote pinning the three-phase contact line on smooth, hydrophobic parafilm support. The initial sessile drop volume was 30 μL, however, the evaporation must decrease the water volume to about 1.5 μL to reach the water solubility of BSF. Further evaporation will induce BSF crystallization with crystals embedded in the film formed as the CMC:BSF mixtures dry. Electrophoresis measurements of the CMC:PAE hydrogel particles with and without BSF gave the same electrophoretic mobilities (Table S 1), suggesting little binding of BSF to the polyelectrolyte complexes in dilute solution. The absence of a significant burst in the release experiments suggests that all of the BSF crystals were encapsulated in CMC:PAE in the compact dry deposit.

CuChl deposit structure. In the case of CuChl deposits, the initial spray solution is a mixture of CMC:PAE complex particles, dispersed CuChl particles, and dissolved CuChl components. The electrophoresis results (Table S 1 and Figure S 2) suggest that CMC adsorbs onto CuChl nanoparticle surfaces, before PAE addition. After PAE addition, the CMC:PAE hydrogel complexes form. The overall average particle size of the spray dispersion was of the same magnitude as the CuChl particles, suggesting no heteroflocculation of CuChl and CMC:PAE hydrogel nanoparticles. During evaporation the diameter of sessile drop increases a little after which the three-phase contact line is effectively pinned giving a coffee ring deposit structure (photograph in Figure 2, diameters in Figure 4). Previous work showed that CuChl nanoparticles adsorb on pristine polystyrene surfaces in the buffer, presumably reflecting hydrophobic interactions. Therefore we anticipate a sparse coating of adsorbed CuChl nanoparticles across the entire footprint of the sessile drop. However most of the CuChl is present as nanoparticles in the annulus, imbedded in the CMC:PAE hydrogel film.

CuChl burst release (Figure 7). With low dosages of CMC:PAE, virtually all of the hydrogel is present in the annual ring of the dried deposit. Therefore, some CuChl present inside the ring is not protected and is immediately released upon exposure to buffer. Note, CuChl does not have to dissolve to be released. Instead, hydrophilic CuChl nanoparticles detach from parafilm when there is no adhesive adjuvant. Higher CMC:PAE concentrations in the spray solution result in more hydrogel in the center of the deposit lowering the fraction of unprotected CuChl and given less burst. By contrast, with BSF the deposit footprint is small, facilitating the CMC:PAE encapsulation of all the BSF crystals, preventing a burst release.

Low or no after-burst CuChl release. Most of the CuChl particles are located in the annular ring where the particles are embedded in the CMC:PAE complex gel. The CMC:PAE acts as an adhesive preventing the detachment of CuChl nanoparticles. In addition, the low solubility of CuChl (0.01% wt/wt, 100 times lower than the solubility of BSF [20]) coupled with a coating of CMC:PAE polyelectrolyte complex inhibits CuChl dissolution and diffusion upon immersion of the deposit into water.

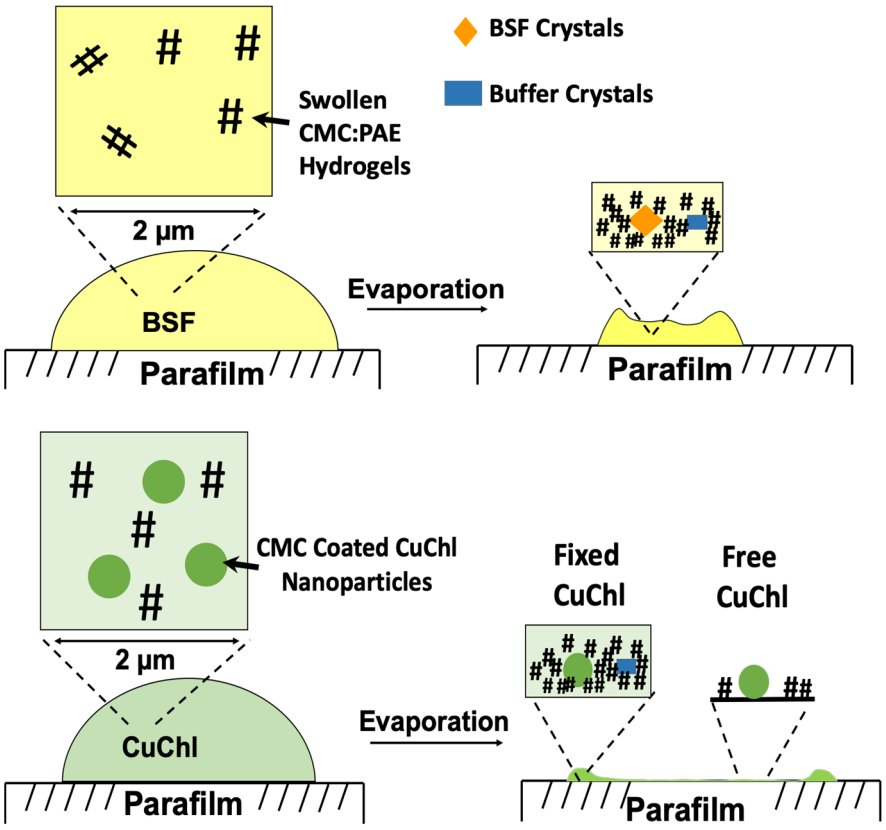

Figure 10 Illustration of sessile spray drops and deposits properties.

Conclusions

A large portion of the added CuChl is fixed to a hydrophobic parafilm surface when a sessile drop of spray solution containing CuChl and a mixture of anionic CMC and cationic PAE, dries to form a deposit. The small unfixed fraction of CuChl is immediately (burst) released upon exposure to water. These behaviors are in contrast to the behavior of an anionic, water-soluble dye brilliant sulfaflavine (BSF) whose release follows a square root of time dependence, typical of small molecules diffusing through a polymer film. The main conclusions herein are:

1. Most of the CuChl in the spray solution ends up as nanoparticles embedded in a hydrogel CMC:PAE matrix present as an annular (coffee) ring in the dried deposit. The low solubility of CuChl, particularly when coated with CMC:PAE complex, fixes CuChl on the parafilm. A small amount of CuChl in the center of the deposit is not embedded in complex and exhibits burst release. Although solid BSF is also encased in CMC:PAE complex, upon exposure to water, the very soluble BSF crystals rapidly dissolve and diffuse into the aqueous phase.
2. The mass of CMC:PAE complexes required to fix most of CuChl on parafilm surfaces is equal to the mass of CuChl, indicating that CMC:PAE complexes are very efficient adjuvants.
3. The role of CMC is critical. The negatively charged hydrophilic polymer helps stabilize colloidal species in the solution and ensuring all particles maintain a negative net charge. Without CMC, PAE flocculates both BSF and CuChl into large precipitates not suitable for spray application.
4. From a practical perspective, by tuning the composition and concentration of CMC:PAE polymers, it is possible to control the fraction of CuChl strongly fixed to leaf surfaces versus the amount available to enter the leaf upon re-wetting of dried spray deposits.

Acknowledgments

We thank the National Sciences and Engineering Research Council of Canada (NSERC) and Suncor Energy for funding this project. Most of the experiments were conducted at the McMaster Biointerfaces Institute, funded by the Canadian Foundation for Innovation. R. H. Pelton holds the Canada Research Chair in Interfacial Technologies. Carla Abarca and Dong Yang are thanked for useful discussions.

Reference

1. Nagini, S.; Palitti, F.; Natarajan, A. T., Chemopreventive Potential of Chlorophyllin: A Review of the Mechanisms of Action and Molecular Targets. *Nutr. Cancer* **2015,** *67* (2), 203-211.
2. Tumolo, T.; Lanfer-Marquez, U. M., Copper chlorophyllin: A food colorant with bioactive properties? *Food Research International* **2012,** *46* (2), 451-459.
3. Viera, I.; Pérez-Gálvez, A.; Roca, M., Green Natural Colorants. *Molecules* **2019,** *24* (1), 154.
4. Ryan, A. A.; Senge, M. O., How green is green chemistry? Chlorophylls as a bioresource from biorefineries and their commercial potential in medicine and photovoltaics. *Photochem. Photobiol. Sci.* **2015,** *14* (4), 638-660.
5. Hou, X.; Yang, R.; Xu, H.; Yang, Y., Adsorption Kinetic and Thermodynamic Studies of Silk Dyed with Sodium Copper Chlorophyllin. *Ind. Eng. Chem. Res.* **2012,** *51* (25), 8341-8347.

6. Zhang, X.; Goatley, M.; Conner, J.; Wilkins, M.; Teshler, I.; Liu, J.; Fefer, M.; Ckurshumova, W., Copper Chlorophyllin Impacts on Growth and Drought Stress Tolerance of Tomato Plants. *HortScience* **2019,** *54* (12), 2195-2201.
7. Green, J. M.; Beestman, G. B., Recently patented and commercialized formulation and adjuvant technology. *Crop Prot.* **2007,** *26* (3), 320-327.
8. Baibakova, E. V.; Nefedjeva, E. E.; Suska-Malawska, M.; Wilk, M.; Sevriukova, G. A.; Zheltobriukhov, V. F., Modern Fungicides: Mechanisms of Action, Fungal Resistance and Phytotoxic Effects. *Annual Research & Review in Biology* **2019**, 1-16.
9. Albert, I.; Hua, C.; Nurnberger, T.; Pruitt, R.; Zhang, L., Surface sensor systems in plant immunity. *Plant Physiology* **2020**, pp.01299.2019.
10. Walters, D. R., Disguising the Leaf Surface: The Use of Leaf Coatings for Plant Disease Control. *Eur. J. Plant Pathol.* **2006,** *114* (3), 255-260.
11. Salin, M. L.; Alvarez, L. M.; Lynn, B. C.; Habulihaz, B.; Fountain iii, A. W., Photooxidative bleaching of chlorophyllin. *Free Radical Res.* **1999,** *31* (sup1), 97-105.
12. Selig, M. J.; Gamaleldin, S.; Celli, G. B.; Marchuk, M. A.; Smilgies, D.-M.; Abbaspourrad, A., The stabilization of food grade copper-chlorophyllin in low pH solutions through association with anionic polysaccharides. *Food Hydrocolloids* **2019**, 105255.
13. Wang, F.; Terazono, Y.; Liu, J.; Fefer, M.; Pelton, R. H., Adsorption of aqueous copper chlorophyllin mixtures on model surfaces. *Colloids and Surfaces A: Physicochemical and Engineering Aspects* **2020,** *592*, 124578.
14. Gaskin, R. E.; Steele, K. D., A comparison of sticker adjuvants for their effects on retention and rainfastening of fungicide sprays. *N. Z. Plant Prot.* **2009,** *62* (0).
15. Symonds, Brett L.; Lindsay, C. I.; Thomson, N. R.; Khutoryanskiy, V. V., Chitosan as a rainfastness adjuvant for agrochemicals. *RSC Advances* **2016,** *6* (104), 102206-102213.
16. Symonds, B. L.; Thomson, N. R.; Lindsay, C. I.; Khutoryanskiy, V. V., Rainfastness of Poly(vinyl alcohol) Deposits on Vicia faba Leaf Surfaces: From Laboratory-Scale Washing to Simulated Rain. *ACS Appl. Mater. Interfaces* **2016,** *8* (22), 14220-14230.
17. Burnet, M.; Gressel, J. Pesticide formulations with substituted biopolymers and organic polymers for improving residual activity, droplet size, adherence and rainfastness on leaves and reduction in soil leaching. US 2007/0149409 A1, 2007.
18. Yu, M.; Yao, J.; Liang, J.; Zeng, Z.; Cui, B.; Zhao, X.; Sun, C.; Wang, Y.; Liu, G.; Cui, H., Development of functionalized abamectin poly (lactic acid) nanoparticles with regulatable adhesion to enhance foliar retention. *RSC Advances* **2017,** *7* (19), 11271-11280.
19. Pelton, R., The streaming current detector(SCD) - What does it really tell us? *Appita J.* **2010,** *63* (3), 196-198.
20. Wilson, J. F., *Fluorometric procedures for dye tracing*. Department of the Interior, US Geological Survey: 1986.
21. Siqueira, E. J.; Salon, M.-C. B.; Belgacem, M. N.; Mauret, E., Carboxymethylcellulose (CMC) as a model compound of cellulose fibers and

polyamideamine epichlorohydrin (PAE)–CMC interactions as a model of PAE–fibers interactions of PAE-based wet strength papers. *J. Appl. Polym. Sci.* **2015,** *132* (26).
22. Gardlund, L.; Norgren, M.; Wagberg, L.; Marklund, A., The use of polyelectrolyte complexes (PEC) as strength additives for different pulps used for production of fine paper. *Nord. Pulp Pap. Res. J.* **2007,** *22* (2), 210-216.
23. Espy, H. H., The mechanism of wet-strength development in paper: a review. *TAPPI* **1995,** *78* (4), 90-99.
24. Ritger, P. L.; Peppas, N. A., A simple equation for description of solute release I. Fickian and non-fickian release from non-swellable devices in the form of slabs, spheres, cylinders or discs. *J. Controlled Release* **1987,** *5* (1), 23-36.
25. Deegan, R.; Bakajin, O.; Dupont, T.; Huber, G.; Nagel, S.; Witten, T., Capillary flow as the cause of ring stains from dried liquid drops. *Nature* **1997,** *389* (6653), 827-828.
26. Faers, M. A.; Pontzen, R., Factors influencing the association between active ingredient and adjuvant in the leaf deposit of adjuvant-containing suspoemulsion formulations. *Pest Manage. Sci.* **2008,** *64* (8), 820-833.

Supporting Information

Controlling the Release of Copper Chlorophyllin From Crop Spray Deposits on Hydrophobic Surfaces

Fengyan Wang, [a] Wenzi Ckurshumova ,[b] Jun Liu, [b] Michael Fefer,[b] and Robert H. Pelton*[a]
[a] Department of Chemical Engineering, McMaster University, 1280 Main Street West, Hamilton, ON, L8S 4L7, Canada
[b] Suncor AgroScience, 2489 North Sheridan Way, Mississauga, ON L5K 1A8, Canada
*Corresponding author: peltonrh@mcmaster.ca

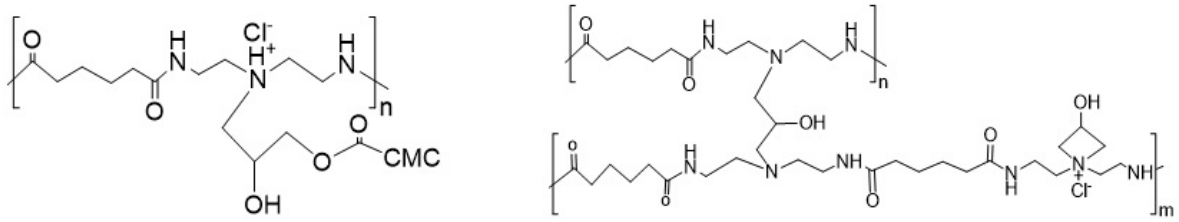

Figure S 1 Crosslinked structures formed by heating mixtures of CMC + PAE.

Table S 1 Some properties of dye:CMC:PAE colloidal complexes in phosphate buffer at pH 7.

$\frac{[dye]}{[polymers]}$	Formulations	DLS[a] Diameter (nm)	PDI	Charge Density (meq/g)	EM (*10^{-8} $m^2/(V \cdot s)$)
-	0.05% CuChl			-1.8	-1.7 ± 0.3
0.5	0.05% CuChl + 0.1 % CMC				-1.9 ± 0.5
0.25	0.05% CuChl + 0.1% CMC + 0.1% PAE				-3.0 ± 0.3
0	0.01% CMC + 0.01% PAE	230 ± 16	0.25	-0.77	-2.2 ± 0.1
0	0.1% CMC + 0.1% PAE	314 ± 16	0.18	-0.77	-2.1 ± 0.3
10	0.05% CuChl + 0.0025% CMC + 0.0025% PAE	176 ± 8	0.24	-1.72	-2.4 ± 0.4
5	0.05% CuChl + 0.005% CMC + 0.005% PAE	195 ± 10	0.22	-1.64	-3.3 ± 0.3
2.5	0.05% CuChl + 0.01% CMC + 0.01% PAE	243 ± 17	0.21	-1.52	-3.3 ± 0.2
0.25	0.05% CuChl + 0.1% CMC + 0.1% PAE	286 ± 8	0.17	-0.98	-3.0 ± 0.1
0.08	0.05% CuChl + 0.3% CMC + 0.3% PAE	379 ± 17	0.19	-0.85	-2.5 ± 0.1
5	0.05% BSF + 0.005% CMC + 0.005% PAE	-	-	-2.10	-2.4 ± 0.2
2.5	0.05% BSF + 0.01% CMC + 0.01% PAE	259 ± 12	0.21	-1.84	-2.0 ± 0.1
0.25	0.05% BSF + 0.1% CMC + 0.1% PAE	336 ± 22	0.21	-0.69	-2.4 ± 0.2

[a] All DLS samples were diluted with buffer by a factor of 100.

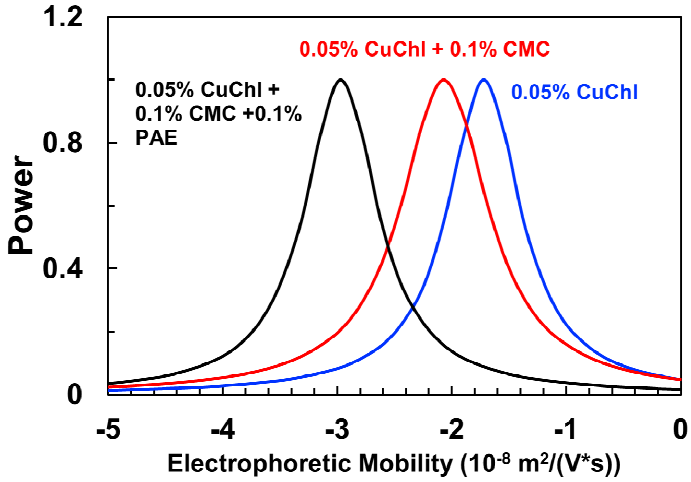

Figure S 2 Electrophoretic mobility distributions of CuChl, CuChl + CMC, and CuChl + CMC + PAE.

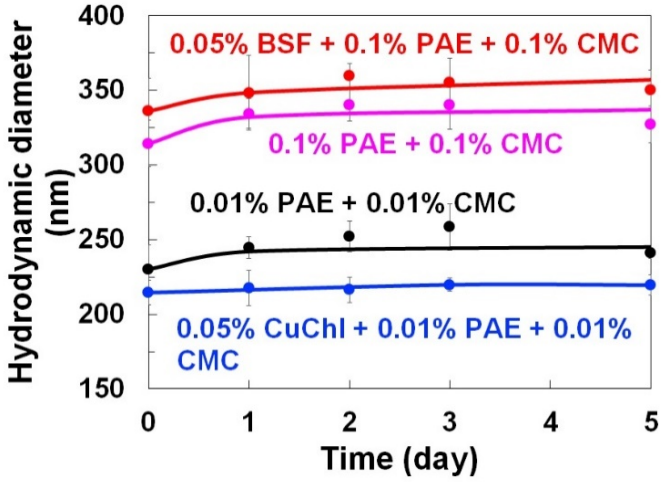

Figure S 3The hydrodynamic sizes of spray solutions were measured as a function of time with dynamic light scattering (DLS). The error bars represent the standard deviation of three replicates.

Table S 2 Dry deposit compositions as a function of spray composition for CMC:PAE deposits.

Spray Solution Composition (% wt/wt)				Deposit Composition (mass fraction)		
Dye	CMC	PAE	Buffer *	Dye	CMC	PAE
0.05%	0.1%	0.1%	0.30	0.14	0.28	0.28
0.05%	0.01%	0.01%	0.60	0.28	0.06	0.06
0.05%	0.005%	0.005%	0.64	0.30	0.03	0.03
0.05%	0.1%	0.05%	0.35	0.16	0.33	0.16
0.05%	0.1%	0.075%	0.32	0.15	0.30	0.23

*Assuming buffer dries as $Na_2HPO_4 \cdot 7H_2O$ and $NaH_2PO_4 \cdot H_2O$ crystals.

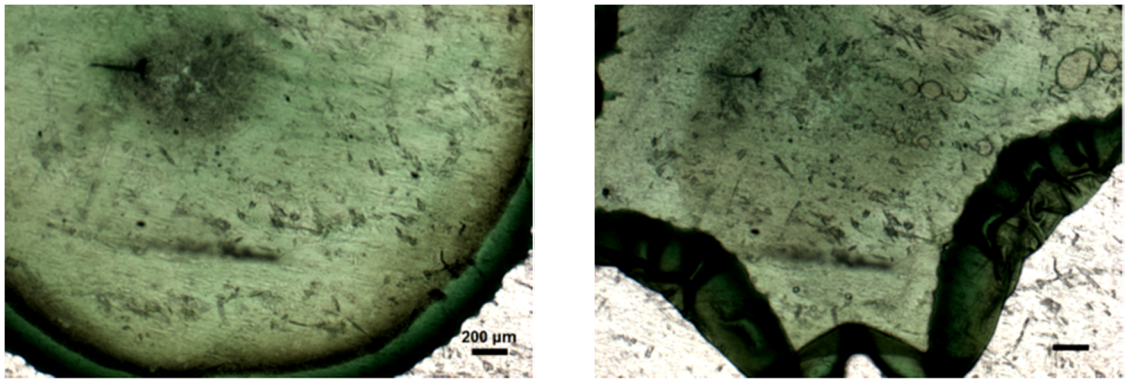

Figure S 4 Optical micrographs of a CuChl deposit air-dried from 15 µL of the spray solution with a composition of 0.05% CuChl + 0.1% PAE + 0.1% CMC on the PARAFILM® M before (left) and after (right) 3-minute release. Images were taken under identical settings. All scale bars represent 200 µm.

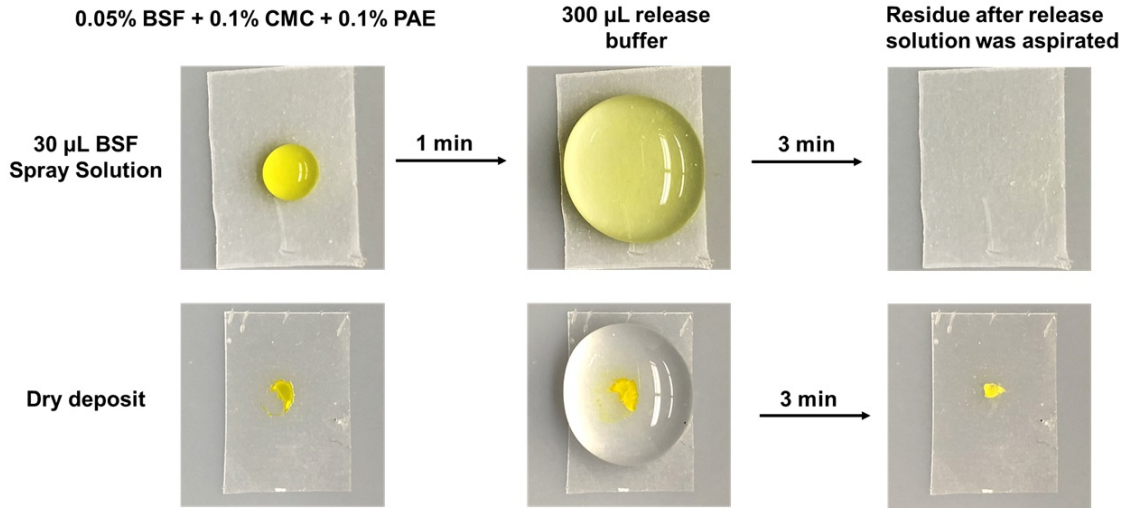

Figure S 5 Comparing BSF release from dried deposit to release from sessile spray drop.

Influence of CMC:PAE crosslinking. When CMC:PAE polyelectrolyte complexes are dried and heated, the AZ groups in PAE form covalent crosslinks with carboxyl groups in CMC and with secondary amine groups in PAE – see chemistry in Figure S 1. Although high temperature crosslinking is not relevant to agricultural applications, we were curious and compared BSF release from crosslinked versus non-crosslinked CMC:PAE deposits. Because parafilm melts at elevated temperatures, polystyrene petri dishes were used as the supporting substrates. The dry deposit diameters on polystyrene were about 1.6 times greater than the diameters on parafilm. The fluorescent images of a BSF deposit before and after release are shown in Figure S 7– most of the BSF was in the annulus (coffee ring).

Figure S 6 compares BSF release for crosslinked versus non-crosslinked CMC:PAE deposits. The deposits dried a low temperature (i.e. no crosslinking) released BSF faster and to a greater extent compared to parafilm results above. The crosslinked deposits, formed at 70 °C, released BSF more slowly, supporting the conclusion that at least some of the BSF diffused through the polymer network. It is well known that crosslinking attenuates the diffusion of polymers through hydrogels. In control experiments, we confirmed there was no decomposition of BSF at 70 °C.

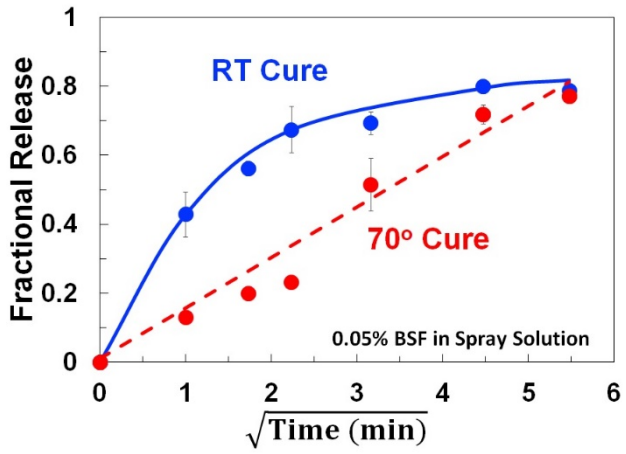

Figure S 6 The influence of PAE crosslinking at 70 °C on BSF release. The spray solution composition was 0.05% BSF+ 0.1% CMC + 0.1% PAE. Deposits were formed on polystyrene petri dishes.

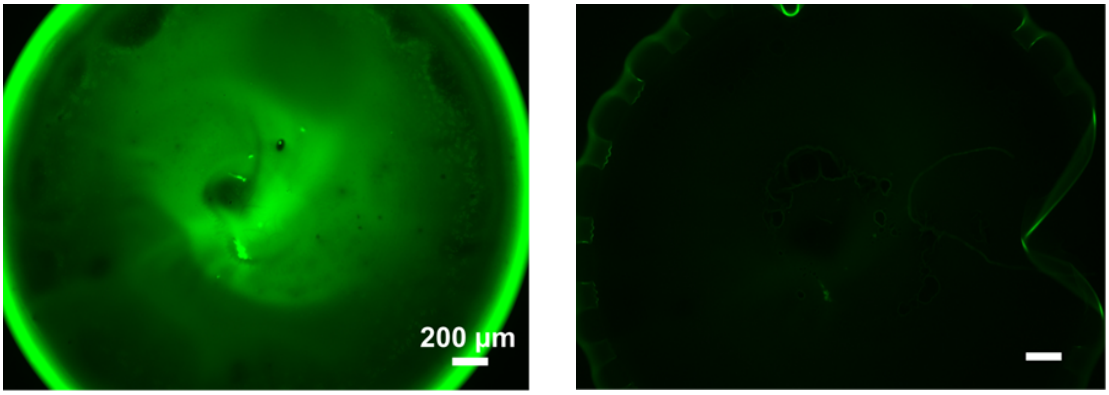

Figure S 7 Fluorescent micrographs of a BSF deposit dried at 25 ºC on a polystyrene petri dish. The left image is the original deposit, the right image is after three minutes release with release solution removed. The spray solution composition was 0.05% BSF + 0.1% PAE + 0.1% CMC. Images were taken under identical settings with a FITC filter. The scale bars represent 200 µm.

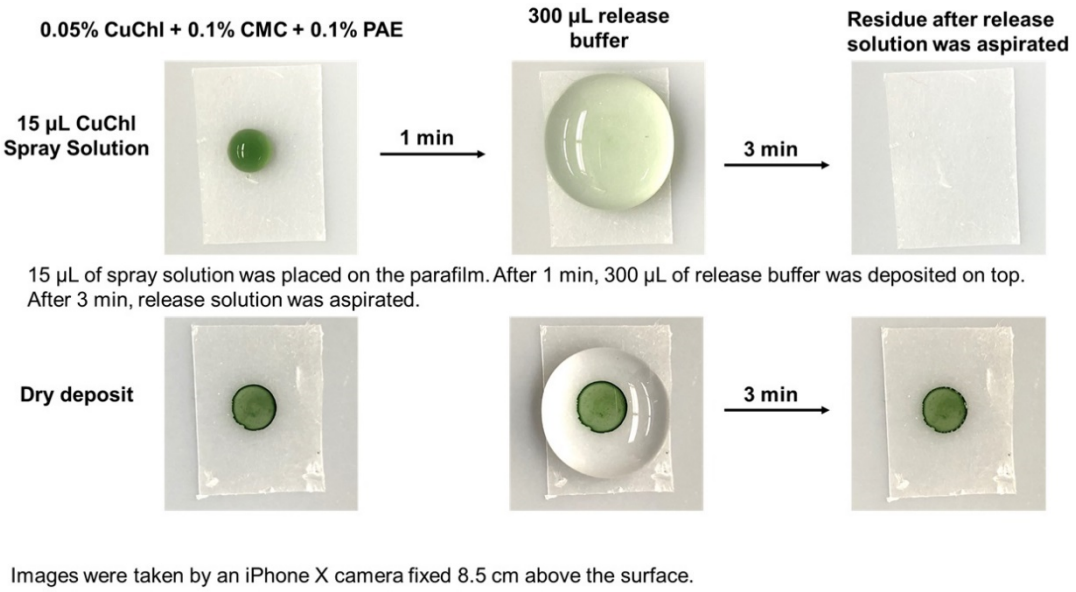

Figure S 8 Comparing CuChl release from a sessile drop with release from a dried deposit.

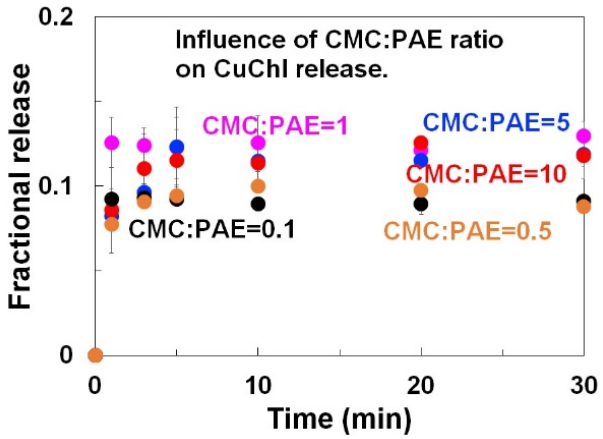

Figure S 9 The influence of CMC:PAE on the release of 0.05% CuChl. The PAE spray solution content was 0.01% and the CMC was varied.

Chapter 4

Factors Influencing Deposit Structures on Hydrophobic Surfaces

This chapter illustrates how formulation variables affect the distribution of PG7 particles in dried deposits. The distribution of PG7 particles is demonstrated to be an indication of the extent to which dispersed particles are bound to or entrained in oil droplets. The results are beneficial for us to understand the relationship between the solution properties of suspoemulsions and the resulting dried deposits on hydrophobic surfaces.

Sample preparations, size and contact angle measurements, and sessile drop imaging were carried out by myself. Optical micrographs and scanning electron microscope images were obtained by Dr. Hu. The first draft was written by Dr. Hu and myself. Dr. Abarca, Dr. Liu, Dr. Fefer and Dr. Brook reviewed the paper and provided useful comments. Robert Pelton helped me analyze the data and rewrite the draft to the final version.

Factors influencing agricultural spray deposit structures on hydrophobic surfaces

Fengyan Wang, Zhen Hu, Carla Abarca, Michael Fefer, Jun Liu, Michael A. Brook, Robert Pelton

Colloids and Surfaces A: Physicochemical and Engineering Aspects 2018, 553, 288–294.

https://doi.org/10.1016/j.colsurfa.2018.05.074

Colloids and Surfaces A 553 (2018) 288–294

Contents lists available at ScienceDirect

Colloids and Surfaces A

journal homepage: www.elsevier.com/locate/colsurfa

Factors influencing agricultural spray deposit structures on hydrophobic surfaces

Fengyan Wang[a], Zhen Hu[a], Carla Abarca[a], Michael Fefer[c], Jun Liu[c], Michael A. Brook[b], Robert Pelton[a,*]

[a] Department of Chemical Engineering, McMaster University, 1280 Main Street West, Hamilton, ON L8S 4L7, Canada
[b] Department of Chemistry and Chemical Biology, McMaster University, 1280 Main Street West, Hamilton, ON L8S 4L7, Canada
[c] Suncor Energy, 2489 North Sheridan Way, Mississauga, ON L5K 1A8, Canada

GRAPHICAL ABSTRACT

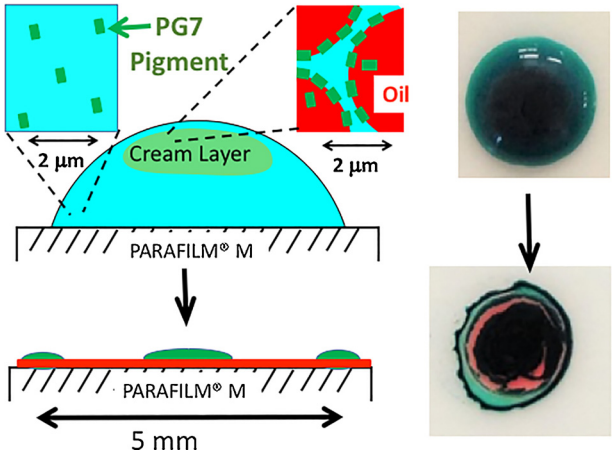

ARTICLE INFO

Keywords:
Emulsions
Suspoemulsions
Agricultural sprays
Coffee-ring

ABSTRACT

The properties of dried deposits formed by placing drops of a commercial turf grass fungicide spray formulation on smooth, waxy PARAFILM® M surfaces were measured as functions of formulation variables. The deposit structure reveals the extent to which dispersed active ingredient particles are bound to oil droplets in agricultural spray dispersions, before drying. The dilute spray dispersion (herein called Green Emulsion) was a suspoemulsion, which is a mixed dispersion of large (2–50 μm) mineral oil drops and small (~430 nm) polychlorinated Cu (II) phthalocyanine (PG7) pigments, also known as Green 7. The distribution of PG7 pigment in the dried spray drop deposit depended upon the partitioning of PG particles in the suspension before drying. Individually dispersed PG7 particles in the aqueous phase mainly ended up in the annulus (coffee ring), whereas PG7 particles adsorbed on the oil emulsion droplets ended up as a central oily deposit (the dome). After most of the water evaporated, some oil migrated beyond the dome and slowly beyond the annulus. Increasing the oil-soluble surfactant concentration inhibited PG7 binding to the oil/water interface, giving a very small dome area and a wide annulus after drying. The deposit structure is sensitive to the mixing intensity when spray concentrates are diluted in a mix-tank. Increased intensity of mixing the suspoemulsion gives smaller oil droplets, more PG7 bound to the oil/water interface and a larger dome. The ASTM E2044 "Standard Test Method for

* Corresponding author.
E-mail address: peltonrh@mcmaster.ca (R. Pelton).

https://doi.org/10.1016/j.colsurfa.2018.05.074
Received 25 January 2018; Received in revised form 18 May 2018; Accepted 25 May 2018
Available online 26 May 2018

Spreading of Liquid Agricultural Spray Mixtures" involves placing a drop of crop spray dispersion on PARAFILM® and measuring the dimensions of the resulting sessile drop. This work demonstrates that allowing the sessile drops on PARAFILM® to dry and analyzing the resulting deposit structure gives a direct measure of the extent to which active ingredient particles, initially dispersed in water, are transferred on or into oil drops in suspoemulsions.

1. Introduction

Modern agriculture depends upon the effective use of fertilizers and plant protection chemicals. In many cases, the chemicals are applied as sprays on leaves (foliar application). Typically, farmers dilute one or more concentrates in a large quantity of water. The mixture is agitated continuously and sprayed on the crops. Ideally, spray application consists of the following steps: the spray drops impact and adhere to leaf surfaces [1]; the adsorbed (sessile) drops spread on the leaf surfaces [2]; the water evaporates, leaving a deposit [3,4]; and, the active ingredient (s) migrate from the deposit to target sites on or in the plants, a process often called uptake. In this paper, we examine a commercial turf grass fungicide we call "Green Emulsion", focusing on the factors influencing the nature of the deposit when sessile Green Emulsion drops dry on both leaves and model surfaces.

Green Emulsion fungicidal activity results from the synergistic interactions between mineral oil, a well-known compound in pesticide formulation [5], and polychlorinated Cu (II) phthalocyanine (PG7) pigment, also known as Green 7 [6]. PG7 crystals are water and oil insoluble. In one variation of the commercial product, oil concentrate with oil-borne surfactants and pigment concentrate with hydrophilic surfactants are added separately to the spray water to form a dilute dispersion with a mixture of oil emulsion droplets (2–50 μm diameter) and suspended PG7 particles (~430 nm diameter). CropLife International have categorized the physical forms of agrichemicals and by their definition, Green Emulsion is a "suspoemulsion" [7]. From a colloid science perspective, suspoemulsions are particularly complex mixtures of oil droplets, colloidal particles and multiple surfactants.

1.1. The literature – deposits from suspensions

Before considering suspoemulsion literature, we now summarize some features of deposits formed when drops of colloidal dispersion dry on a surface. In other words, these dispersions are suspoemulsions minus the oil-in-water emulsion component. There is a large literature describing annulus (coffee-ring) structures formed by drying drops of solutions and dispersions on surfaces, sessile drops [8]. Drying a sessile drop of an aqueous suspension usually produces an annulus containing most of the solid material – the coffee ring. Annulus formation occurs when a sessile drop is pinned during evaporative drying. The flux of liquid to the drop periphery drives a buildup of suspended material near the three-phase contact line [9]. An elegant report from Binks' group demonstrated the effects of colloid hydrophobicity and concentration on the deposit structure from dried drops [10]. Hydrophilic silica particles concentrate in the annulus, whereas more hydrophobic silica is concentrated in what Binks calls a "dome" in the center of the dried drops. Dome formation results from particle association (gelation or aggregation) forming large structures that are not easily transported to the periphery of the sessile drop – Fig. 1. Surfactants [11], volatile solutes [3], particle shape [12], and particle adsorption at the air water interface[10] all influence coffee ring structures in systems much simpler than the suspoemulsions of interest herein.

1.2. Literature – deposits from emulsions

Surfactant stabilized oil-in-water emulsions are another subset of suspoemulsions in which there are no dispersed solid particles. In the absence of high concentrations of superwetting surfactants, emulsion droplets form sessile drops on hydrophobic surfaces, including leaves. The dispersed oil droplets rise towards the surface in gravity driven flow. We will show in our results below that creaming time is more than an order of magnitude shorter than the drying time. As emulsions droplets concentrate near the air/water interface, the oil drops may aggregate and coalesce into larger droplets or remain as individual droplets in a concentrated cream layer. Emulsion droplets adjacent to an air/water interface may: 1) do nothing; 2) penetrate the interface to form a lens; or, 3) penetrate the interface and completely spread. For systems governed by thermodynamics, the outcome, paths 1) 2) or 3), can be predicted by the entry and spreading coefficients. Hotrum et al. give a clear description of the coefficients, which are calculated from the various interfacial tensions [13]. However, their experimental results indicate a significant kinetic barrier for oil droplet penetration of the air/water interface, not predicted by the entry coefficients. There exists a stable water film between smooth solid particles or oil drops and the air water interface, preventing entry. We see examples of this kinetic barrier to entry in many technologies. For example, in defoamer technology, silicone oil emulsion drops are poor foam breakers because the oil droplets cannot penetrate the air/water interface. However, when the oil drops are supporting spikey, hydrophobic particles, these drops can penetrate the thin water film when an oil droplet approaches the air/water interface, ultimately leading to foam collapse [14]. Further evidence for thin water films between emulsion droplets and the surface of sessile drops comes from the analysis of evaporation rates for emulsions made using volatile solvents [3]. Whereas the continuous water phase evaporates at the same rate as bulk water, the volatile oil phase evaporation rate is much lower compared to bulk solvent. The solvent must diffuse through the thin water layer, lowering evaporation rates.

1.3. Literature – deposits from suspoemulsions

Many of the early suspoemulsion publications focused on the colloidal stability of concentrated dispersions, presumably with a view to understanding the factors influencing the shelf life [15–19]. Tadros explains that suspoemulsions can undergo a number of processes including: homoflocculation of the suspended particles (i.e., the PG7 particles in our work); emulsion coalescence; heteroflocculation of the emulsion droplets and the suspended particles giving either aggregates or emulsion drops coated with particles embedded in the oil/water interface; and, solubilization of the suspended particles in the oil [20].

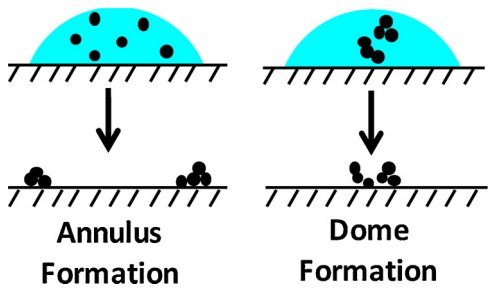

Fig. 1. Cross-sectional illustration of deposits formed by drying sessile drops formed with aqueous colloids. Stable, hydrophilic particles mainly form an annulus (coffee ring) whereas hydrophobic, aggregating particles form a dome. Adapted from Anyfantakis et al. [10].

In an excellent paper involving suspoemulsions, Faers and Pontzen reported a detailed study of deposit structure after drying on leaf surfaces [21]. They hypothesized that the oil was most effective in promoting uptake of the active agent when the oil was in direct contact with the active ingredient – a state they called association. This is a reasonable hypothesis, as mechanisms proposed for oil adjuvants include modification of the transport properties of leaf surfaces [22,23] and solubilization of oil-soluble adjuvants [24]. For both of these oil adjuvant mechanisms, the active ingredients must be in contact with the oil – association. Faers' experiments involved characterizing deposits formed by spraying a suspoemulsion on grape leaves. They showed that suspoemulsion deposit structures were sensitive to surfactant concentration and the extent of dilution at constant coverages of the dispersed active particles. Parallel experiments involving measuring uptake in a measuring the uptake of a different active in apple cuticles gave some support for the association hypothesis.

Although suspoemulsions are often prepared as independent suspensions of active ingredient particles and oil droplets, one can imagine that hydrophobic actives could be engulfed and/or dissolved in the oil phase before spraying. Recently an Australian group reported studies simulating what happens to a suspoemulsion in the mixing tank before spraying. They measured the transfer of small oil-soluble, dispersed particles into the oil phase using X-ray diffraction and found that complete dissolution was rapid (< 200 s) [24]. Of course this may not be a general conclusion. Strongly adsorbing or grafted stabilizing polymers onto the particles surfaces could prevent the particles from entering the oil phase [25].

Motivated by Faers and Pontzen [21], we believe that by controlling deposit structure, we can influence the impact of Green Emulsion on plants. Characterization and control of deposit structure is the first step and thus the focus of this work. Herein we report the influence of formulation variables on the structure of the dried deposits that form when a drop of Green Emulsion suspoemulsion dries on PARAFILM® M, a smooth waxy film used in ASTM E2044 "Standard Test Method for Spreading of Liquid Agricultural Spray Mixtures" [26]. We demonstrate that the deposit structure depends upon the extent to which dispersed pigment particles adsorb at the oil/water interface before evaporative drying.

2. Experimental section

2.1. Materials

HARMONIZER™, an aqueous dispersion of 40 wt% Pigment Green 7 (PG7) plus 17 wt% of a surfactant mixture, CIVITAS, 98% mineral oil and 2% oil-borne surfactant and pure mineral oil were supplied by Suncor Energy (Mississauga, ON, Canada). Oil Red O and PARAFILM® M were purchased from Sigma-Aldrich. All water used was deionized and further purified with a Barnstead Nanopure Diamond system (Thermo Scientific).

2.2. Sessile drop imaging

Images of sessile drops drying on PARAFILM® M were recorded with an iPhone 5 camera fixed 9 cm above the surface. In many cases, Oil Red O was added to the oil concentrate to enhance the oil images. For contact angle measurements, the sessile drops were characterized with a Krüss Drop Shape Analysis System DSA1.

2.3. Green Emulsion preparation

Green Emulsion is an aqueous dispersion of 0.54% HARMONIZER™ and 4.46 wt% CIVITAS. The overall Emulsion composition is shown in Table 1. For Green Emulsion-VM, 20 mL of the mixture in a 50 mL Falcon tube was dispersed using a vibromixer (Mini Vortex Mixer, VWR) at 3000 rpm for 1 min. Green Emulsion-US was emulsified using a probe sonicator (Sonifier 450, Branson Ultrasonics), in an ice bath for 1 min at an intensity level 6 and 50% pulses. In some cases, a small quantity of Oil Red O was dissolved in the CIVITAS to facilitate visualization of oil spreading.

2.4. Optical microscopy

Optical micrographs were obtained with a Zeiss LSM 510 Meta on an Axiovert 200 M microscope (Zeiss, Gottingen, Germany).

2.5. Dynamic light scattering

The hydrodynamic diameters of PG 7 with water-borne surfactant were measured using a Malvern Zetasizer Nano instrument that possesses a He-Ne 4.0 mW laser operating at 633 nm and a detector angle of 173°. A sample of HARMONIZER™ was diluted with 5 mM NaCl to give an intermediate PG7 dispersion of 0.56 wt%, which was vortexed at 3000 RPM for 1 min. 10 μL of this mixture was diluted with 990 μL 5 mM NaCl solution that was then equilibrated in a light scattering cell for 3 min at 21 °C. Light scattering measurements were made in triplicate with each measurement consisting of 15 cycles. The data were analyzed with Zetasizer software, version 7.01.

3. Results

Green Emulsion suspoemulsions were prepared by dispersing in water a commercial mineral oil concentrate that included surfactants (oil-borne). A concentrated aqueous dispersion of the pigment PG7, stabilized with water-soluble surfactants, was added in a second step, yielding the composition summarized in Table 1. In practice, the suspoemulsions are prepared by farmers in the sprayer mix-tanks just before application. Because the mixing conditions used to disperse concentrates are not clearly defined, we employed two laboratory methods for dispersing the concentrates – a lower intensity dispersion with a vortex mixer (Green Emulsion-VM) and a higher intensity ultrasonic dispersion protocol (Green Emulsion-US). We presume that the low intensity dispersion in the vibromixer (VM) is more representative of commercial mix-tank preparations.

Green Emulsion is dilute. The total volume fraction of dispersed oil and PG7 particles is about 5%. Dynamic light scattering was used to characterize a dilute dispersion of PG7 particles dispersed in 5 mM NaCl. The resulting particle size distribution (see Fig. S1 in the Supporting information) had a main peak that was approximately log normal with a mean diameter of 430 nm. In addition, there was a small peak at 70 nm and another at 5000 nm. This broad particle size distribution is typical of particles produced by milling larger particles.

Fig. 2 shows photographs and optical micrographs of the suspoemulsions one and seven days after mixing. With the low intensity VM dispersion, the oil drops were very large after one day, indicating the surfactant packages were chosen to give limited emulsion stability. Fig. S2 shows micrographs of Green Emulsion-VM one hour after dispersion; the emulsion droplets are much smaller than those in Fig. 2.

By contrast, the suspoemulsion prepared by ultrasonic dispersion

Table 1
Green Emulsion composition.

	wt%
From HARMONIZER™	
PG7 pigment	0.22%
Water-borne surfactants	0.092%
From CIVITAS	
Mineral oil	4.37%
Glycerol Oleate, HLB 3	0.029%
Polyoxyethylene (4) lauryl ether, HLB 16.9	0.059%
Total water content.	95.2%

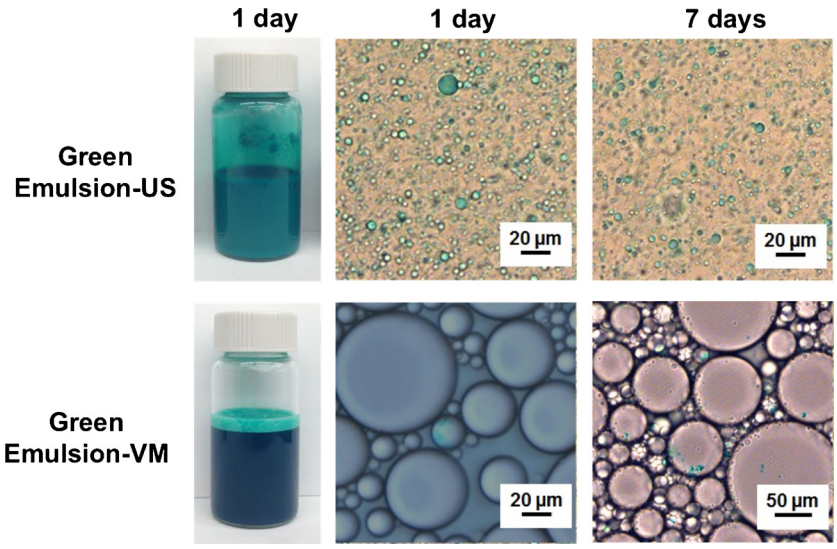

Fig. 2. Comparison of spray dispersions prepared by our standard low energy vortex mixing (Green Emulsion-VM) with emulsions prepared by high energy ultrasonic dispersion (Green Emulsion-US). Optical micrographs of samples taken below the cream layer. (For interpretation of the references to color in this figure legend, the reader is referred to the web version of this article).

(Green Emulsion-US), had much smaller emulsion drop diameters and showed little change over seven days. Furthermore, the emulsion droplets are green, suggesting the PG7 pigment particles are embedded in the oil surface or possibly entrained in the oil phase. The presence of particles at the oil/water interface could explain the exceptional stability of the Green Emulsion-US dispersions. The surface tensions of the two types of green emulsions and some the components are given in Table S1. Most of the combinations had surface tensions between 27- and 33 mN/m. Green Emulsion-US was an outlier with a surface tension of 48 mN/m, reflecting the higher surface area of the in ultrasonicated emulsion.

The contact angles (see images in Fig. S3) of a sessile drop Green Emulsion-VM on PARAFILM® smooth wax film was 56 ± 2°, whereas Green Emulsion-US gave a contact angle of 82 ± 2°. The ultrasonic dispersion produced more oil/water interfacial area, influencing the surfactant distribution and the contact angle on PARAFILM® M.

The spreading and drying characteristics of the two types of Green Emulsion drops on PARAFILM® M are compared in Fig. 3. Oil Red O dye was dissolved in the oil concentrate to facilitate imaging the extent of oil spreading. Under ambient laboratory conditions, it took about 3 h for the water to evaporate leaving the deposit. The Green Emulsion-VM drops showed limited spreading, consistent with the initial contact angle (56°). With drying there was some contraction in drop diameter before the drop was pinned, giving a non-circular drop pattern. The deposit structure in the 6-hour image shows the green PG7 particles are concentrated in two areas – a narrow annulus (coffee ring) and a large central dome.

Green Emulsion-US sessile drops were completely pinned with no evidence of contraction. The dried drops had a dome, occupying most of the drop footprint with no annulus. Additional VM and VS photographs of sessile drops are shown in Fig. S4. The 6-hour Green Emulsion-US image in Fig. 3 showed a slight indication of red beyond the deposit, suggesting oil spreading. Fig. S5 shows that after seven days the oil had spread beyond the deposits formed by both VM and US sessile drops.

The spreading behaviors of dyed oil emulsion (no PG7) and PG7 dispersion (no oil), are compared to Green Emulsion in Fig. 4. The oil emulsion sessile drop did not spread on PARAFILM® M and the oil did not spread after the water evaporated. The PG7 dispersion dried to give a thick annulus and no dome – classic coffee ring behavior. The Green Emulsion-VM deposit shared characteristics of both the oil emulsion deposit, with most of the oil in a dome, and the PG7 dispersion deposit. However, the Emulsion-VM dome was dark green, indicating a significant PG7 content.

The oil-borne surfactant content influences the deposit structure formed by sessile drops on PARAFILM® M. Fig. 5 shows that increasing the oil-borne surfactant concentration beyond the 0.089% (see Table 1)

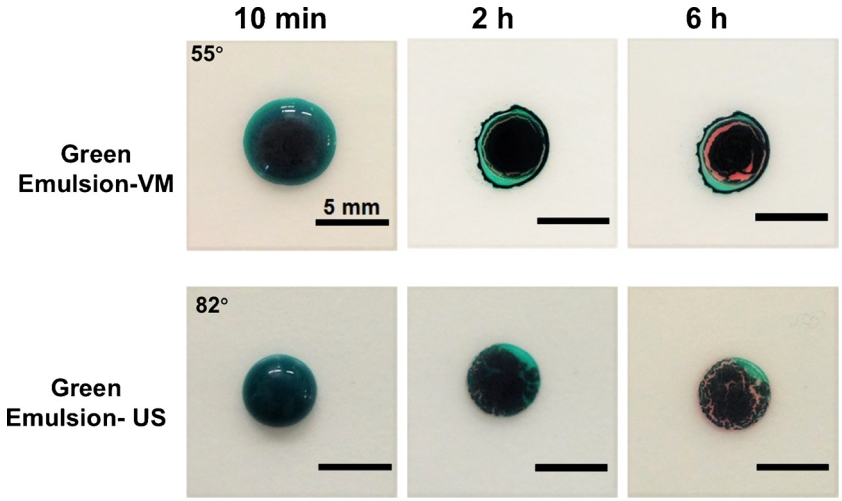

Fig. 3. Green Emulsion-VM and US 30 μL sessile drops drying on PARAFILM® M. The oil contained a red dye. (For interpretation of the references to color in this figure legend, the reader is referred to the web version of this article).

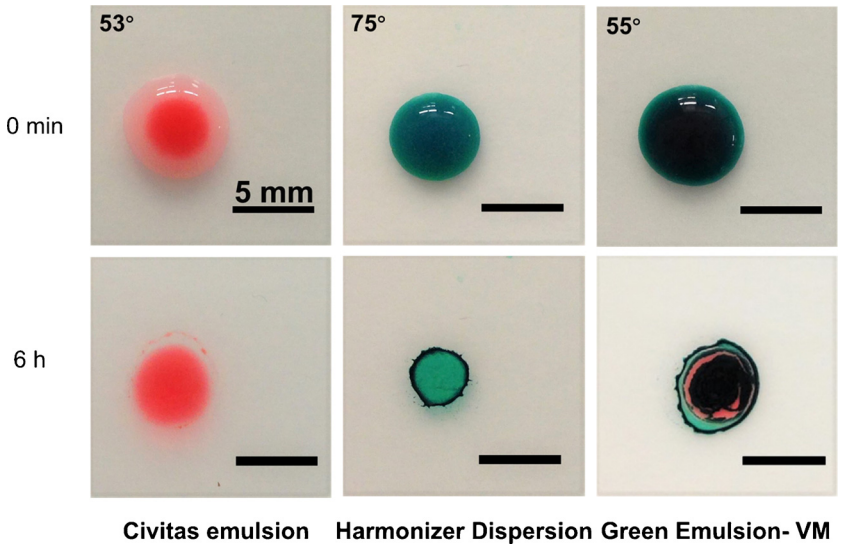

Fig. 4. Comparing Green Emulsion-VM spreading on PARAFILM® M with the corresponding dyed oil emulsion (without PG7) and the PG7 pigments dispersion (without oil). All photographs are shown at the same magnification, and drop volumes were 30 µL. The oil in the Civitas emulsion included an oil-soluble red dye. (For interpretation of the references to color in this figure legend, the reader is referred to the web version of this article).

decreased the dome area, with a corresponding growth in the width of the annulus. The optical micrographs show that all higher surfactant concentrations gave much smaller emulsion drop sizes. The higher two surfactant concentrations also gave slighter larger sessile drop footprints, indicating lower contact angles. More examples of photographs showing the influence of oil-borne surfactant are presented in Fig. S6.

Finally, we applied drops of Green Emulsion-VM on grass and burning bush leaf surfaces. The photographs in Fig. 6 showed that, on grass, no dome or annulus were observed because the oil and PG7 particles spread along the axis of the leaves. The contact angle of water on top side of grass was 91° when viewed parallel to the direction of the veins and 101° when viewed parallel to the veins. Interestingly, the contact angle of water on PARAFILM® M was 96°, between the two grass values. The contact angle of water on the top side of a burning bush leaf was 74°.

To better understand these observations, we prepared silicone rubber molds of the grass leaf. The SEM of the rubber template show ridges, corresponding to grooves, along the direction of the leaf axis. Therefore, we conclude that mineral oil spread along the grooves in the leaf surface. By contrast, the burning bush leaves gave nearly circular annuli encircling a dome. The SEM image of the leaf surface indicated nanoscale asperities but no grooves. The influence of leaf structure on spray drop spreading has been addressed in the literature [27,28].

4. Discussion

Suspoemulsions containing mixtures of 4–6 surfactant types, dispersed particles and emulsified oil are very complicated formulated products. Because the PG7 pigment in Green Emulsion is completely water and oil insoluble, this system is slightly less complex compared to products where the dispersed particles are partially oil soluble.

Most of our results involve 30 µL Green Emulsion-VM sessile drops on PARAFILM® M, a slightly bigger drop than the ASTM method that uses 20 µL [26]. If we assume the sessile drop shapes are ideal spherical caps with a contact angle of 50°, the height of a 30 µL spherical cap before drying is 1.61 mm. By contrast, a typical spray drop diameter applied to a field is 200 µm, corresponding to a drop volume of 0.004 µL [29]. The corresponding drop height for a 0.004 µL spherical cap shape is 81 µm. The dispersed phase volume fraction of Green Emulsion is low (~0.05) suggesting that initial creaming/sedimentation rates can be estimated by Stokes' law. Table 2 summarizes the time required for an oil droplet to rise a distance equal to the sessile drop height, and the

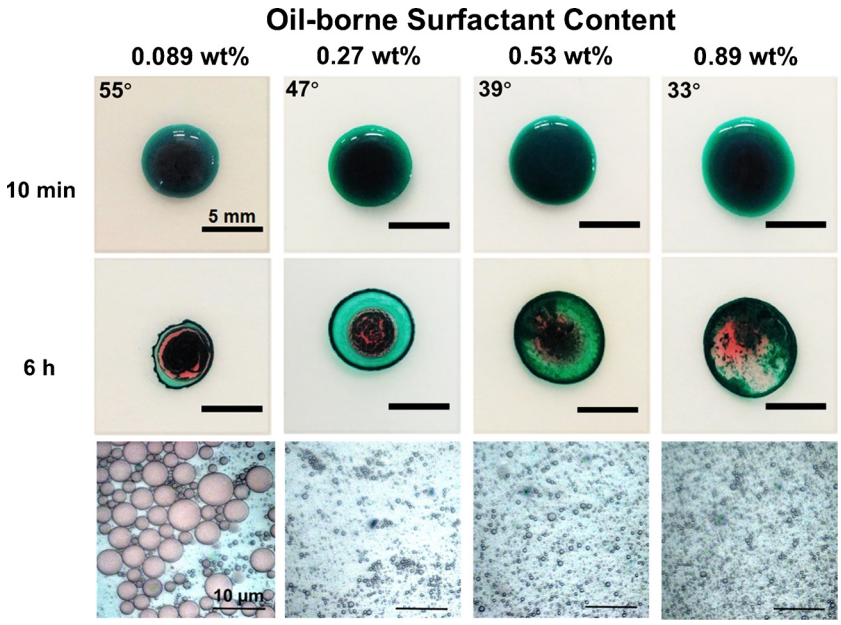

Fig. 5. Photographs showing the influence of the oil-borne surfactant content on Green Emulsion-VM deposit structure. Top row – 30 µL sessile drops on PARAFILM® M 10 min after formation; middle row – the resulting deposits; and, bottom row – optical micrographs of the Green Emulsion-VMs. (For interpretation of the references to color in this figure legend, the reader is referred to the web version of this article).

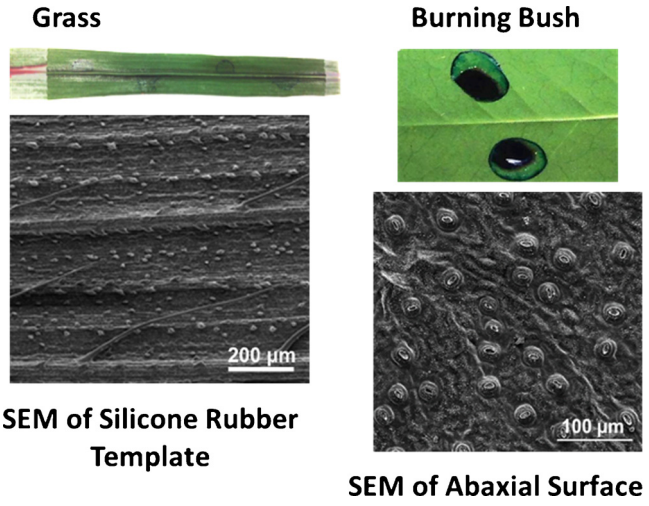

Fig. 6. Photographs of dried Green Emulsion-VM on a grass and on a burning bush leaf. The electron micrographs show a silicone rubber template of a grass leaf, whereas the burning bush micrograph was made directly on the leaf. (For interpretation of the references to color in this figure legend, the reader is referred to the web version of this article).

Table 2
Some properties of Green Emulsion sessile drops assuming a spherical cap shape and Stokes' law sedimentation rates. Oil creaming is rapid and PG7 sedimentation is slow.

	PARAFILM® M Spreading Experiments	Typical Spray Application in Field
Drop diameter	3.9 mm	200 µm
Drop volume	30 µL	0.0042 µL
Contact angle	50°	50°
Maximum height of sessile drop	1.6 mm	81 µm
Maximum creaming time for 5 µm diameter oil drop	587 s	30 s
Maximum 350 nm diameter PG7 sedimentation time.	22 h	1.1 h

corresponding sedimentation time for PG7 particles. Two conclusions can be drawn from the estimates in Table 1: 1) oil creaming times are much shorter than the 3–6 h required to dry 30 µL drops, whereas the PG7 sedimentation times are much longer; and, 2) the creaming/sedimentation times for the 200 µm drops are about 20 times shorter than the times for the large, 30 µL drops we used for the PARAFILM® M experiments. The significance of this calculation is oil drops will cream whereas dispersed pigment particles will not settle before sessile drops evaporate.

Fig. 4 shows that when a sessile drop containing only PG7 particles dries, most of the pigment is present in the annulus. This deposit is a classic coffee ring structure resulting from fluid flow towards the periphery of the pinned drop. By contrast, the oil + PG7 combination in Green Emulsion-VM gave an annulus plus a large dome region. The genesis of the dome is apparent almost immediately after the sessile drop is formed – see the 10 min Green Emulsion-VM images in Fig. 3 where a dark green oil rich phase has formed under the top center of the drop. The creaming time estimates in Table 2 are consistent with the observed accumulation of oil near the drop surface in ten minutes. Why is the oil dark green? We propose that the PG7 pigments adsorb at the oil/water interface possibly giving some Pickering stabilization [30] of the oil drops. These oil-immobilized pigment particles cannot migrate to the periphery to build the annulus but instead are trapped with the oil, ultimately giving a dome structure. Generally, when small particles adsorb at an oil/water interface, the maximum coverage corresponds to monolayer of adsorbed particles. Is there enough oil/water interface to adsorb all of the PG7 particles in Green Emulsion?

Assuming PG7 particles are spheres with a diameter of 430 nm, 1 kg of Green Emulsion contains enough PG7 particles (Table 1) to cover a surface with an area of 6 m^2/kg. The micrographs in Fig. 2 show that emulsion drop size, and thus the oil/water interfacial area, is sensitive to the intensity of dispersion (i.e. VM vs US), and also aging to time (VM images in Fig. 2 versus 1 h images in Fig. S2). The smaller the average oil drop diameter, the greater the corresponding oil/water interfacial area. For the oil concentration given in Table 1, the oil droplet diameter required to give an interfacial area of 6 m^2/kg is 50 µm. Although there are some large oil drops in Green Emulsion-VM, prepared with lower intensity mixing, the VM images in Figs. 2 and S2 suggest values smaller than 50 µm. Therefore, we conclude that there is sufficient oil/water interfacial area in the Green Emulsion-VM to sequester all of the PG7 particles. However, all the Green Emulsion-VM deposit images reveal annuli + domes, indicating only a fraction of the PG7 particles are immobilized at the oil/water interfaces. By contrast, Green Emulsion-US emulsions are much smaller, providing much oil/water interfacial area, leaving few PG7 particles in suspension to form an annulus.

Green Emulsion is an optimized commercial turf grass fungicidal spray that has shown efficacy combating salt and moisture stress. Herein we evaluated the impact on deposit structures of small changes in the composition. Mixing intensity had the greatest impact on emulsion and deposit properties – Fig. 3. Our industry partner compared Green Emulsion-US with Green Emulsion-VM in a salt stress assay using US. Perennial ryegrass (*Lolium perenne* L.). No significant differences between the performance of the two emulsions were observed. We do not know the mechanism by which Green Emulsion improves salt tolerance. However, this work shows that mechanism is not sensitive to deposit structure.

Finally, the ASTM E2044 "Standard Test Method for Spreading of Liquid Agricultural Spray Mixtures" involves placing a drop of crop spray dispersion on PARAFILM® and measuring the dimensions of the resulting sessile drop [26]. The broader implication of the current work is that allowing the sessile drops on PARAFILM® to dry, followed by the analysis of the deposit structure, gives a direct measure of the extent to which active ingredient particles, initially dispersed in water, are transferred on or into oil drops in suspoemulsions.

5. Conclusions

Green Emulsion is a dilute aqueous dispersion formed by diluting in water a mineral oil concentrate plus a PG7 pigment concentrate. We investigated the factors influencing the deposit structure formed when sessile drops of Green Emulsion dry on waxy PARAFILM® M surfaces, and made the following conclusions.

The distribution of PG7 pigment in the dried spray drop deposit depends on the partitioning of PG particles in the suspension before drying. Individually dispersed PG7 particles in the aqueous phase mainly end up in the annulus (coffee ring), whereas PG7 particles adsorbed on the oil emulsion droplets end up as a central oily deposit we call a dome – see the graphical abstract. Therefore, the deposit structure on PARAFILM® M surfaces gives an indication of the extent to which dispersed active ingredient particles are adsorbed on engulfed in oil droplets.

After most of the water evaporates, some oil migrates beyond the dome and beyond the annulus. Increasing the oil-soluble surfactants concentrations inhibited PG7 binding to the oil/water interface, giving a very small dome area and a wide annulus after drying.

The deposit structure is sensitive to the mixing intensity when concentrates are diluted in a mix-tank. The ultrasonically dispersed Green Emulsion-US gave much smaller oil drops compared to Green Emulsion-VM prepared by vortex mixing. Virtually all the PG7 particles were bound to the large oil/water surface area in the Green Emulsion-US, giving very large dome areas.

As reported by others [2,27], nano and micro scale asperities and

trenches in leaves greatly distort the circular drop pattern observed on smooth, wax surfaces.

Acknowledgments

We thank the National Sciences and Engineering Research Council of Canada (NSERC) and Suncor Canada for funding this project. Most of the experiments were conducted at the McMaster Biointerfaces Institute, funded by the Canadian Foundation for Innovation. R.H. Pelton holds the Canada Research Chair in Interfacial Technologies. C. Abarca thanks the National Commission for Scientific and Technological Research of Chile, CONICYT – Becas Chile Scholarship Program.

Appendix A. Supplementary data

Supplementary material related to this article can be found, in the online version, at doi:https://doi.org/10.1016/j.colsurfa.2018.05.074.

References

[1] M. Massinon, N. De Cock, W.A. Forster, J.J. Nairn, S.W. McCue, J.A. Zabkiewicz, F. Lebeau, Spray droplet impaction outcomes for different plant species and spray formulations, Crop Prot. 99 (2017) 65–75.
[2] P. Taylor, The wetting of leaf surfaces, Curr. Opin. Colloid Interface Sci. 16 (2011) 326–334.
[3] I. Aranberri, K.J. Beverley, B.P. Binks, J.H. Clint, P.D.I. Fletcher, How do emulsions evaporate? Langmuir 18 (2002) 3471–3475.
[4] I. Aranberri, B.P. Binks, J.H. Clint, P.D.I. Fletcher, Evaporation rates of water from concentrated oil-in-water emulsions, Langmuir 20 (2004) 2069–2074.
[5] C.J. Wang, Z.Q. Liu, Foliar uptake of pesticides—present status and future challenge, Pestic. Biochem. Physiol. 87 (2007) 1–8.
[6] M. Fefer, J. Liu, T. Ruo, S.E. Hevia, Turfgrass Fungicide Formulation with Pigment, Suncor Energy Inc., Calgary, Alberta, US, 2013.
[7] A. Knowles, Recent developments of safer formulations of agrochemicals, Environ. 28 (2008) 35–44.
[8] R. Deegan, O. Bakajin, T. Dupont, G. Huber, S. Nagel, T. Witten, Capillary flow as the cause of ring stains from dried liquid drops, Nature 389 (1997) 827–828.
[9] A.F. Routh, Drying of thin colloidal films, Rep. Prog. Phys. 76 (2013) 046603.
[10] M. Anyfantakis, D. Baigl, B.P. Binks, Evaporation of drops containing silica nanoparticles of varying hydrophobicities: exploiting particle–particle interactions for additive-free tunable deposit morphology, Langmuir 33 (2017) 5025–5036.
[11] H. Hu, R.G. Larson, Marangoni effect reverses coffee-ring depositions, J. Phys. Chem. B 110 (2006) 7090–7094.
[12] P.J. Yunker, T. Still, M.A. Lohr, A.G. Yodh, Suppression of the coffee-ring effect by shape-dependent capillary interactions, Nature 476 (2011) 308–311.
[13] N.E. Hotrum, T. van Vliet, M.A. Cohen Stuart, G.A. van Aken, Monitoring entering and spreading of emulsion droplets at an expanding air/water interface: a novel technique, J. Colloid Interface Sci. 247 (2002) 125–131.
[14] G. Wang, R. Pelton, A. Hrymak, N. Shawafaty, Y.M. Heng, On the role of hydrophobic particles and surfactants in defoaming, Langmuir 15 (1999) 2202–2208.
[15] T.F. Tadros, Disperse systems in pesticidal formulations, Adv. Colloid Interface Sci. 32 (1990) 205–234.
[16] S. Memula, P. Berger, C. Chellappa, Suspoemulsions with improved stability and correlation of long term stability with the zeta potential, in: H.M. Collins, F.R. Hall, M. Hopkinson (Eds.), Pesticide Formulations and Application Systems: 15th Volume, ASTM International, 1996, pp. 132–144.
[17] R. Pal, Rheology of blends of suspensions and emulsions, Ind. Eng. Chem. Res. 38 (1999) 5005–5010.
[18] P. Mulqueen, Recent advances in agrochemical formulation, Adv. Colloid Interface Sci. 106 (2003) 83–107.
[19] J. Santos, L.A. Trujillo, N. Calero, M.C. Alfaro, J. Muñoz, Physical characterization of a commercial suspoemulsion as a reference for the development of suspoemulsions, Chem. Eng. Technol. 36 (2013) 1883–1890.
[20] Suspoemulsions, in: T. Tadros (Ed.), Encyclopedia of Colloid and Interface Science, Springer Berlin Heidelberg, Berlin, Heidelberg, 2013pp. 1389.
[21] M.A. Faers, R. Pontzen, Factors influencing the association between active ingredient and adjuvant in the leaf deposit of adjuvant-containing suspoemulsion formulations, Pest Manag. Sci. 64 (2008) 820–833.
[22] B.R. Bondada, C.E. Sams, D.E. Deyton, J.C. Cummins, Oil emulsions enhance transcuticular movement of captan in apple leaves, Crop Prot. 26 (2007) 691–696.
[23] D.K. Rodham, Colloid and interface science in formulation research for crop protection products, Curr. Opin. Colloid Interface Sci. 5 (2000) 280–287.
[24] G.R. Webster, N.B. Bisset, D.M. Cahill, P. Jones, A. Killick, A. Hawley, B.J. Boyd, Kinetic resolution of the interactions between agrochemical products and adjuvant systems upon mixing, J. Agric. Food Chem. 64 (2016) 6139–6147.
[25] R. Pons, P. Rossi, T.F. Tadros, Investigation of the interaction between emulsions and suspensions (suspoemulsions) using viscoelastic measurements, J. Phys. Chem. 99 (1995) 12624–12630.
[26] ASTM, ASTM International, Standard Test Method for Spreading of Liquid Agricultural Spray Mixtures, (2012).
[27] L. Boize, C. Gudin, G. Purdue, The influence of leaf surface roughness on the spreading of oil spray drops, Ann. Appl. Biol. 84 (1976) 205–211.
[28] C.G. McWhorter, W.L. Barrentine, Spread of Paraffinic oil on leaf surfaces of Johnsongrass (Sorghum halepense), Weed Sci. 36 (1988) 111–117.
[29] P. Hipkins, R. Grisso, Droplet Chart Selection Guide, Virginia Cooperative Extension, Virginia State University, 2014 Publication 442-031.
[30] B.P. Binks, Particles as surfactants—similarities and differences, Curr. Opin. Colloid Interface Sci. 7 (2002) 21–41.

SUPPLEMENTARY MATERIAL

Factors Influencing Agricultural Spray Deposit Structures on Wax Surfaces

Fengyan Wang[†], Zhen Hu[†], Carla Abarca[†], Michael Fefer[‡], Jun Liu[‡], Michael A. Brook and Robert Pelton[† *]

† Department of Chemical Engineering, McMaster University, 1280 Main Street West, Hamilton, ON L8S 4L7, Canada

‡ Suncor Energy, 2489 North Sheridan Way, Mississauga, ON L5K 1A8, Canada

* E-mail: peltonrh@mcmaster.ca

Table S1 Surface tensions of the two types of Green Emulsions and some of the individual components.

Sample	Surface tension (mN/m)
Green Emulsion-VM	31.5±0.2
Green Emulsion-US	48.1±0.5
Oil emulsion	31.4±0.3
PG7 Dispersion	32.8±0.3
Emulsion-VM (0.27 wt% oil-borne surfactant contained)	27.6±0.2
Emulsion-VM (0.53 wt% oil-borne surfactant contained)	27.5±0.3
Emulsion-VM (0.89 wt% oil-borne surfactant contained)	27.2±0.4

Figure S1 PG7 particle size distribution measured by dynamic light scattering. The dispersion was diluted with 5 mM NaCl at neutral pH.

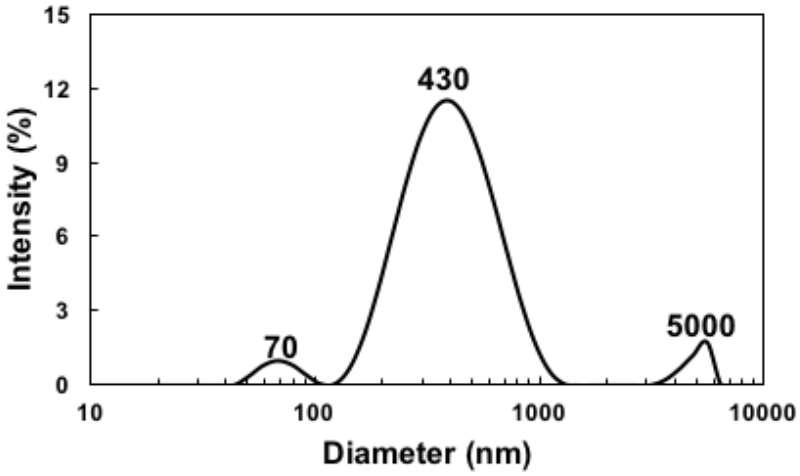
15
12
9
6
3
0
Intensity (%)
430
70
5000
10
100
1000
10000
Diameter (nm)

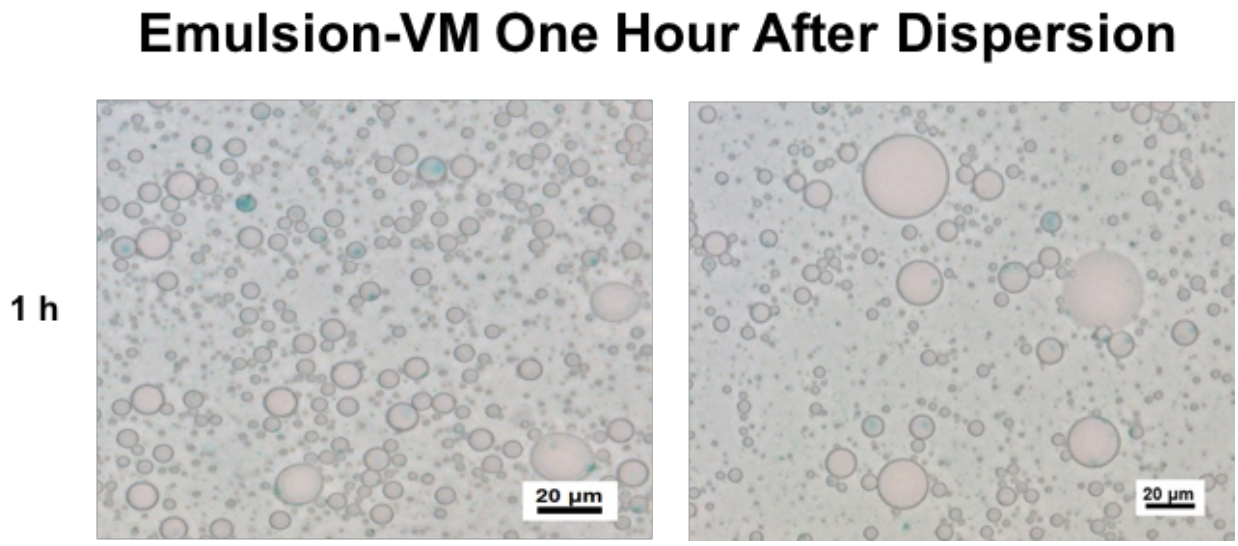

Figure S2 Photographs of Green Emulsion-VM taken 1 hour after dispersion in a vibromixer

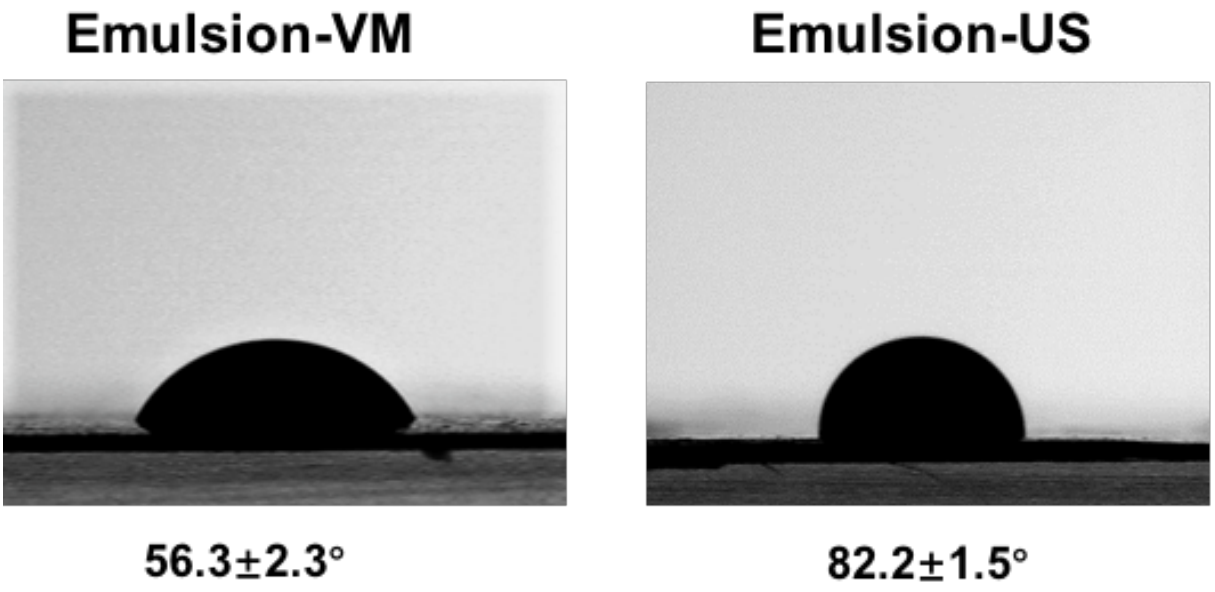

Figure S3 Initial contact angles of Green Emulsion on PARAFILM® M.

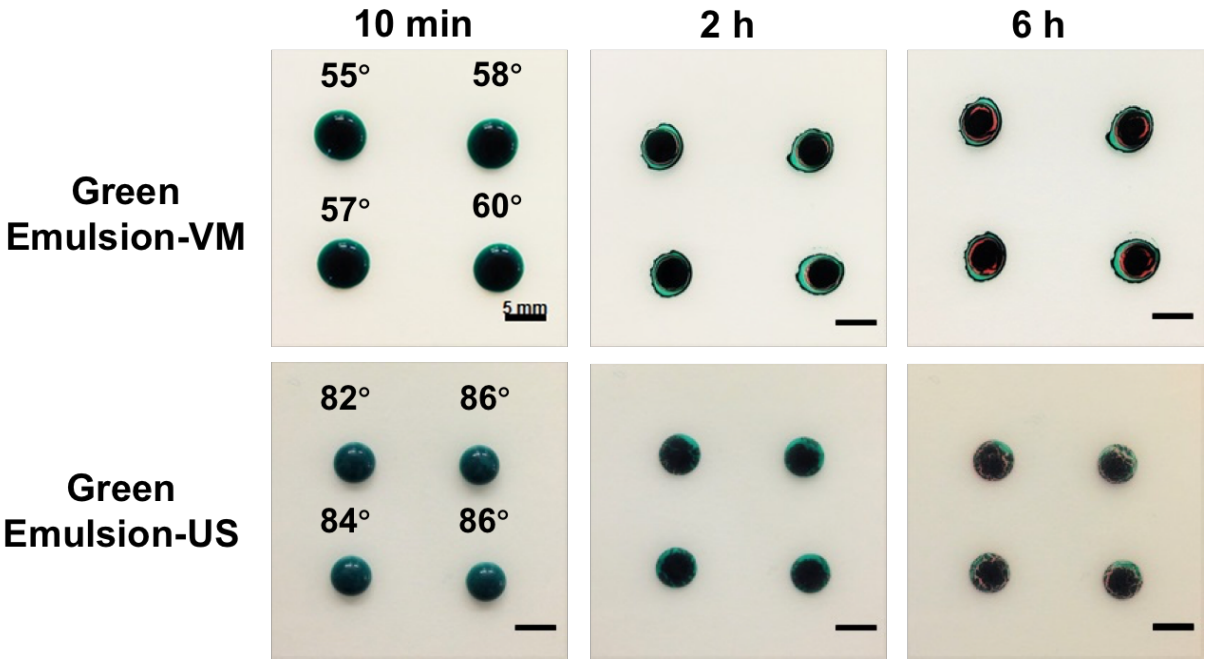

Figure S4 More examples of Green Emulsion-VS sessile drops on PARAFILM® M

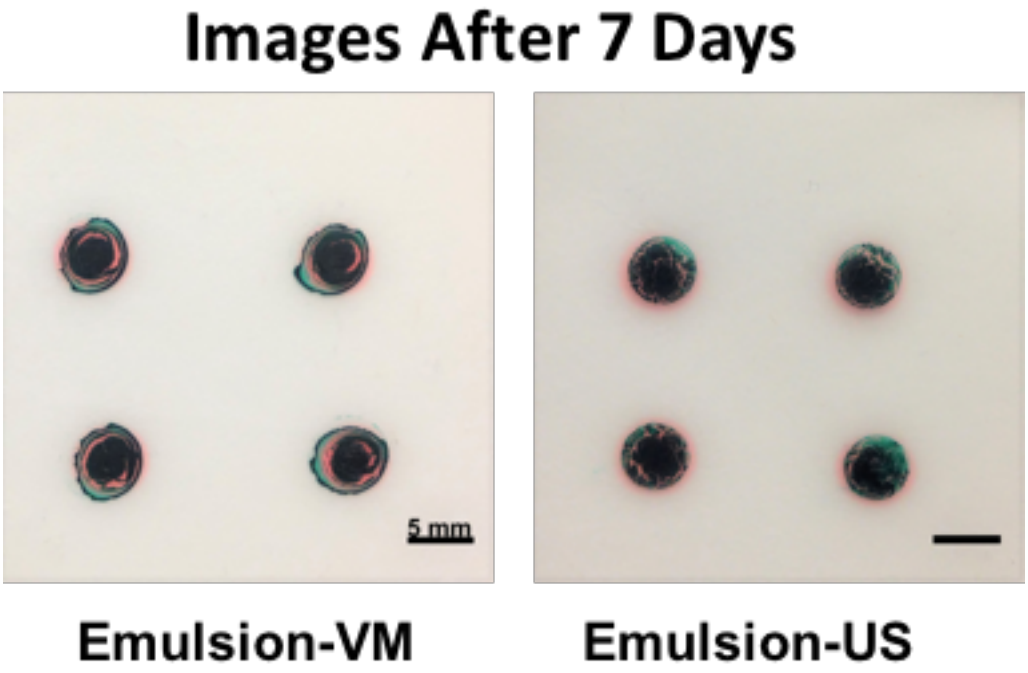

Figure S5 Dyed oil slowly spreads beyond the annulus of the dried drops.

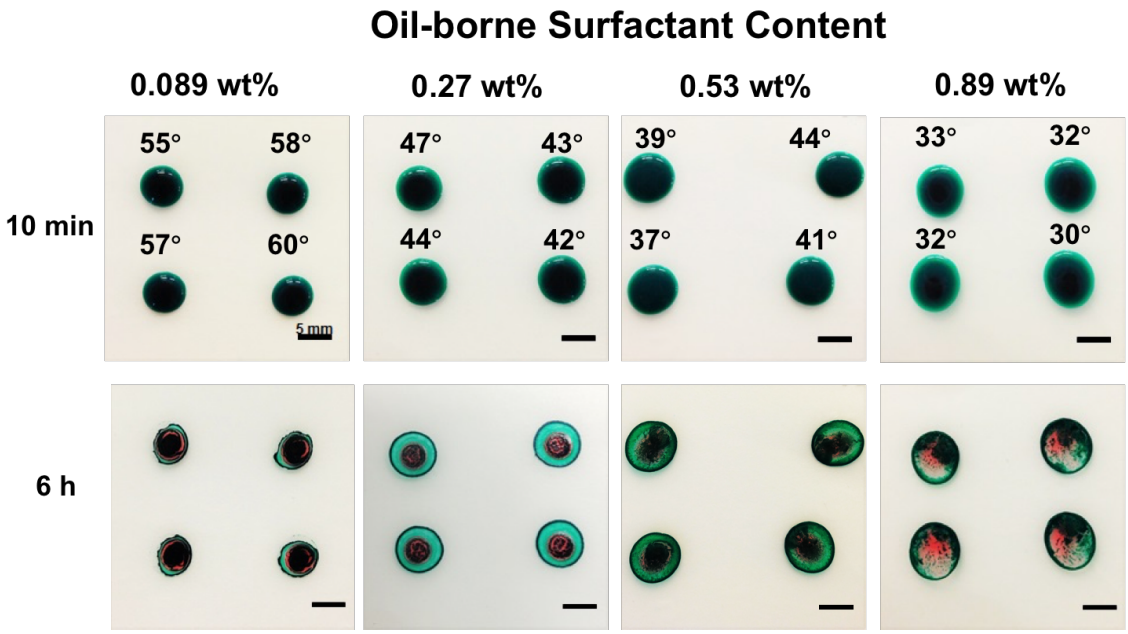

Figure S6 More examples showing influence of oil-borne surfactant content on deposit structure.

Chapter 5

My contributions

To employ CuChl as a new agricultural active ingredient, this research characterized CuChl's colloidal properties and binding tendencies for model surfaces. In addition, a potential strategy was given for solving the problem of CuChl's poor intrinsic rainfastness performance. Furthermore, a method for analyzing the relationship between the properties of suspoemulsions and the resulting dried deposits on hydrophobic surfaces was also presented. Thus, this thesis makes the following major contributions:

1. This work was the first to measure the adsorption of CuChl on model surfaces by QCM-D in order to help understand how CuChl interacts with relevant plant surfaces. Of the model surfaces, cellulose adsorbed the most CuChl, followed by polystyrene and pullulan. The surfactants, SDS or DTAB, were able to displace CuChl that had been adsorbed onto cellulose when they were used in concentrations above the critical micelle concentration. This result suggests that surfactants in commercial products can affect the transport of active ingredients by altering binding tendencies.

2. A polymer combination of CMC and PAE was demonstrated as a spray adjuvant that is capable of providing water-soluble/dispersed CuChl with efficient rainfastness protection. A unique feature of this polymer combination is that it can form a structure that controls the release of an active ingredient after it dries down. In the release experiments, an unfixed amount of CuChl was immediately released whereas water-soluble BSF exhibited a square root of time-dependent behavior. In the CuChl solution, the present nanoparticles were coated with CMC:PAE complexes, as well as CuChl's low solubility, caused the immobilization of CuChl on parafilm. A small amount of CuChl that was not embedded in complexes exhibited a burst release. In contrast, highly water-soluble BSF dissolved rapidly and diffused through complexes upon exposure to water. In addition, this research demonstrated the ratio between the release of CuChl and the amount that is available to enter plants upon re-wetting can be controlled by adjusting the compositions and concentrations of polymers.

3. This work is the first to show how the distribution of active ingredient particles in dried deposits can be used to determine the extent to which dispersed particles are bound to or entrained in oil drops in suspoemulsions. As the finding showed, the PG7 particles that were bound to or entrained in oil drops ended up in the center (dome) area after drying, whereas individually dispersed particles ended up in the annulus.